Susana Costa de Oliveira

Licenciatura em Engenharia de Micro e Nanotecnologias

Biomimetic Mineralization: Encapsulation in Calcium Carbonate Shells

Dissertação para obtenção do Grau de Mestre em
Engenharia de Micro e Nanotecnologias

Orientador: Professora Doutora Isabel Maria das Mercês Ferreira, Professora Associada, Faculdade de Ciências e Tecnologia da Universidade Nova de Lisboa

Co-orientador: Professora Doutora Susana Isabel Pinheiro Cardoso de Freitas, Professora Associada, Instituto Superior Técnico da Universidade Técnica de Lisboa

Júri:

Presidente: Prof. Doutor Rodrigo Ferrão de Paiva Martins
Arguente: Doutora Verónica Cristina Baião Martins Romão
Vogal: Prof. Doutora Isabel Maria das Mercês Ferreira

FACULDADE DE CIÊNCIAS E TECNOLOGIA
UNIVERSIDADE NOVA DE LISBOA

Setembro, 2015

Biomimetic Mineralization: Encapsulation in Calcium Carbonate Shells

Acknowledgments/Agradecimentos

Antes de mais quero agradecer à minha orientadora, Professora Isabel Ferreira pelo apoio dado nesta etapa e por me ter deixado tentar concretizar o que imaginei. Desde montes de objetivos traçados, falhados e frustrações, cheguei até aqui e sei que evoluí com toda esta experiência. Resiliência é a palavra-chave desta tese.

Quero também agradecer ao meu co-orientador, Professor João Paulo Borges, que esteve sempre pronto para partilhar conhecimento, e como não podia deixar de ser, deixo uma linha especial para a Doutora Ana Baptista, que esteve sempre disponível mesmo quando não podia. A todo o restante grupo, Paulo Duarte, Inês Ropio, Filipe, Xana, Marisa, um obrigado, pois todos ajudaram de alguma forma, a que este projeto andasse sempre um pouco mais para a frente.

Não podia ainda deixar de referir a Professora Carmo Lança, a Professora Helena, a Professora Suzete, o CJ e a Coro pela ajuda prestada e pelo acesso à câmara e ao microscópio, e tenho ainda de deixar um agradecimento à Ana Almeida pela análise dos ângulos de contacto, ambas ajudas essenciais para este trabalho.

Por fim mas não por último, quero agradecer imenso à instituição INESC-MN, à Professora Susana, que me recebeu e me deu acesso às instalações como se desde sempre tivesse feito parte da vossa casa. Obrigado por ter permitido que eu pudesse aprender com o seu grupo, ter ido para o INESC-MN desenvolver o dispositivo de microfluídica foi um passo importante que eu queria para este projeto, e uma aprendizagem fundamental ter passado da teoria à prática - deixo aqui também os parabéns pela organização das instalações. De todas as pessoas que aí conheci tenho de agradecer (e muito) ao Tomás e ao Tiago que me deram muito do seu tempo sem nada em troca, partilhando o seu conhecimento comigo e ajudando ativamente a resolver questões técnicas que foram surgindo. Obrigado ainda ao Zé e ao Eng. Fernando pela ajuda com o fabrico da máscara e pela boa disposição, à Virgínia pelas mais variadas ajudas e em particular com o perfilómetro e à Andreia pelo tempo disponibilizado na *mill*.

A vossa ajuda e paciência permitiu-me estar aqui hoje.

Aos amigos,

Do Lab, Dj Fi in tha House, Tomás-Talheres-de-Peixe, Susana sista do bronze, Cláudia Nails on Gels e à mascote Ana Sardine Hip Hop 2000, que tornaram os dias muito mais divertidos! "Porque quando uma pessoa acredita e trabalha, as coisas acontecem!", T.M.;

Do Ceni, Rachel, Inês, Tomás, obrigado pelas *pipe connections* e apoio moral, e ao AFM master Mestre Tomás Calmeiro um muito obrigado pelo melhor filme 3D-AFM que já vi;

À team fibras, B e Richie, que se há-de encontrar no gym para mais aventuras: #6pack_thereturn

E aos mais antigos: Melissa, Ana A., Carlos, Diogo I., Miguel e Diogo S.

À família, mãe, pai, irmã e ao meu Diogo, obrigado pelo apoio incondicional de sempre.

Rita, agora é a tua vez!

Abstract

Calcium carbonate biomineralization is a self-assembly process that has been studied to be applied in the biomedical field to encapsulate biomolecules. Advantages of engineering mineral capsules include improved drug loading efficiencies and protection against external environment. However, common production methods result in heterogeneous capsules and subject biomolecules to heat and vibration which cause irreversible damage.

To overcome these issues, a microfluidic device was designed, manufactured and tested in terms of selectivity for water and oil to produce a W/O/W emulsion. During the development of this work there was one critical challenge: the selective functionalization in closed microfluidic channels. Wet chemical oxidation of PDMS with 1M NaOH, confirmed by FTIR, followed by adsorption of polyelectrolytes - PDADMAC/PSS - confirmed by UV-Vis and AFM results, render the surface of PDMS hydrophilic. UV-Vis spectroscopy also confirmed that this modification did not affect PDMS optical properties, making possible to monitor fluids and droplets. More important, with this approach PDMS remains hydrophilic over time. However, due to equipment constrains selectivity in microchannels was not achieved.

Therefore, emulsion studies took place with conventional methods. Several systems were tried, with promising results achieved with $CaCO_3$ *in-situ* precipitation, without the use of polymers or magnesium. This mineral stabilizes oil droplets in water, but not in air due to incomplete capsule formation.

Keywords: $CaCO_3$; biomineralization; microfluidic; selective functionalization; emulsion.

Resumo

A biomineralização do carbonato de cálcio é um processo auto-regulado que tem sido estudado para aplicar na área biomédica para encapsulamento de biomoléculas. Entre as vantagens destas cápsulas encontram-se a melhor eficiência de encapsulamento e a proteção contra fatores externos. Contudo, os métodos tradicionais de produção resultam em cápsulas heterogéneas, e sujeitam as biomoléculas a calor e vibração, o que causa danos irreversíveis.

Para ultrapassar estes problemas, um dispositivo de microfluídica foi desenhado, fabricado e testado em termos da seletividade para a água e o óleo para produzir um emulsão A/O/A. Durante o desenvolvimento deste trabalho houve um desafio crítico: a funcionalização seletiva em canais de microfluídica selados.

A oxidação por solução química do PDMS com 1M NaOH, confirmada por FTIR, seguida da adsorção de polielectrólitos - PDADMAC/PSS - confirmada por UV-Vis e AFM, tornou a superfície do PDMS hidrofílica. A espectroscopia UV-Vis também confirmou que o PDMS mantinha as suas propriedades óticas, possibilitando monitorizar os fluídos e as gotas. Mais importante, com esta modificação química o PDMS mantém a hidrofilicidade ao longo do tempo. Devido a constrangimentos de equipamento, a seletividade nos microcanais não foi alcançada.

Devido a isso, fez-se um estudo de emulsões por métodos convencionais. Vários sistemas foram testados, com resultados promissores para a precipitação *in-situ* do $CaCO_3$, sem uso de polímeros ou magnésio. Este mineral estabiliza gotas de óleo em água, mas não no ar devido à formação de uma cápsula incompleta.

Palavras-chave: $CaCO_3$; biomineralização; microfluídica; funcionalização seletiva; emulsão.

Abbreviations

3D	Three dimensional
Ad 5	Adenovirus 5
AFM	Atomic Force Microscope
BL	Bilayer
BSA	Bovine Serum Albumin
$CaCO_3$	Calcium carbonate
CaP	Calcium phosphate
DMAc	Dimethylacetamide
DMSO	Dimethyl Sulfoxide
DNA	Deoxyribonucleic Acid
EDS	Energy Dispersive Spectroscopy
fps	Frames per second
FTIR	Fourier Transform Infrared Spectroscopy
I 1,2	Intersection 1, 2
IBU	Ibuprofen
INESC-MN	Instituto de Engenharia de Sistemas e Computadores para os Microssistemas e as Nanotecnologias
IPA	Isopropyl alcohol
JEV	Japanese Encephalitis Vaccine
LbL	Layer-by-layer
MAA	Methacrylic acid
MilliQ	Ultrapure water
NaOH	Sodium hydroxide
Out	Outlet channel
O/W	Oil in water
PAA-Na	Polyacrylic acid sodium salt
PAH	Poly(allylamine hydrochloride)
PBS	Phosphate-buffered saline
PDADMAC	Poly(diallyldimethylammonium chloride)
PDMS	Polydimethylsiloxane
PEEK	Polyether ether ketone
PEG-b-PMAA	Diblock poly(methacrylic acid) and poly(ethylene glycol)
PGMEA	Propylene glycol monomethyl ether acetate
PMMA	Polymethyl methacrylate
PSS	Polystyrene sulfonate
PVA	Poly(vinyl alcohol)
PVP	Polyvinylpyrrolidone

RT	Room temperature
SBF	Simulated Body Fluid
SDS	Sodium Dodecyl Sulfate
SEM	Scanning Electron Microscope
Si	Silicon
TEM	Transmission Electron Microscopy
UV	Ultraviolet
UV-Vis	Ultraviolet-visible
$V_{W,A,B,C,D,E,F,G,I,J,K}$	Volume of Water or respective solutions
W/O, W/O/W	Water in oil, water in oil in water
w/w, v/v, w/v	Weight or volume per total weight or volume of solution
WCA, DWCA	Water contact angle, Dynamic WCA
XRD	X-Ray Diffraction

Symbols

$CaCO_3$	Calcium carbonate
Mg^{2+}	Magnesium ion
pH	Potential of hydrogen
CO_2	Carbon dioxide
O_2	Oxigen
º	Degree
m	Meter (SI) - cm, mm, µm
G	Gauge
L	Liter (SI) - mL, µL
M_w	Molecular weight
g	Gram
mol	Mol
HCl	Hydrochloric acid
H_2O_2	Hydrogen peroxide
H_2SO_4	Sulfuric acid
NaOH	Sodium hydroxide
ρ	Density
H_2O	Water
η	Viscosity
cP	Centipoise
@	At
ºC	Degree Celsius
$CaCl_2.2H_2O$	Calcium chloride dihydrate
Na_2CO_3	Sodium carbonate
$MgCl_2.6H_2O$	Magnesium chloride hexahydrate
h	Hour
', min	Minutes
M	Molar
rpm	Revolutions per minute
'', s, sec	Seconds
Hz	Hertz
N^1	Newton
λ	Wavelength
Å	Angström
V	Volts
A	Ampere
-OH	Hydroxyl group
-COOH	Carboxilic Acid group
$-CH_3$	Methyl group
$-CH_2$	Methylene group
rms	Roughness mean square
Ca	Calcium (element)
Ca^{2+}	Calcium ion
[X]	Concentration of X
$Q_{c,d}$	Flow rate of continuous or disperse phase

Table of Contents

List of Figures

List of Tables

Objectives

One of the aims of this work is to develop a microfluidic device to produce monodisperse droplets directed to encapsulation. The development of such advanced system will allow the homogenous production of W/O/W emulsion, for future application in multifunctional particles for biomolecules encapsulation. For this type of emulsion, a selective microchannel surface modification is required. So, the first challenge is to achieve a stable wet chemical modification, and then apply it to closed microchannels.

Regarding encapsulation, this work takes biomimetic mineralization as inspiration to construct $CaCO_3$ microcapsules. The influence of Mg^{2+} and organic matrices, namely PVA, PAA-Na and PVP, will be accessed. Finally, after carrying a continuous process of biomimetic mineralization the stabilization of these capsules in dry environment will be evaluated.

1 Introduction

1.1. Biomimetics and Biomineralization

Nature presents uncountable examples of living organisms and structural materials with superior properties, which inspire the development of new advanced materials, devices and processes. This approach, known as biomimetics, is not new. Along with the development of micro and nanotechnology came the possibility to study the microstructure of the materials in natural organisms and to mimic these to develop new improved materials. [1] Some current popular examples of biomimetics include the lotus flower effect for water repellence, the gecko feet structure for high adhesion tape, insect eyes and wings microstructure for antireflective surfaces and sea shells and pearls for high mechanical strength composites and protective capsules. [1]
Taking sea shells and pearls as examples, their formation either through biological or biomimetic controlled processes is referred to as biomineralization. This is a self–assembly process by which these living organisms produce mineralized hard tissues under physiological conditions. [2]

1.1.1. Mimicking Shells and Pearls: Calcium Carbonate

There is a variety of natural mineralized structures, like teeth and bone (composed of calcium phosphate minerals), sea shells, pearls and egg shells (composed of calcium carbonate), and others. [3] These mineralized structures are a ceramic–organic assembly that have calcium as common element and a complex multi-organic component that act as a glue. This last controls the size of minerals, their structure and morphology. [3] [4]
In particular, calcium carbonate appears in six different polymorphs, of which three are hydrated forms (calcium carbonate monohydrate, calcium carbonate hexahydrate and amorphous calcium carbonate) and three are anhydrous polymorphs (calcite, aragonite and vaterite in **Figure 1.1**).

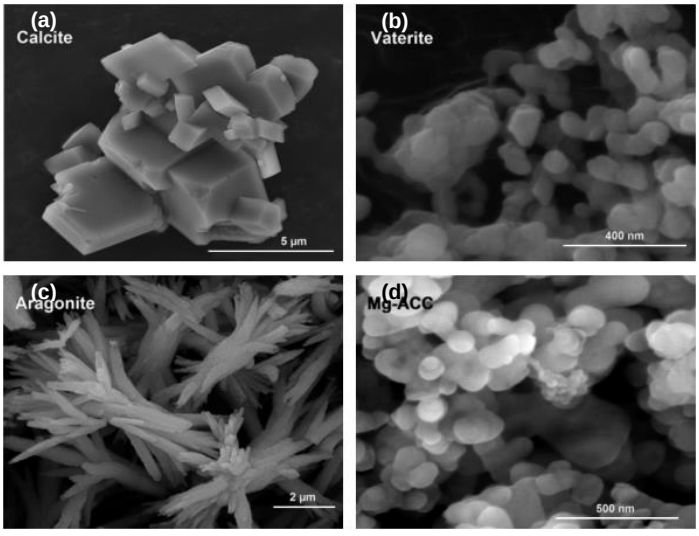

Figure 1.1. SEM images of $CaCO_3$ anhydrous polymorphs: (a) calcite; (b) vaterite; (c) aragonite; (d) magnesium-doped amorphous calcium carbonate. [5]

Regarding the regulating organic component in sea shells, there is a range of biopolymers involved, like acidic proteins with carboxyl groups, collagen, keratin, chitin and also silk fibroins. [6] [7] However, the function concerning each organic matrix, the cooperative role between them and the conjoin influence of the system specific parameters - like the concentrations of precipitants, presence of promoting or inhibitor ions as Mg^{2+}, pH and temperature - remains unclear. [4] [8]

Inspired by natural biomineralization, researchers have been using biomimetic methods (**Figure 1.2**) for mineral synthesis. Using additives to mimic the organic matrix role, various types of crystal morphologies and sizes were synthesized. An extensive review can be found in reference [9]. Additives used include surfactants as SDS, synthetic polymers as PEG-b-PMAA, biomolecules as cellulose and proteins as DNA and BSA. The function of these additives is to interact with calcium ions, triggering $CaCO_3$ heterogeneous (site specific) nucleation and subsequent growth into nano or microparticles. [3] [4]

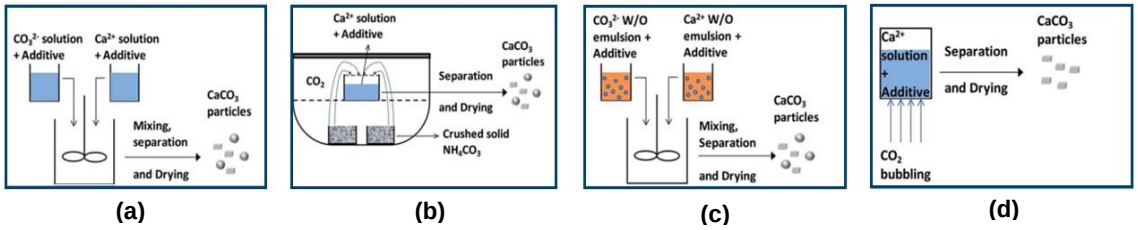

Figure 1.2. $CaCO_3$ synthesis methods: (a) precipitation, (b) slow carbonation, (c) reverse (W/O) emulsion and (d) CO_2 bubbling method. The biomimetic method is represented by (a), (b) and (c). [9]

1.1.2. State of the Art Applications

Nowadays calcium carbonate is used as paper, plastic and paint additive to reinforce mechanical properties; in biomedical and pharmaceuticals for bone regeneration and drug delivery, and for biosensors used in food industry and environmental analysis. [7] [9]

In the biomedical field, particularly referring to the encapsulation for drug delivery, typically soft materials as polymers are used. However inorganic based capsules have been attracting attention due to their biodegradability, biocompatibility, simple preparation, low-cost procedures under mild conditions and simple triggering mechanisms by pH or mechanical force. [10]

Calcium-based minerals as $CaCO_3$ and CaP are used to produce hollow shell-like capsules or compact particles (beads) to encapsulate bioactive molecules using emulsion methods. [2]

$CaCO_3$ capsules were already produced with O/W emulsion using MAA polymer to trigger mineralization and PVP in ionic solution to grow a thick shell [11]. Other methods include using pristine commercial $CaCO_3$ particles with posterior mineralization by CO_2 bubbling method [10] or ionic solution [12] without the aid of polymers. These methods allow the encapsulation of hydrophobic substances as limonene [10]. To encapsulate hydrophilic biomolecules W/O/W double emulsions are employed [13], as in the synthesis of hydroxyapatite-graft-poly(D,L-lactide) capsules with mineralization carried in SBF [14].

As for compact mineral particles, those are used mainly as sacrificial templates to assemble polymeric capsules and to improve drug loading, as in BSA mineralization [15] or IBU loading on previously prepared $CaCO_3$ particles [16]. But mineral particles are also used to directly protect biomolecules as JEV, Ad 5 and yeast [3]. A detailed review can be found in [3] and [17].

Constructing biocompatible capsules offers protection to biomolecules against environmental degradation, allows a controlled release and reduces the risk of unwanted immune response. Traditional methods of encapsulation as spray and freeze-drying, crystallization, encapsulation into liposomes or polymeric particles, do not produce equal particles, which will result in heterogeneous properties. Besides that, encapsulated biomolecules are often exposed to high temperatures, gas–water interface or organic solvents, surfactants, and reactive cross-linking agents (Appendix 1). These factors can turn biomolecules unviable, for example in case of proteins it can lead to their denaturation.

So, the main challenge here is to control the properties of produced capsules, through homogenous production, regarding size, shape, morphology and biomolecule content, preserving the properties of encapsulated biomolecules during the process. [17]

One way to get that particle control and safe biomolecule manipulation is through microfluidics.

1.2. Microfluidics

Microfluidics is the science and technology of systems that manipulate small amounts of fluids in channels with dimensions of tens to hundreds of micrometers. These systems are generally characterized by a low Reynolds number, which makes all fluid flows essentially laminar. [18]

The need of such field, was born from the necessity to carry out separations and detections with high resolution and sensitivity. Advantages of these systems include the use of very small quantities of fluids (sample and reagents) for fast and low-cost medical and environmental analysis, in a very precise environment (pH, ionic strength, concentration, etc.). [19]

1.2.1. Droplet Microfluidics

Manipulation of multiphase flows is one strength of microfluidic systems. If immiscible fluids are pumped into the device, it is possible to generate droplets with a discrete fluid dispersed in a second continuous phase fluid (**Figure 1.3 - a**). Then, through a number of operations, specifically transport, fusion, fission, mix and sort it is possible to manipulate the droplets (**Figure 1.3 – b to f**). [19]

These operations can be used to produce polymer particles, emulsions and foams to be applied as particles for therapeutic delivery, biomedical imaging, drug discovery, biomolecule synthesis, and diagnostics. The great advantage of these systems is the precise control to produce monodispersed droplets in size and shape which is of great importance for the above mentioned applications. [20] [21] [22]

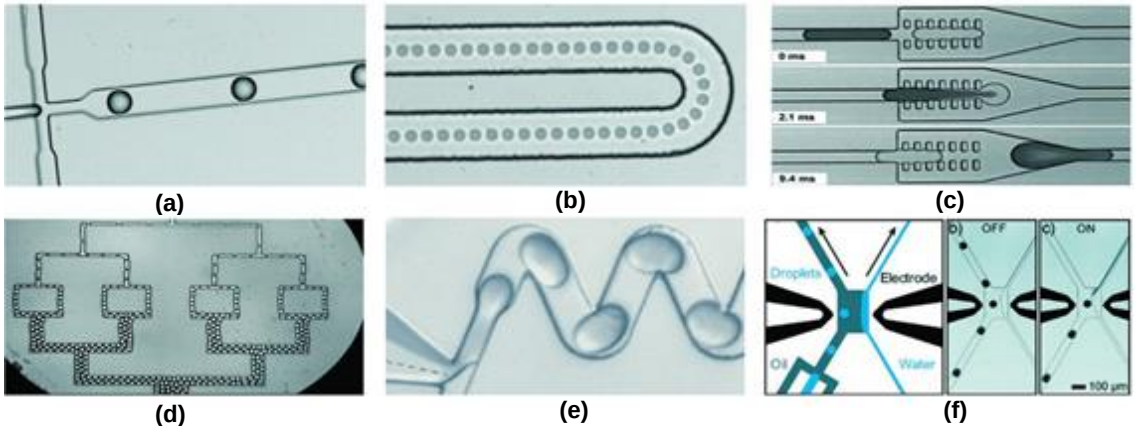

Figure 1.3. Droplet microfluidics operations: a) production; b) transport; b) fusion; d) fission; e) mix; f) sort. Adapted from [23] and [22].

1.2.2. Device Geometries, Materials and Surface Chemistry

Typical geometries of these microfluidic devices include T-junctions, co-flow and step emulsification devices, as represented in **Figure 1.4.** [20]

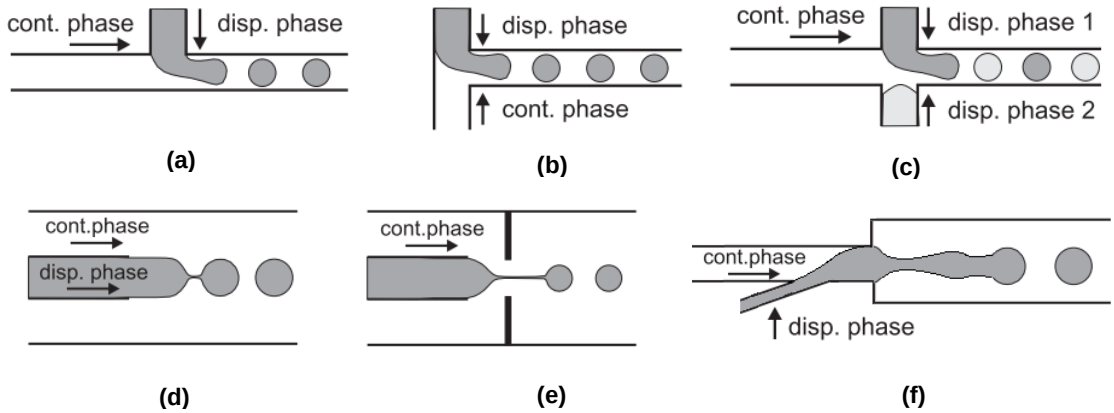

Figure 1.4 Device geometries for droplet production: (a) regular T-junction; (b) head-on T-junction; (c) T-junction for two species of droplets; (d) co-flow without flow-focusing; (e) co-flow with flow-focusing; (f) step-emulsification. Adapted from [20].

For the T-junctions, the design and demands to manufacture the device as well as fluids manipulation are simpler. However, for larger flexibility in generated droplets, co-flow devices must be chosen, even though these require more complex channel geometries and more fluidic inlets. [20]

Besides device geometry, to achieve a stable droplet production and also the type of emulsion desired, the wettability of the walls of the microchannels is crucial. This factor depends on the material's surface chemistry. Microfluidic devices are commonly made out of glass or silicon-glass, polymeric and metallic materials. [20] But for research purposes, it is important to minimize the technological and temporal effort using soft lithography techniques. This can be done with polymeric materials like PDMS, PMMA and PEEK, with the first being the most popular

due to its enhanced chemical resistance [24] and low fabrication cost when compared to others. [25] [26]

Concerning the type of emulsion possible, since PDMS is hydrophobic, water droplets in an oil continuous phase will be generated. The importance of PDMS surface chemical modification, is to manufacture devices capable to produce complex emulsions for multifunctional particles, and also prevent protein adsorption to channels' walls in biological applications.

For this purpose, a variety of protocols can be found in literature to render PDMS hydrophilic and produce oil droplets instead. Some examples include UV radiation and O_2 plasma treatments which can lower PDMS water contact angle from 105º to 27°. By these methods hydrophobic recovery is commonly achieved in few hours, even though it has been reported hydrophilic stability up to 15 days. [27] Other methods include chemical vapor deposition, metal and metal oxide coatings, but these are time consuming and expensive, requiring specialized equipment and facilities. [28]

To solve these issues, wet chemical approaches rises as promising candidates since these are simpler and can be applied in closed channels, as many times as needed. For this goal, acid [29] [30] [31] and basic solutions [32] were used to change PDMS functional groups, turning its surface hydrophilic. More complex chemical treatments to the walls of microchannels include sol–gel routes to deposit thin glass coatings [33] [34], polymeric grafting with PVP [35] or acrylic acid coatings [33], and layer-by-layer deposition of polyelectrolytes. For this latter case a positively charged polymer and a negatively charged one are required, as PAH/PSS. [18] [36] The main drawback of this last method is that PDMS has to be oxidized first, to introduce hydroxyl groups capable to bond with polyelectrolytes, and this is mainly done during bonding process by O_2 plasma, which is a clear disadvantage. [36]

Another issue is related to selective modification of microchannels, which with wet chemical approaches is achieved with flow confinement, controlling the flows of fluids only in certain channels. [33] [36] After that step, the microfluidic device should be capable of producing a double emulsion (**Figure 1.5**).

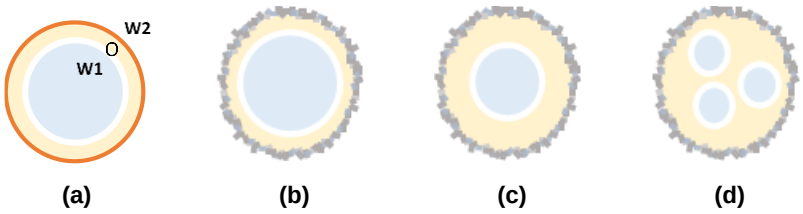

Figure 1.5. W1/O/W2 emulsion stabilized by (a) soft materials (polymers or surfactants represented by white and orange lines) or (b) solid particles; (c) and (d) represent possibilities of each phase with microfluidic devices by controlling the flow of fluids.

In this work, a microfluidic system is designed, constructed and tested in terms of selectivity to fluids of emulsion for droplet production. However some challenges have to be overpassed, related to the wet chemical modification applied, to the selective functionalization of microfluidic channels, the emulsion compatibility with microfluidic device material and the stability of produced mineral capsules.

.

2 Experimental Section

2.1. Materials

Glass and silicon substrates (5 × 5 cm^2, 0.7 mm thick, International Wafer Service), needles (21G 26G and 28G, Itec), 1 ml and 5 ml syringes (Injekt-F, BBraun), teflon tubes, MilliQ purified by E-POD (Elix).

SU-8 (Micro-Chem), PGMEA (M_w = 132.16 g/mol, assay > 99.5% Sigma-Aldrich), PDMS (Sylgard 184 Silicone Elastomer Kit, Dow Corning), IPA (M_w = 67-63 g/mol, assay ≥ 99.5 %, Fisher Scientific), HCl 37% (M_w = 36.461 g/mol, Carlo Erba Reagents), H_2O_2 35% (M_w = 34.01 g/mol, Valente e Ribeiro), H_2SO_4 (M_w = 98.08 g/mol, assay = 95-97%, Sigma-Aldrich), NaOH pellets (M_w = 40 g/mol, ρ = 1.99 g/mL, Eka), PVP (M_w = 1300 000 g/mol, Sigma-Aldrich), PDADMAC solution 20% in H_2O (M_w = 100 000-200 000 g/mol, ρ = 1.04 g/mL, η = 60-180 cP @ 25 °C, Sigma-Aldrich), PSS (M_w = 70 000 g/mol, ρ = 0.801 g/mL @ 25 °C, Sigma-Aldrich), $CaCl_2.2H_2O$ (M_w = 147.01 g/mol, assay > 99.0%, Sigma-Aldrich), Na_2CO_3 (M_w = 105.99 g/mol, assay ≥ 99.5%, Sigma-Aldrich), $MgCl_2.6H_2O$ (Mw = 203.3 g/mol, assay > 99%, Roth), PVA (M_w = 95000 g/mol, 95% hydrolyzed, Acros Organics), PAA-Na (M_w = 5100 g/mol, ρ = 0.55 g/mL @ 25 °C, Sigma-Aldrich), PVP K15 (Mw = 6000 – 15000 g/mol, ρ = 0.6-0.7 g/mL @ 25 °C, ISP), oleic acid (M_w = 282.46 g/mol, assay = 97%, Fisher Scientific), commercial vegetable oil Alvolino used without further purification or treatment.

Current lab equipment included scale (Kern), oven (Memmert), magnetic stirrer (Agimatic-N, P-Selecta), centrifuge (1-13, Sigma), flow controllers (model KDS-100-CE, KdScientific), ultrasonic processor (UP400S, Hielscher-Ultrasound Technology) and disperser (Ultra-Turrax, IKA).

2.2. Methods

2.2.1. COMSOL Multiphase Fluids Simulations

COMSOL Multiphysics® Software (version 4.4v, https://www.comsol.com) was used to simulate droplet production capability of microfluidic devices with different geometries and wetting wall conditions. The protocol followed for simulation can be found in http://altsoft.co.kr/wp-content/uploads/2014/02/COMSOL_V4.4_heat.pdf (pages 28-48). Simulations were carried with default water and vegetable oil applying mass conservation. Time-dependent studies were carried from 0 to 0.160 s with 0.002 s step. More details of input data along with results in Appendix 2.

2.2.2. Development of Microfluidic Device for W/O/W Emulsion

2.2.2.1. Microfluidic Device Assembly

Based on results from simulations carried on COMSOL and on devices reported in literature [37] [36], two microfluidic devices were designed with AutoCAD 2015 (Appendix 3 - Figure A3.1.).

The optimized protocol and the equipment for manufacturing the mask and the SU-8 mold using soft lithography methods, and the PDMS microfluidic device, were provided by INESC-MN (Illustrated Run Sheets in Appendix 4). A brief experimental description follows.

Mask was manufactured by coating a glass substrate with aluminum using Nordiko 7000, followed by patterning a deposited photoresist layer with Lasarray DWL 2.0 (Direct Write Laser system, Heidelberg). On a silicon substrate SU-8 was spin coated using WS-650MZ-23NPP/LITE spin-coater and patterned by contact UV lithography with previously fabricated mask. Three PMMA plates (10 × 10 cm^2, two with 2 mm one with 4 mm thick) were micro machined using TAIG Micro Mill (Super tech & Associates) controlled by a high frequency motor and the controlling software Mach2Mill CNC control program (ArtSoft Corporation, 2000-2004). With DesKAM2000 a certain function - contour, pocketing or drilling - was associated to each designed area in AutoCAD file (Appendix 3 - Figure A3.2)

For device fabrication, PDMS was prepared by mixing the base and the curing agent in 10:1 (w/w) ratio, which was then degassed and injected trough the top PMMA plate hole. A PDMS non-patterned layer was also prepared in a petri dish. Curing process was carried at 70ºC for 1h and 30 minutes in an oven. Microfluidic devices were assembled by bonding the two PDMS substrates (patterned and smooth) after corona discharge for 2 minutes per surface.

2.2.2.2. Post-Bonding Selective Channel Modification

Preliminary tests to evaluate surface modification were carried in PDMS substrates, prepared as previous mentioned on a smooth rectangular dish, and cut with 4 × 1 cm^2. Prior to chemical modification these were cleaned in ultrasound bath of IPA, at 30ºC for 30 minutes.

Different types of chemical solutions were tested namely acid, basic and polymeric. On the basis of the layer-by-layer method, a novel method was tested combining a first step of chemical oxidation with adsorption of polyelectrolytes. Details of prepared solutions and methods of chemical modification are in **Table 2.1**.

Table 2.1. Wet chemical modifications applied to PDMS substrates. For A), B), C) and F) at the end of modification substrates were rinsed in MillliQ water and dried at RT.

Wet Chemical Modification		Method	Based on Reference
A	H_2O:H_2O_2:HCl, 5:1:1 (v/v), 5’	Immersion	[31]
B	H_2O_2:H_2SO_4, 2:3 (v/v), 15’ Rinse in MilliQ 1M NaOH, 15’	Immersion	[29]
C	1M NaOH, 24h	Immersion	[32]
D	0.25% (w/v) PVP Thermal treatment at 110ºC for 10’	Drop Casting	[35]
E	0.25% (w/v) PVP Thermal treatment at 110ºC for 10’ Cross-linking in UV 254 nm for 24h	Drop Casting	-
F	1M NaOH, 15’ 0.4% (w/v) PDADMAC, 15’ 0.4% (w/v) PSS, 15’	Immersion (LbL)	[36]

A more detailed study was conducted for modification **F** (**Table 2.1**). The influence of several parameters was evaluated, in particular NaOH solution concentration (1, 3, 6, 10 M) and time of immersion (5 and 15 minutes), time of immersion in each polyelectrolyte solution (5 and 15 minutes) and number of bilayers adsorbed (1 to 3). To study duration capabilities of the modification, hydrophilic character of substrates was evaluated in three distinct times. In this case immediately after modification, after 8h immersion in MilliQ (with 100 rpm agitation) and also following 5 days storage in air.

For hydrophilic outlet channel modification, the setup in Appendix 5 was used. This included flow controllers, syringes, tubes, and needles. As a blocking solution water or oil were used and as wet chemical treatment modification **F** (**Table 2.1**) was applied, with 1 or 3 polyelectrolyte bilayers.

2.2.3. Mineralization Applied to Emulsions: $CaCO_3$ Capsules

2.2.3.1. Mineralization of $CaCO_3$

To study the influence of mixing speed and time of reaction in $CaCO_3$ crystal size, a modified protocol of [16] for synthesizing $CaCO_3$ microparticles was used. Aqueous solutions of 0.5 M $CaCl_2.2H_2O$ (A) and Na_2CO_3 (B) were prepared. Equal volumes of A and B were rapidly mixed, with solution B added to solution A. The reaction took place for mixing speeds of 300 and 1200 rpm, during 30 minutes and 2h.

To study the influence of magnesium in $CaCO_3$ synthesis, aqueous solutions of 1, 2 and 4 M $MgCl_2.6H_2O$ (C) were prepared and added to solution A in equal volume. Solution B was added as before, with equal volume to total volume of solution A and C together. This time, a mixing speed of 1200 rpm was used for a 2h reaction.

After precipitation reaction, $CaCO_3$ minerals were triple centrifuged and washed at 10000 rpm for 2 minutes, and finally dried at RT.

2.2.3.2. Simple Emulsions

With the future goal of a double W/O/W emulsion, simple emulsions were studied to evaluate how to stabilize W/O and O/W interface, through mineralization, adding polymers or both. To try stabilization by $CaCO_3$ minerals, both pre-synthesized and *in-situ* precipitated crystals were used.

For first case, protocol similar to [10] was followed (volumes and mass fractions were maintained). Briefly 0.2 g of $CaCO_3$ pre-synthesized particles were dispersed in 4 ml of MilliQ. A volume of 0.4 ml of vegetable oil was added and the mixture was sonicated with cycle value of 1 and amplitude of 100% for 1 minute.

For emulsions with polymers and *in-situ* precipitation of $CaCO_3$, the ratio between two phases was maintained at 1:10 (v/v) for W/O and O/W.

As water phase, solutions in **Table 2.2** were prepared and used with volumes indicated.

Table 2.2. Prepared solutions for emulsions, volume ratios and identification.

Solution ID	Aqueous solution of	Volumes	Emulsion ID
A	1% (w/v) PVA	$V_W = V_A$	**1**
B	1% (w/v) PAA-Na	$V_W = V_B$	**2**
C	1% (w/v) PVA in 0.5 M $CaCl_2.2H_2O$	$V_W = V_C + V_D$	**3**
D	1% (w/v) PVA in 0.5 M Na_2CO_3	$V_C = V_D$	
E	1% (w/v) PAA-Na in 0.5 M $CaCl_2.2H_2O$	$V_W = V_E + V_F$	**4**
F	1% (w/v) PAA-Na in 0.5 M Na_2CO_3	$V_E = V_F$	
G	0.5 M $CaCl_2.2H_2O$	$V_W = V_G + V_H$	**5**
H	0.5 M Na_2CO_3	$V_G = V_H$	
I, J, K	1, 2 and 4 M of $MgCl_2.6H_2O$	$V_W = V_G + V_{I,J,K} + V_H$ $V_G + V_{I,J,K} = V_H$ $V_G = V_{I,J,K}$	**6, 7,8**

Because of immediate precipitation reaction between calcium containing solutions and carbonate containing solutions, for cases where salts were involved, $CaCl_2.2H_2O$ aqueous solution was added first to glass, followed by oil volume fraction and in last place Na_2CO_3 aqueous solution. The mixtures were rapidly sonicated with same parameters as before. The tip of sonicator was washed with acetone between samples preparation.

For emulsion **5**, **6**, **7**, **8**, since these were respective to main goal of producing mineral capsules with diameter similar to that of microfluidic outlet channel, Turrax was used with 3000 rpm for 1 minute, to obtain larger particles.

2.2.3.3. Continuous Mineralization

Emulsion stabilized by $CaCO_3$ particles (**Table 2.2 - 5**) was subjected to a posterior crystallization process, based on protocol in [11] and [14]. Emulsion **5** was incubated in a 0.1% (v/v) ratio in different solutions. Incubation was carried for 3 days with reposition of aqueous medium every 24h as indicated in **Table 2.3**.

Table 2.3. Mineralization aqueous solutions.

	Ionic Solutions		**0.5% (w/v) PVP in B**	
ID	**A**	**B**	**C**	**D**
	10 × PBS	2.5mM $CaCl_2.2H_2O$ 2.5mM Na_2CO_3	High M_w “PVP 1300”	Low M_w PVP K15
Refreshed with	A	B	B	B

Stabilization in air was evaluated by placing a droplet of sample in a microscope slide, and letting water evaporate at RT.

2.3. Characterization

2.3.1. Profilometer

Using Alpha Step 200 profiler (Tencor Instruments, INESC-MN) six height measures were taken of SU-8 mold in the 6 inlets available. SU-8 height result is presented as mean value with standard deviation.

2.3.2. WCA

For preliminary tests WCA was registered with a Casio EX-F1 Exilim Pro using the setup described in [38]. Photographs were taken after 30 seconds of placing a 5 µl droplet in the PDMS substrate. The photograph was converted to grayscale and contrast was enhanced using Adobe Photoshop Elements 8.0. Images were analyzed with Image J (version 1.48v, http://imagej.nih.gov/ij/)) software using Drop Analysis- DropSnake plugin, which allows an active contour to shape the drop. In this study, 12 to 16 dots per droplet were used, 6 droplets per substrate were dispensed and photographed, and each image was measured 6 times. WCA results are presented as mean value with standard deviation by propagation of uncertainty.
For modification **F** (**Table 2.1**), dynamic water contact angle measurements were performed using an OCA15 contact angle measuring instrument (DataPhysics Instruments GmbH, Filderstadt, Germany). Water microdrops (volume ≈ 5 µl) were generated with an electronic micrometric syringe and deposited on the sample surface. A film was recorded during 300 seconds at a rate of 2 fps, starting from the moment of the drop deposition. WCA was determined by fitting the shape of the drop to the Young-Laplace equation, which relates interfacial tension to drop shape. A total of six drops were dispensed and each drop was placed in a different region of the sample. The results correspond to the mean value with standard deviations. Image acquisition, analysis and contact angle determination were performed using the SCA15 v.4.3.12 and v.4.3.16 software (Dataphysics Instruments GmbH, Filderstadt, Germany). All measures were taken immediately after chemical modification and substrate drying at RT, except for substrates stored for 5 days in air.

2.3.3. UV-Vis spectroscopy

Oxidation effect and polyelectrolyte film growth was monitored in T90+ UV/VIS Spectrometer, PG Instruments Ltd, with UVWin software. Spectrums were acquired in 190-900 nm range, with an air baseline and an unmodified PDMS spectrum registered before different modifications.

2.3.4. FTIR

To elucidate about surface modification, FTIR was performed on a Thermo Nicolet 6700 spectrometer in ATR. The equipment was operated from 4500 to 525 cm^{-1} with a 2 cm^{-1} step. A baseline was made before analysis. Samples were allowed to completely dry before any measure.

2.3.5. AFM

To evaluate the effect of modification **F** (**Table 2.1**) on PDMS roughness and surface coverage, images of PDMS unmodified and modified surfaces were acquired using Asylum Research MFP-3D Standalone AFM system. This equipment was operated in alternate contact mode, using commercially available Si probes (Olympus AC160TS) with a resonant frequency of 300 kHz and a spring constant of 26.1 Nm^{-1} at 1 Hz scan rate. Areas of 10 x 10 μm^2 and 2 x 2 μm^2 were scanned and images plane fitted. 3D images were also generated.

2.3.6. Optical Microscopy

Optical microcopy for general monitoring was conducted with CETI microscope coupled with PC-Ocular Camera (Type 049002-VGA by Meade Instruments (Rhede, Germany), connected to a laptop for live recording using Window Movie Maker 12 software (http://windows.microsoft.com/pt-pt/windows-live/movie-maker). This setup was used to monitor microfluidic channels selective modification.

For studies on emulsions, images were acquired with Olympus Optical Microscope (U-TV0.5XC-3, Tokyo, Japan) coupled with the light source Olympus- KL2500 and using the micro-imaging software, Olympus Stream Basic. Emulsions were analyzed immediately after preparation and for a time where alterations were observed. Sample preparation required to place a small sample volume in a microscope slide, without coverslip in case of mineralized capsules.

2.3.7. XRD

Samples of $CaCO_3$ obtained by precipitation reaction with and without magnesium, were characterized by X-ray diffraction (X'PerPRO, PANalytical) with CuKα radiation (λ = 1.5418 Å) at 45 kV and 40 mA, with the linear detector X'Celerator. The diffraction pattern was collected in Bragg-Brentano configuration in 2θ ranging from 20° to 90° at a scanning rate of 0.0167º.

2.3.8. SEM-EDS

Images of synthesized $CaCO_3$ minerals and capsules were obtained using the scanning electron microscope of high resolution EOL JSM-7001F/Oxford 250/HKL INCA Energy, at Microlab-IST. A drop of the diluted sample was placed into the sample holder using a carbon tape. The solvent was left to evaporate at RT and a very thin layer of gold-palladium was deposited on top of the sample to enhance the detection.

2.3.9. TEM

Transmission electron microscopy images were obtained using a Hitachi H-8100 II with thermo ionic emission LaB6, at Microlab-IST. TEM analysis was performed in a little quantity of resuspended $CaCO_3$ capsules placed in a Kevlar 25 mesh grid after solvent drying.

3 Results and Discussion

3.1. COMSOL Simulations and Microfluidic Device Assembly

Results from simulation can be consulted in Appendix 2. Some main conclusions follows.

For water droplets production, a wetted wall condition had to be introduced in the simulation using a contact angle of 90º with walls (hydrophobic channels). If a smaller angle was chosen, the droplets slide through microchannels or appeared as plugs (elongated). To produce spherical droplets, water contact angle with the walls, as well as flow rates, have to be taken into account. With this information, it is possible to predict that to produce oil droplets instead, hydrophilic/lipophobic channels are required. Comparing between different geometries, it was easier to use flow-focusing device to produce spherical droplets, with channel after intersection with 45º walls and dimensions similar to droplet size (**Figure 3.1 - a**). Using protocols provided by INESC-MN, and considering microscope equipment available, it was possible to scale down dimensions in half compared to the ones used for simulation. **Figure 3.1** shows the process for development of the device from simulation to drawing and finally the assembly and test.

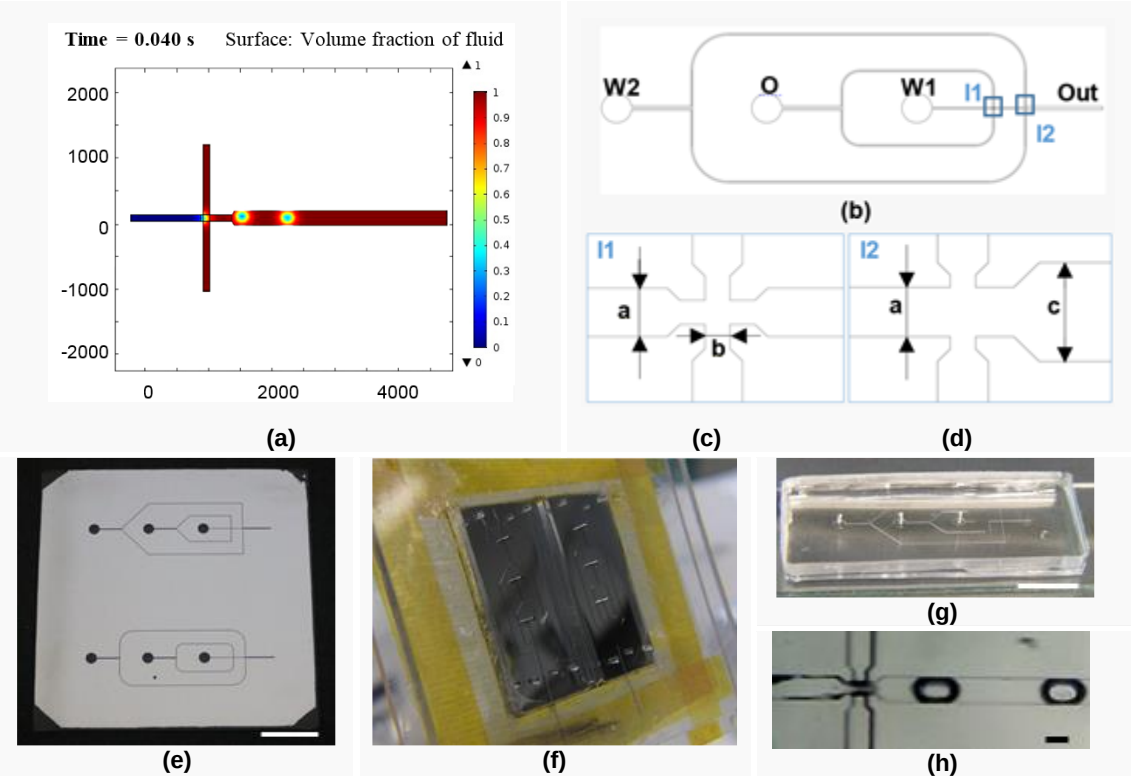

Figure 3.1. (a) Simulation of flow-focusing device of intersection 1 (**I1**) - More details in Appendix 2; (b) AutoCAD drawing of microfluidic device with round corners: inlets **W1, O, W2** named after fluid phase of required emulsion (Water 1, Oil, Water 2) and outlet named **Out;** (c) Magnification of first Intersection, **I1**, same width for equal channels; (d) Magnification of second intersection, **I2**. Channel width dimensions: a = 100 µm, b = 50 µm, c = 200 µm. More details of dimensions in Appendix 3; (e) Mask showing both geometries designed (scale bar = 1 cm); (f) Manufacture of PDMS devices: photograph showing SU-8 mold (**120.2 ± 6.9 µm height**) mounted between PMMA plates with outlet needles inserted before PDMS curing; (g) Microfluidic device after bonding (scale bar = 1 cm); (h) Water/Oil test on **I1**: only water droplets were produced (scale bar = 100 µm).

3.2. PDMS Surface Properties Characterization

3.2.1. Preliminary Studies on Modifying PDMS Surface

3.2.1.1. Water Contact Angle

For this work the outlet channel of the microfluidic device has to be hydrophilic. Thus a selective surface modification has to be found to be applied in closed channels. **Table 3.1** summarizes the chemical solutions tested and both measured and expected WCA. Images analyzed are in Appendix 6.

Table 3.1. WCA values obtained for PDMS with wet chemical modifications based on literature, with example of photographs analyzed (scale bar = 500 µm).

Wet Chemical Modification			WCA (°)		
			Measured		Literature Review
	Unmodified PDMS		-		105 [27], 109.28 [34]
Acid	A	H_2O:H_2O_2:HCl, 5:1:1 (v/v), 5'	106 ± 4	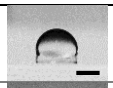	22.82 [34]
	B	H2O2:H2SO4, 2:3 (v/v), 15' 1M NaOH, 15'	100± 4	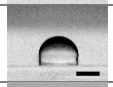	90-100 [30], 27 [29]
Basic	C	1M NaOH, 24h	96 ± 5	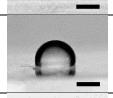	106 [32]
Polymeric	D	0.25% (w/v) PVP	87 ± 4	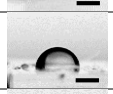	-
	E	0.25% (w/v) PVP UV 254 nm, 24h	69 ± 4	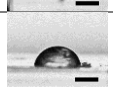	56 [39]
	F	1M NaOH, 15' 0.4% (w/v) PDADMAC, 15' 0.4% (w/v) PSS, 15'	**81 ± 4**	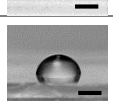	Hydrophilic Based in [36]

- *Acid solutions*

During modification **A** and **B**, air bubbles formed by reactants interfered in a way PDMS was little or nothing affected, so WCA remained unchanged. This modification couldn't be selectively applied to microchannels because air bubbles destabilized the fluids flows (**Figure 3.2**).

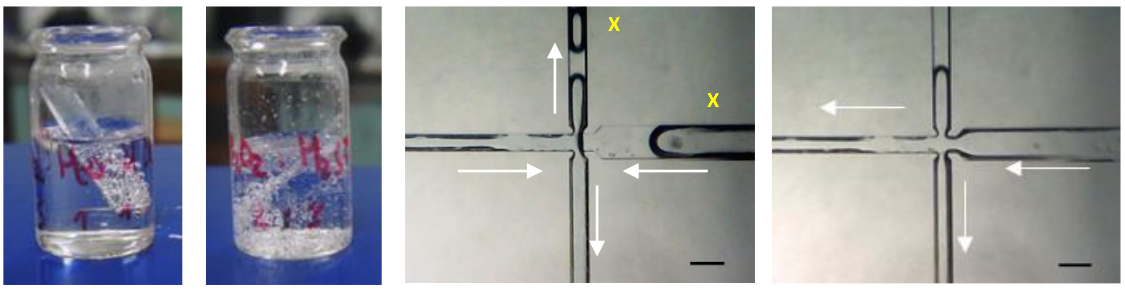

(a) **(b)** **(c)** **(d)**

Figure 3.2. Immersion of PDMS substrates in acid solutions: (a) **A** and (b) **B**. Both acid modifications form air bubbles from H_2O_2 decomposition; Modification **A** was applied into micro channels: (c) air bubble (yellow cross) was injected in microfluidic channels through outlet against water (blue); (d) air blocks upper channel and HCl solution advances to left channel. White arrows show fluids' direction. It can be seen hydrophobic nature of PDMS by dark lines of water-based fluids against the walls. Scale bar = 200 µm.

- *Basic solutions*

In modification **C,** oxidation was expected and WCA obtained is similar to the reported value in literature, with PDMS maintaining its hydrophobicity. This seems contradictory. Further FTIR and AFM analysis may help to clarify this issue.

- *Polymeric solutions*

PDMS does not have functional groups to attract non-ionic PVP, so drop casting was chosen to deposit a thin PVP film followed by temperature treatment at 110ºC for PVP grafting (**Figure 3.3 - a**). In **Figure 3.3 - b and c**, comparing modification **D** and **E**, one can see that cross-linking prevented PVP dissolution. This is the reason that explains a higher WCA comparing **D** to **E** recipe, with WCA value between the one of PVP film (68°) and PDMS. With PDMS absorbing for wavelengths lower than 250 nm, it is impossible to use **E** recipe in closed channels. Besides that, in microfluidic device it is also impossible to control PVP solution flow when subjected to heat (**Figure 3.3 - d**), and so a controlled selective modification cannot be achieved.

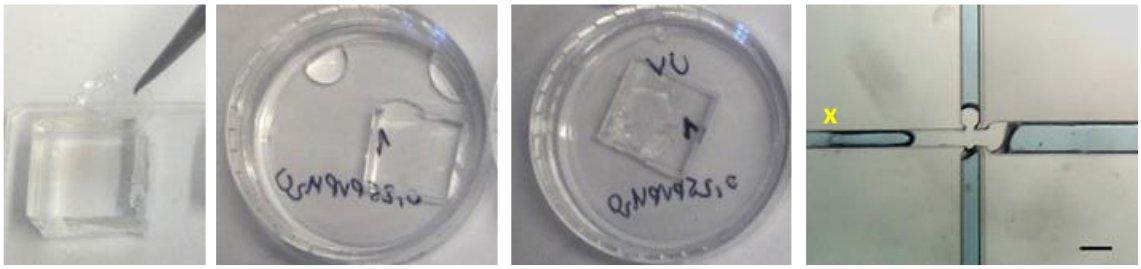

(a) **(b)** **(c)** **(d)**

Figure 3.3. (a) PVP film detaches from PDMS surface; (b) Modification **D** - when placed in water for few minutes PVP dissolves; (c) Modification **E** – PVP film swells if cross-linked in UV 254 nm for 24h; (d) PVP traveled for other channels during temperature process as shown by hydrophilic nature of wetting walls (yellow cross). Scale bar = 200 µm.

Since for oxidation in microfluidic device, with closed channels, only modification **C** is possible of being applied, in test **F** a new approach is proposed. This combines chemical oxidation stabilized with adsorption of oppositely charged polyelectrolytes. Results obtained for just 1 BL (a pair of adsorbed polyelectrolytes: PDADMAC and PSS) render PDMS hydrophilic.

3.2.2. Proposed Method for PDMS Selective Surface Modification

Based on previous results for modification **F** (**Table 3.1**), a deep study on the chemical oxidation of PDMS followed by surface modification with polyelectrolytes was performed.

3.2.2.1. Oxidation by NaOH

- *Dynamic Water Contact Angle*

It has been described the role of NaOH to oxidize the surface of PDMS. Common oxidation processes referred in **Introduction** are known to introduce –OH, –COH, –COOH hydrophilic groups by $–CH_3$ substitution. [40] This experiment was set to find a condition where PDMS turned hydrophilic in shorter time possible. It was verified that WCA could change in a dramatic way over time for some substrates, so a 5 minute video was recorded for one of the droplets**. Figure 3.4** shows DWCA results, summarized in **Table 3.2**.

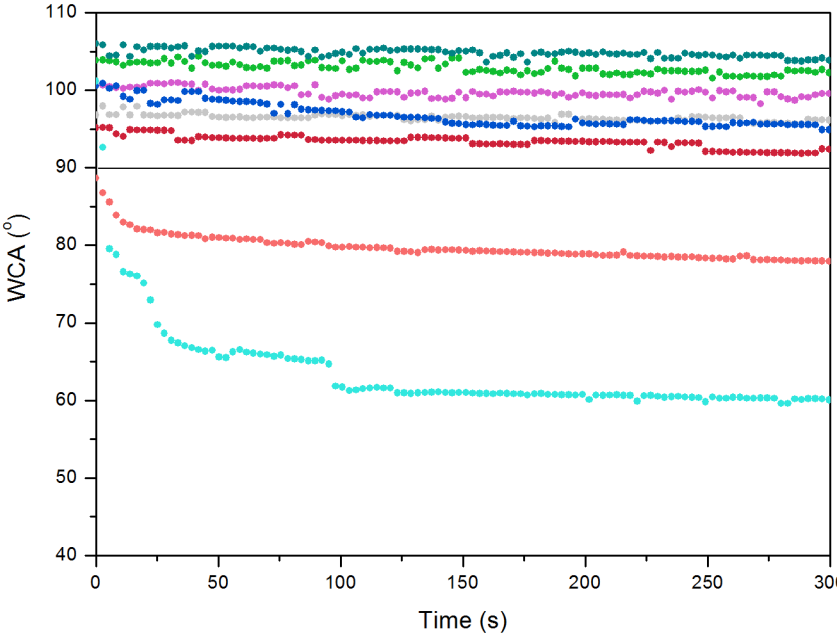

Table 3.2. Legend with correspondent values of initial WCA (°).

	WCA (°) t = 0 s
1M (5')	95 ± 6
3M (5')	97 ± 1
6M (5')	101 ± 2
10M (5')	100 ± 5
1M (15')	106 ± 4
3M (15')	100 ± 4
6M (15')	95 ± 3
10M (15')	94 ± 4

Figure 3.4. DWCA for one droplet on PDMS chemically oxidized with NaOH; 90º line in black. Oxidation treatment indicated as follows: Concentration of NaOH solution in Molar (time of immersion in minutes).

It can be assumed that deviation for results in **Figure 3.4** are the same registered for initial time (t = 0 s). No correlation of WCA is observed between NaOH concentration and time of immersion. Also, WCA results for time zero and for when the angle became stable don't always match (see sample 10M (5') vs. 10M (15')). A reason for all of that may be the dissolution of non-cross-linked chains of PDMS in such oxidizing solutions, which creates heterogeneity in surface modification. Associated to this, low molecular weight PDMS chains can migrate from the substrate to surface which decreases the available hydrophilic polar groups. [27] A less plausible reason is hydrophobic recovery, which is a phenomenon vastly reported in literature. This process refers to recombination of newly introduced –OH groups and reversal of hydrophilic PDMS to hydrophobic in few hours. [27] However, WCA analysis was conducted immediately after substrate drying, which took only a few minutes, and therefore that hypothesis is not probable.

For the application required it is more significant to analyze transient PDMS behavior, which refers to analyzing WCA when stable. In that case it was possible to render PDMS surface hydrophilic with 10M NaOH immersion for 5 or 15 minutes. Even though it could be expected that a prolonged immersion time resulted in a lower WCA, that didn't happen. WCA results for these samples may be explained by the possible breakage of PDMS chains resulting in increased surface roughness. There must be a competing event between oxidation and surface roughness, the first contributing to lower WCA and the second to increase it. If this is true, it explains that a more hydrophilic substrate was obtained for immersion in 10M NaOH only for 5 minutes instead of 15, since a prolonged time in such concentrated solution may have increased a lot the roughness. As for other modifications, it cannot be concluded that they didn't oxidize PDMS surface, however PDMS remained hydrophobic. FTIR and AFM analysis should help clarifying these questions.

3.2.2.2. Oxidation Followed by LbL of Polyelectrolytes

- *UV-Vis Spectroscopy*

UV-Vis spectroscopy of samples was used to set best conditions for hydrophilic PDMS modification, keeping its optical properties (transparency) unchanged as possible. This was monitored by absorbance increase in PDMS samples when modified with NaOH and deposition of polyelectrolytes for 1, 2, or 3 BL, which is possible since PSS has a maximum absorbance at 224 nm. [41] The results are in **Figure 3.5**. Note that 1BL means an adsorbed pair of a positive (PDADMAC) and negative (PSS) polyelectrolyte.

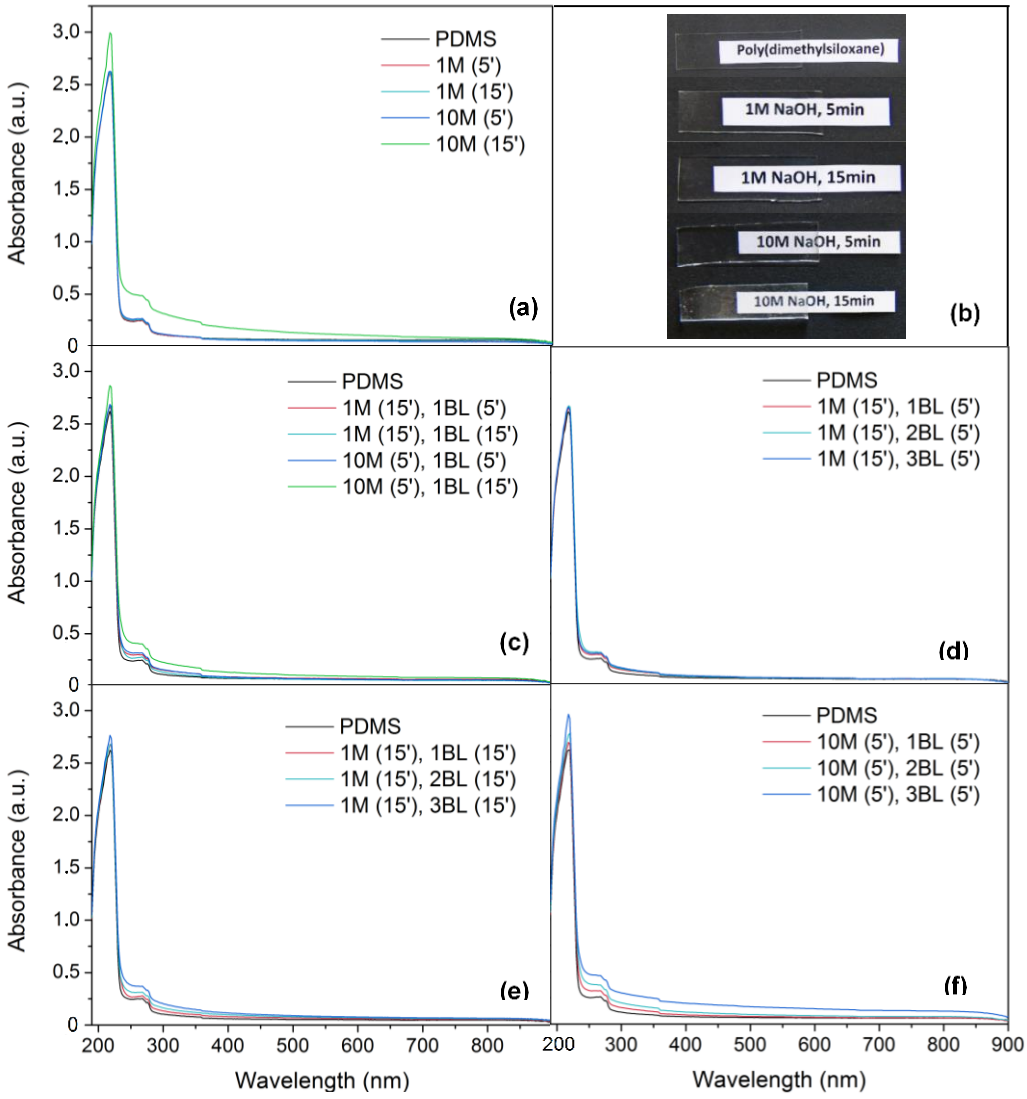

Figure 3.5. (a, c, d, e, f) UV-Vis spectra recorded in 190-900 nm range of modified PDMS substrates with thickness of 2.069 ± 0.027 mm. Respective modifications are indicated as follows: Concentration of NaOH solution in Molar (time of immersion in minutes), number of bilayers (time of immersion in minutes for each layer); (b) Photographs of PDMS 4 × 1 cm^2 substrates correspondent to spectrum in (a). Note whitish color for "10M NaOH, 15min" photograph.

From **Figure 3.5 - a and b** it can be seen that at extreme conditions - higher concentration and longer time of immersion, 10M (15') - PDMS substrate turns white, which excludes such modification to be carried. To select conditions for polyelectrolyte adsorption study, it was chosen as oxidation parameters immersion in less concentrated solution for longer time (1M NaOH for 15 minutes), and in higher concentrated solution for less time (10M NaOH for 5 minutes). The goal here was to verify if similar results could be obtained in shorter times using a concentrated NaOH solution.

As shown in **Figure 3.5 - c,** for 10M (5'), 1 BL (15') there's a greater increase in absorbance which eliminates that condition as a viable option for modification, since more layers need to be deposited, which would correspond to even higher absorbances.

For the remaining three hypothesis, 3 BL were deposited. It can be noted that increasing time of immersion leads to an increase in absorbance, related to the thickness of film adsorbed, as shown by **Figure 3.5 - d vs. e**. Also, using 10M NaOH solution even for short time, resulted in higher absorbances (**Figure 3.5 - f**), even when polyelectrolyte adsorption occurred for only 5 minutes. This means that thicker layer of polyelectrolyte was adsorbed. However this last substrate turned white, and this condition was eliminated. This sets as best conditions the immersion in 1M NaOH for 15 minutes, with polyelectrolyte adsorption for 5 or 15 minutes per layer. As for absorbance variation in general, which increases only slightly between bilayers, it was reported elsewhere a variation of less than 0.1 magnitude, similarly to this study. [41] It is noticeable in literature about this matter, that has been referred along this work, the use of polyelectrolyte solutions with salt (as NaCl).This factor lowers polymers solubility in water contributing for a thicker layer deposited (Appendix 7). This in turn results in less transparent PDMS and for this case was not considered.

- *Dynamic Water Contact Angle*

DWCA was measured for 1, 2 and 3 BL deposited for 5 or 15 minutes. Results are in **Figure 3.6.**

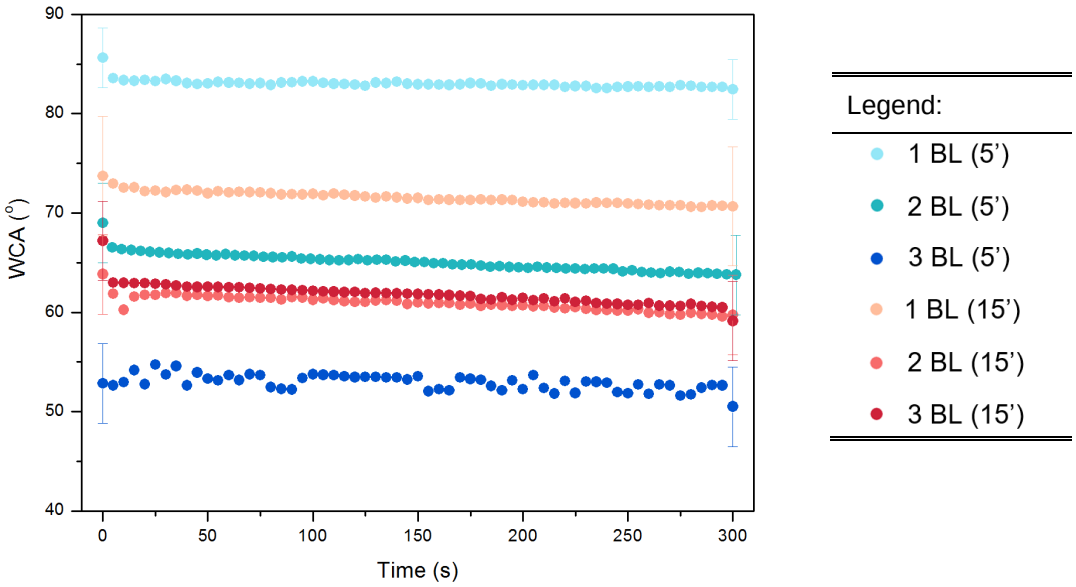

Figure 3.6. DWCA results for oxidation in 1M NaOH (15') followed by adsorption of 1, 2, 3 BL for 5' (blues) and 15' (reds). Respective modifications are indicated as follows: Number of bilayers (time of immersion in minutes for each layer). Detailed WCA values in Appendix 8.

It can generally be seen that increasing number of bilayers as well as time of immersion in polyelectrolytes, lowers WCA gradually, probably from a better surface coverage (**Figure 3.6**). For 3 BL deposition, stability of polyelectrolyte layers was evaluated in three conditions, namely measuring DWCA immediately after modification, after immersion in water for 8h and also for substrates stored 5 days in air (**Figure 3.7**).

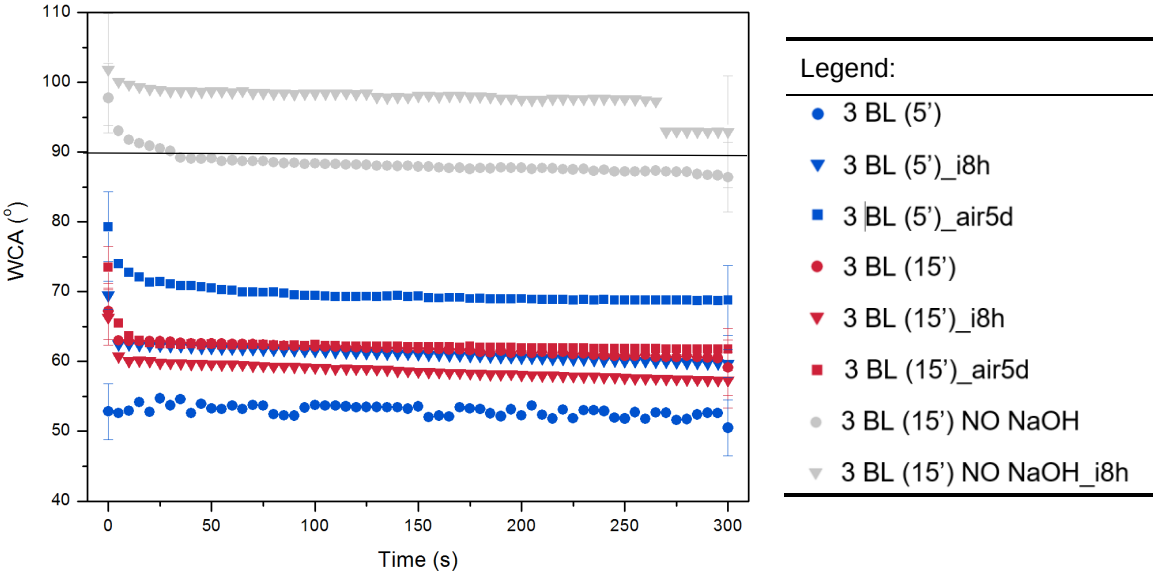

Figure 3.7. DWCA results for oxidation in 1M NaOH (15') followed by adsorption of 3BL for 5' (blue dots) and 15' (red dots), with 8h immersion (X = i8h: triangles) in MilliQ and air storage for 5 days (X = air5d: squares). Comparison with non-oxidized samples (NO NaOH). Respective modifications are indicated as follows: Number of bilayers (time of immersion in minutes for each layer)_X. 90º line in black. Detailed WCA values in Appendix 8.

As it is expected that polyelectrolytes are electrostatically bonded, immersion may wash only excess polymer. That condition was verified for 3 BL (15') when PDMS remained hydrophilic even after 8h immersion in water, with similar WCA (**Figure 3.7**: ●→ ▼). In the case of 3 BL (5') there was a greater increase in WCA for same situation (**Figure 3.7**: ●→ ▼). Once this sample had the lowest WCA immediately after modification, this can only mean that the final washing step of LbL method wasn't effectively done. This can be also confirmed by WCA pattern that shows more variations (**Figure 3.6**: ●). When substrates were stored in air for 5 days, WCA raised about 10º for 3 BL (5') (**Figure 3.7**: ▼→ ■) and 4º for 3 BL (15') (**Figure 3.7**: ▼→ ■). This may be due to complete water evaporation, which made polyelectrolyte layers more compact. In this case WCA could be influenced by underlying polyelectrolyte [42] or even PDMS surface if this last wasn't fully covered. Considering previous UV-Vis results, a greater absorbance was obtained for 3 BL (15') correlated to thicker polyelectrolyte layers. So, it makes sense a smaller WCA variation for this substrate. With future hydration it is expected that polymer chains swell and sulfonic acid groups of PSS dominate polar surface properties, with a resulting lower WCA. [42] Regarding the role of NaOH, it can be noted that when NaOH is not used, WCA drops only slightly from PDMS original value. This happens possibly from adhered polyelectrolytes that tend to be washed, with substrate turning hydrophobic. This indicates that NaOH has an important role in stabilizing

polyelectrolytes. In terms of WCA best results were obtained for 3 BL (15'), but for time efficiency condition 3 BL (5') could be equally satisfying.

- *FTIR*

To try to elucidate about chemical modification with NaOH solution, FTIR was performed to compare chemical oxidation in 1M solution for short time of immersion (15 minutes) and prolonged time (24h). Results are displayed in **Figure 3.8**.

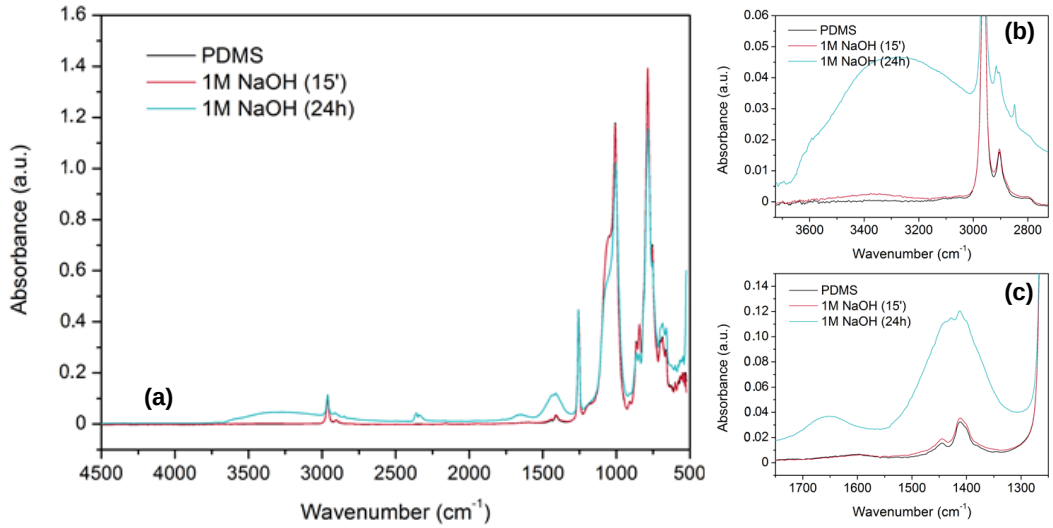

Figure 3.8. FTIR spectrum in 4500-500 cm^{-1} range for (a) unmodified PDMS (black), and oxidized PDMS with 1M NaOH (15') and for extreme time of 24h as in [32]; (b) Detail of 3750-2700 cm^{-1} region; (c) Detail of 1750-1250 cm^{-1} region. Near 2350 cm^{-1} there is the peak of CO_2 for 1M NaOH (24h) resultant from absence of a baseline subtraction before that sample analysis.

FTIR spectra shows PDMS characteristic bands at 2962, 2915, 2904 and 1256 cm^{-1} attributed to $Si–CH_3$, $Si(CH_3)_2–O–Si(CH_3)_2$ and $Si–CH_2$ stretching vibrations [27] [43]; at 1653 cm^{-1} and 1410 cm^{-1} from C=C of $Si–CH=CH_2$ (present in siloxane oligomer) stretching [43]; from 1000-1100 cm^{-1} and at 844 cm^{-1} due to Si–O–Si stretching [27][32]; at 910 cm^{-1} and 865 cm^{-1} the Si–OH stretching bands [27][32]; at 785 cm^{-1} from $–CH_3$ rocking [27] and at 760 cm^{-1} the Si–C stretching [32].

When PDMS is treated with NaOH same oxidation modification occur for different times, being more intense at 24h immersion. Oxidation can be seen by a new broad band between 3000-3670 cm^{-1} attributed to newly introduced Si–OH groups (stretching) [32][43], even for 15 minutes immersion (**Figure 3.8 - b**), and an increase of intensity of bands between 1750-1250 cm^{-1} (**Figure 3.8 - c**). In this last region, before modification it seems to exist only three bands and after 24h immersion more than three are seen, suggesting hidden bands from species other than $Si–CH=CH_2$. Increase of this band is attributed to O–H bending, from carboxylic acid (-COOH) or alcohol (–OH) groups, suggesting other type of oxidation of $–CH_3$ groups (**Figure 3.9**). This is supported by findings in published results in [40].

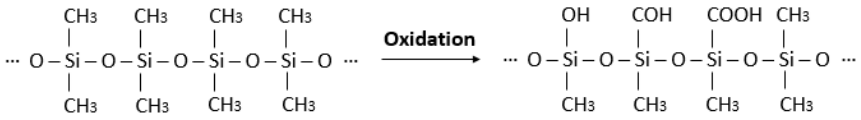

Figure 3.9. Schematic diagram showing the oxidation of PDMS by alcohol, ester or carboxylic acid groups. Based on [40].

Oxidation implies substitution of $–CH_3$ groups, but it is not obvious to quantitively evaluate bands related to these groups since they are in positions where others interfere. For example, it is easy to see a slight increase of 910 cm^{-1} band, but for 3000-3670 cm^{-1} region these bands may have been simply dislocated by Si–OH band. So it is not possible to relate increase of new oxidation groups with $–CH_3$ substituted groups.

- *AFM*

With FTIR confirming the presence of hydrophilic groups after NaOH immersion, and relating that with previous results of WCA (**Figure 3.4**), surface roughness was evaluated by AFM. This analysis was also used to confirm surface coverage with polyelectrolytes.

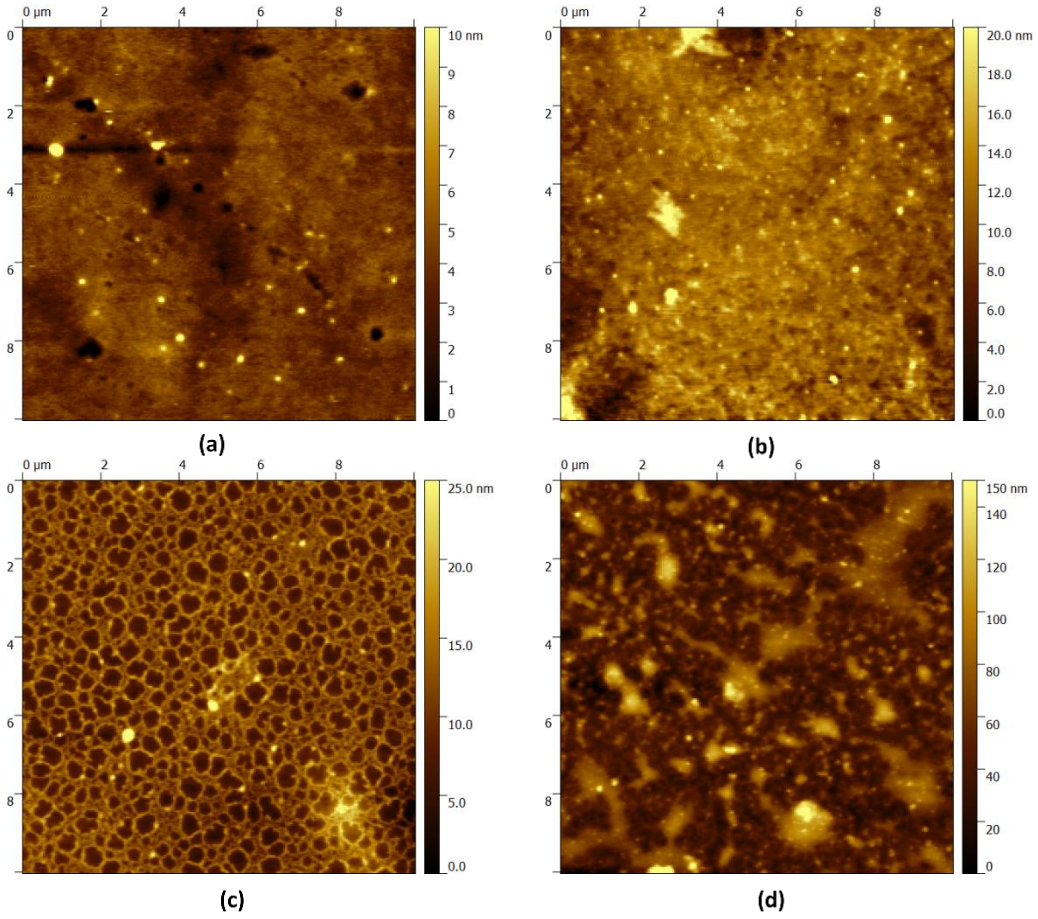

Figure 3.10. AFM 10 × 10 μm^2 topographic images of (a) unmodified PDMS, rms = 1.15 nm; (b) modified PDMS in 1M NaOH (15'), rms = 2.54 nm; (c) with 3 BL (5') deposition, rms =3.27 nm; (d) with 6 BL (5') deposition, rms= 20.4 nm. 3D images in Appendix 9.

PDMS is very smooth (**Figure 3.10 - a**) and roughness increases even for 15 minutes of oxidation in NaOH solution, being proportional to time in solution: rms of 2.54 nm or 22.6 nm if immersion occurs during 15 minutes or 24h. According to FTIR, oxidation is obvious for 24h of immersion, however from preliminary studies the substrate remained hydrophobic (**Table 3.1 - C**). For 15 minutes immersion WCA of PDMS also did not changed. In this situation it is clear that surface roughness is the predominant factor in determining surface properties.

However, when polyelectrolytes are adsorbed, even without total surface coverage (**Figure 3.10 - c vs. d**) WCA drops significantly and PDMS becomes hydrophilic. This is mainly due to the new chemical groups interaction with water, even with increased roughness. Rms values increase from 3.27 nm (3 BL) to 20.4 nm (6 BL), approaching a roughness similar to the surface treated with NaOH for 24h but substrates are hydrophilic. This confirms the success of this approach.

3.2.3. Microfluidic Device Selective Modification

The main attempts to turn the outlet channel of the microfluidic device selectively hydrophilic are in **Figure 3.11**. More in Appendix 10.

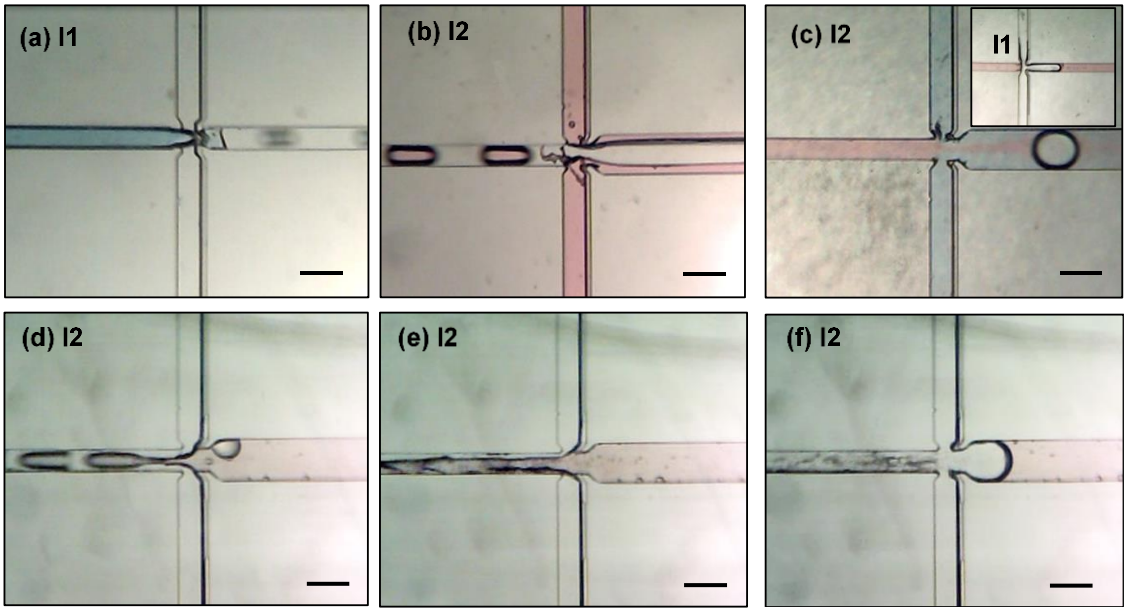

Figure 3.11. Microscope images of (a) hydrophobic unmodified microchannels: water droplets; (b) 1M (15'), 1 BL (15') injected in **W2** and MilliQ as blocking solution injected in **W1** and **O**: water droplets; (c) 1M (15'), 3 BL (15') injected in **Out** and MilliQ in **W1** and **O**: oil droplets; (d) Equal modification to (b) injected in **Out** but with oil as blocking solution injected in **W2**: produces droplets of the chemical solution; (e) Reaction between NaOH aqueous soution and oil stopped droplet production promoting chemical attack on left channel; (e) advancing oil contaminated outlet channel, limiting the modification. Water as colored liquid. Scale bar = 200 µm.

Figure 3.11 - b shows that the deposition of 1 BL seemed to be insufficient on turning the outlet channel hydrophilic. Due to difference in fluids viscosity or due to incomplete surface coverage by polyelectrolytes (incomplete modification) water can not involve oil. But with 3 BL deposition (**Figure 3.11 - c**) the outlet turned hydrophilic. However, channel between **I1** and **I2** that was

supposed to maintain its hydrophobicity for water droplets production, only kept water repellence property when 1 BL was deposited.

This raised the question that a prolonged time of flushing MilliQ (pH = 5.9) was turning PDMS hydrophilic. So, untreated water (pH = 7) and phosphate buffer (pH = 7) were used as blocking solutions to verify if it was the pH or ions the responsible factor for such modification. Results were inconclusive since for all the approaches the respective channel turned hydrophilic (Appendix 10)

Therefore, inert fluids are necessary to carry this modification. Hypothesis for that include oil and air. So, oil was tried, but it was extremely hard to control its flow (**Figure 3.11 - f**), and from the moment when it advanced to the outlet channel, it was impossible to eliminate its residues from the walls, limiting the chemical modification. This made this type of approach unsuccessful. Also some reaction between oil and NaOH occurred damaging the device. An attempt without NaOH was carried, but again it was unsuccessful because of uncontrollable oil flow (Appendix 10).

Recording all the modification process, allowed to find out the real reason why channel between **I1** and **I2** was turning hydrophilic. The blocking solution was supposed to protect that channel, keeping wet chemical solutions flowing through other channels. Video recorded images in **Figure 3.12** shows chemical solutions advancing to channel between **I1** and **I2**.

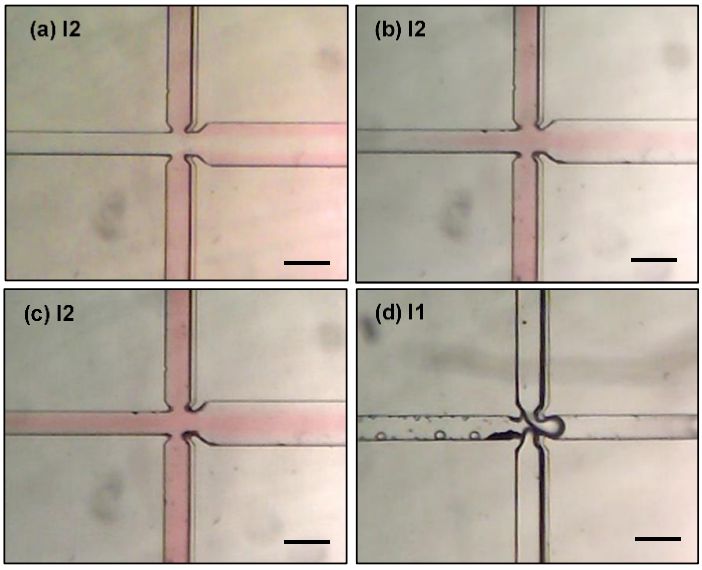

Figure 3.12. Without any vibration the fluids that are (a) controlled only on the **Out** (red) (b) start flowing to channel behind **I2**, (c) eventually filling that channel with chemical solution. This turns that channel also hydrophilic as seen in (d) and oil droplets form. Scale bar = 200 µm.

This situation was noticed to occur randomly, without any vibrations or disruptive events (for example, tubes oscillation or exchange between chemical solutions). The only reason found for this occurrence, was the step motor of the flow controller. The movement of this motor isn't continuous, and for multiphase fluids microfluidics it revealed very disadvantageous.

Ideally air could be pumped as blocking fluid, but that may only work with pressure controllers. With flow controller air is simply compressed and liquid chemical solutions advance for unwanted channels. Because of this equipment constraint, selective modification could not be performed.

3.3. Mineralization Applied to Emulsions: $CaCO_3$ Capsules

For these studies, a system compatible with PDMS had to be chosen for future processing in the device. Although PDMS is the best alternative in terms of chemical resistance as stated in **Introduction**, this material can't be used with organic solvents. This raises a problem since emulsion common processing methods use organic solvents (as DMAc, DMSO, etc.), to be further extracted. [44] So, the emulsion idea here is to create a mineral capsule surrounding an oil phase. That oil can't be evaporated, which can be seen as a disadvantage. However, this way also avoids using methods of solvents extraction (Appendix 1) that may damage or release biomolecules from internal water phase. So this oil layer can act as soft protective barrier to encapsulate hydrophilic molecules, with a surface favorable to mineralization.

3.3.1. Mineralization of $CaCO_3$

3.3.1.1. SEM-EDS

The synthesis protocol of $CaCO_3$ was performed according to results stated in reference [45]. First, it was studied the role of time and stirring speed in controlling crystal size. **Figure 3.13** shows that $CaCO_3$ crystals synthesized are rhombohedral in shape, and generally smaller with increasing time and mixing speed. This is due to a larger number of nuclei (heterogeneous nucleation) related to better salt intermixing. [17] Best condition regarding size was achieved with **Figure 3.13 - d** parameters, with smaller and similar sized crystals. In reference [17] sizes of 3-20 µm of crystals were obtained. Results are in accordance.

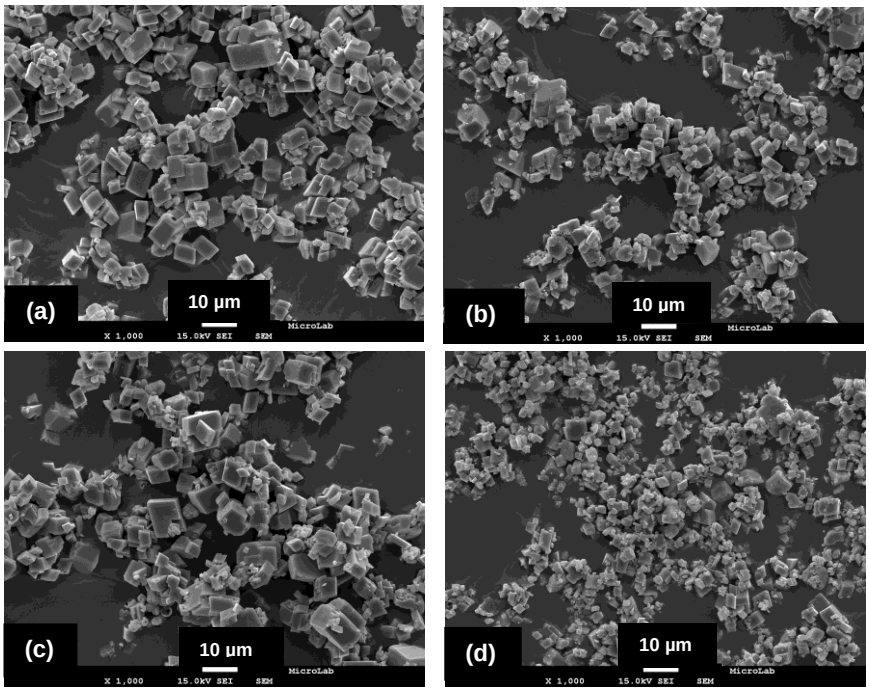

Figure 3.13. SEM micrographs of $CaCO_3$ synthesized by precipitation reaction between 0.5 M aqueous solutions of $CaCl_2.2H_2O$ and Na_2CO_3 at (a) 300 rpm, 30'; (b) 300 rpm, 2h; (c) 1200 rpm, 30'; (d) 1200 rpm, 2h. More in Appendix 11.

Inclusion of magnesium in precipitation reaction, allowed for different structures as seen in **Figure 3.14**. Under certain conditions Mg^{2+} can act either as an effective inhibitor of nucleation and crystal growth of calcite or as a promoter of aragonite nucleation.[6] In this case it seems to have favored aragonite formation by morphology obtained, where structures became sharper [5] with increase of Mg content. The results of EDS (Appendix 12) confirms the presence of calcium and oxygen from $CaCO_3$, gold and palladium from sample preparation, Mg when the respective element was used for synthesis, and also a contamination of sodium chloride (**Figure 3.14: X mark**) that must be due to an incomplete removal of that salt in washing steps.

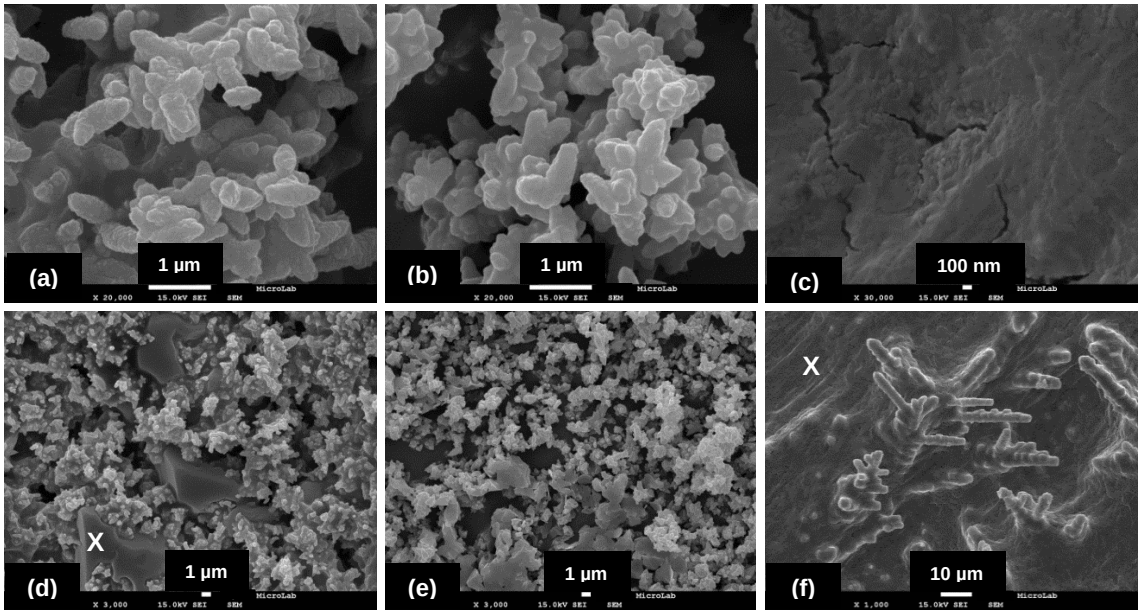

Figure 3.14. SEM micrographs of $CaCO_3$ synthesized by precipitation reaction between 0.5 M aqueous solutions of $CaCl_2.2H_2O$ and Na_2CO_3 with 1200 rpm for 2h and [Mg]/[Ca] of (a, d) 2 (b, e) 4 and (e, f) 8. X marks NaCl contamination.

3.3.1.2. XRD

The confirmation of the obtained $CaCO_3$ crystals polymorph came from XRD analysis, showed in **Figure 3.15.** Results from XRD analyses identify $CaCO_3$ rhombohedral crystals as calcite. When analyzing conditions where magnesium was included, it can be seen an intensity decrease from calcite characteristic peaks (see for example at 30º), with increasing Mg content. It can also be seen new peaks with increasing intensity, for example at 26.3º, 27.3º and 33.5º. By comparison these are related to the appearance of orthorhombic aragonite.

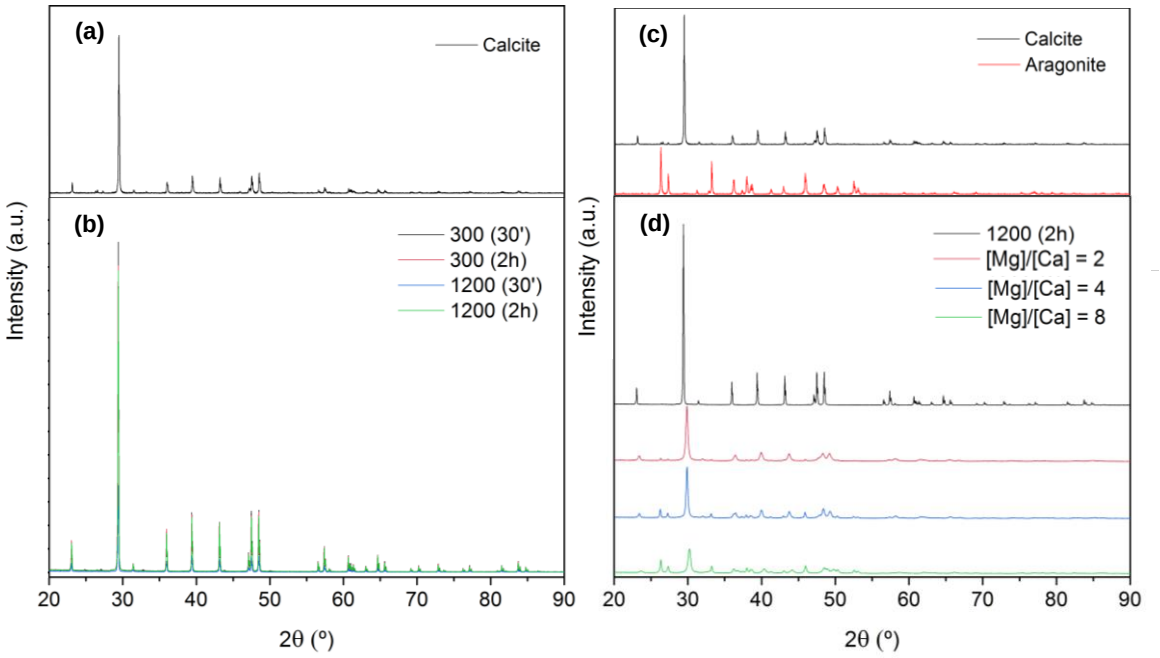

Figure 3.15. XRD analysis of (a) Calcite; (b) $CaCO_3$ synthesized for different mixing speed and time of reaction in absence of magnesium and; (c) Calcite and Aragonite; (d) $CaCO_3$ synthesized with magnesium inclusion with [Mg]/[Ca] of 2, 4 and 8 for a reaction at 1200 rpm during 2h. (a) and (c) from database: http://rruff.info/.

3.3.2. Simple Emulsions

Generally, an O/W Pickering emulsion is stabilized by hydrophilic particles with a contact angle less than 90º, while a W/O emulsion is preferably stabilized by hydrophobic particles with a contact angle larger than 90º. $CaCO_3$ particles have a contact angle of around 40º, therefore they should be capable of stabilize O/W emulsion. [10] Previously prepared $CaCO_3$ calcite crystals produced with 1200 rpm for 2h (smaller), were used in an attempt to stabilize O/W emulsion, as done in references [12] and [10] with pristine commercial $CaCO_3$ particles. No emulsion was obtained (Appendix 13), possibly due to larger particles compared to pristine (less than 2 µm [12]). This approach was put aside and following attempts relied on *in-situ* precipitation.

Simple W/O and O/W emulsions were studied with and without polymers and with Mg inclusion. Results were registered by photographs and microscope images when appreciable changes were noticed.

As for organic matrices PVA and PAA-Na were the polymers chosen. The first due to the already established role as emulsion stabilizer. [44] The second, because of the functional groups present, compatible with posterior mineralization. [46]

3.3.2.1. Stability of W/O

Photographs of prepared emulsions at initial time and 24h late are showed in **Figure 3.16**, with obvious differences.

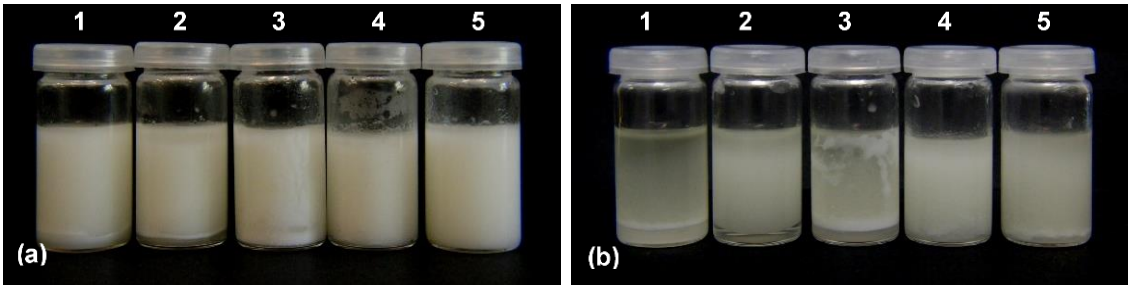

Figure 3.16. Photographs of W/O emulsion (a) immediately after emulsified and (b) 24h later. Emulsion ID: 1 - PVA, 2 - PAA-Na, 3 - PVA + salts, 4 - PAA-Na + salts, 5 - $CaCO_3$.

This is a type of emulsion difficult to stabilize, with majority of water volume separating from oil almost immediately (microscope images in Appendix 14). Photographs from emulsions with PVA (1), PAA-Na (2) and PVA with salts (3) show clearly the phase separation after 24h. Even though some water droplets still remain in the oil phase (as showed by microscope images), those are coalescing, and therefore these emulsions are unstable. Emulsion with PAA-Na with salts (4) don't show very good results, even though by photographs it seems that there is a stable emulsion. Microscope images don't shown water droplets, but a sort of film deposited on bottom with no sign of $CaCO_3$ crystals. PAA-Na seems to have suppressed crystal growth.
When used $CaCO_3$ *in-situ* precipitation no water droplets were obtained, but some oil droplets were seen by microcopy indicating phase inversion, proving hydrophilic nature of these particles in stabilizing only oil droplets in water.

With all W/O emulsions in **Figure 3.16** unsuccessful, and with the goal to stabilize this interface, oleic acid [47] was used in 1%, 5% and 10% (w/v). Good and similar results with stable emulsions even after 3 days were obtain with 5% and 10% solutions (**Figure 3.17**).

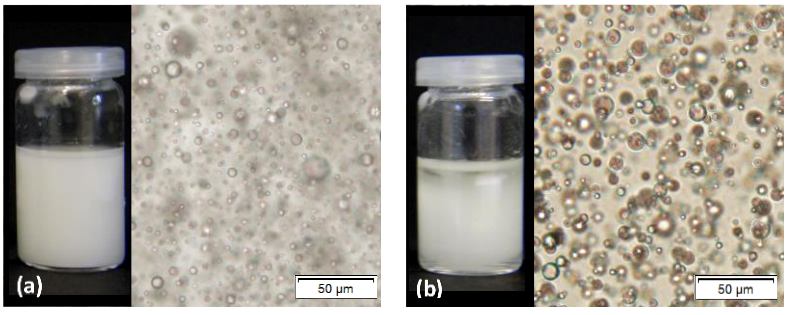

Figure 3.17. W/O emulsion stabilized with 10% (w/v) oleic acid in oil phase: (a) Photograph and microscope image immediately after preparation and (b) 3 days after preparation. Other results in Appendix 15.

3.3.2.2. Stability of O/W

This time O/W emulsions were prepared, with same polymers and minerals as before. Photographs for initial time and 24h later show clearly differences (**Figure 3.18**).

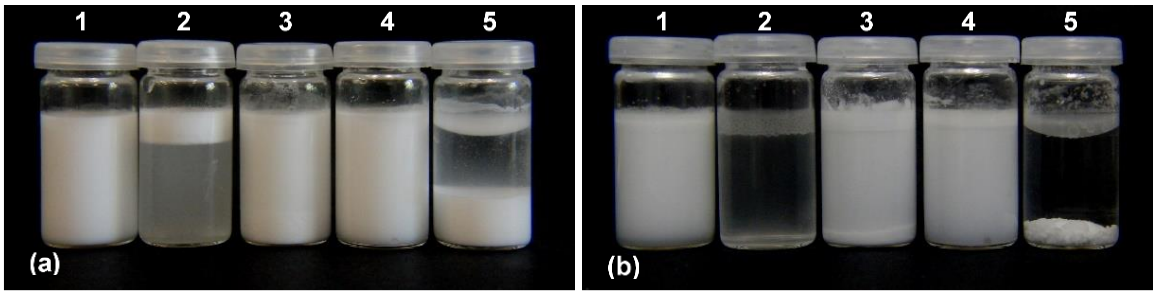

Figure 3.18. Photographs of O/W emulsion (a) immediately after emulsified and (b) 24h later. Emulsion ID: 1 - PVA, 2 - PAA-Na with fluctuating oil droplets, 3 - PVA + salts, 4 - PAA-Na + salts, 5 - $CaCO_3$ with depositing oil droplets.

Considering emulsion stability an important factor for posterior mineralization steps, best results for O/W were obtained with PVA (1) and $CaCO_3$ (5) *in-situ* precipitation when no polymers were simultaneously added. In the cases where solutions of respective polymer and salts were mixed together (3 and 4) deposits of crystals were observed on glass walls, with water starting to separate from oil phase at 24h. Polymers might be competing with Ca^{2+} ions to bond to oil-water interface. This is a plausible reason since when only polymers were used, emulsions were obtained. In the case of PAA-Na (2) emulsion droplets started to coalesce at 24h, which might be due to insufficient polymer concentration. Microscope images in Appendix 16 help clarifying this analysis. The case where $CaCO_3$ was used showed promising results, with crystals stabilizing oil droplets event though not covering all droplet surface (**Figure 3.19**)**.**

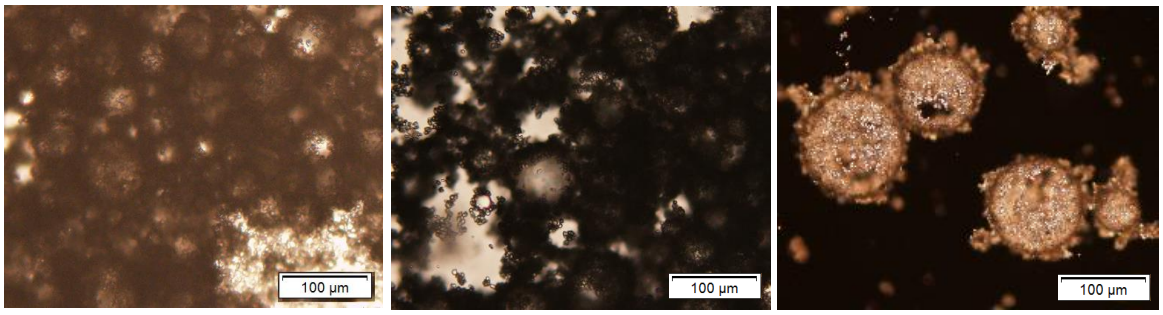

(a) **(b)** **(c)**

Figure 3.19. Microscope images of oil droplets stabilized by $CaCO_3$ particles for (a) initial time; (b) 24h after preparation; (c) under crossed polarizer showing crystal birefringence and incomplete surface coverage. Notice dispersion in sizes.

3.3.2.3. Stability of O/W introducing magnesium

Knowing by previous XRD analysis that magnesium induces different polymorph formation, O/W emulsion using variable magnesium content were prepared. Photographs can be seen in **Figure 3.20**.

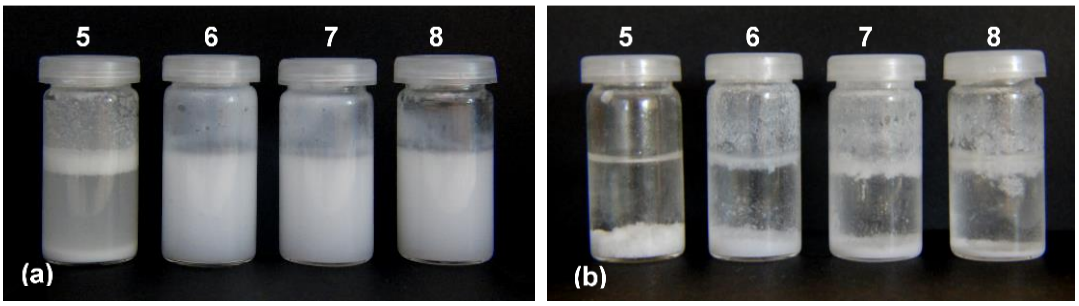

Figure 3.20. Photographs of O/W emulsion (a) immediately after emulsified and (b) 7 days later. Emulsion ID: 5 - $CaCO_3$, 6 - [Mg]/[Ca] = 2; 7 – [Mg]/[Ca] = 4; 8 – [Mg]/[Ca] = 8.

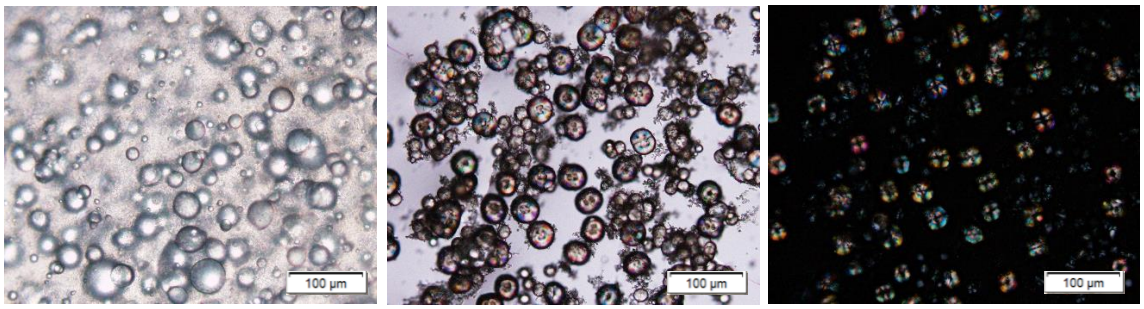

(a) **(b)** **(c)**

Figure 3.21. Microscope images of oil droplets of emulsion **6** at (a) initial time; (b) after 7 days; (c) under crossed polarizer showing birefringence. Other emulsions were similar and can be seen in Appendix 17.

When magnesium was introduced with other $CaCO_3$ precursors, one might expected to form $CaCO_3$ capsules with a different polymorph, in this case aragonite. Emulsion using Mg was successful, maintaining the appearance in **Figure 3.20 - a** for few days, but no mineral was observed in droplets surface - seen by transparent droplets - or in any place of the emulsion. After 7 days, some white powder deposited, as shown by photographs. It can be seen by **Figure 3.20 - b** that there is less volume of this power with increase of Mg content, and also an increase of oil fluctuating layer indicating that less oil was emulsified. Because of this, Mg seems to have suppressed crystal nucleation, with this being the predominant factor for a higher oil volume emulsification. Also, small crystals deposits can be seen after 7 days in microscope images (**Figure 3.21 - b**), which appear to be the result of delayed crystallization. It could be expected that aragonite formed under these situations, due to previous SEM and XRD analysis results. But no opaque capsule was verified on droplets as seen in absence of Mg (**Figure 3.19**). However, droplets show spherulitic birefringence, unlike in initial time. This can only mean that some sort of mineral different from calcite is surrounding oil droplets, or there wouldn't be any oil emulsified neither that birefringent effect. This can be caused by polymorphs as aragonite or vaterite. [48] Since this system is different than the one evaluated in XRD, vaterite is also possible to have occur. If aragonite or vaterite were indeed formed during this process, they may have recrystallized into calcite (more thermodynamically stable) in the solution where crystals are seen, and maintained the polymorph around oil droplets. Overall there must exist a competing situation between Mg^{2+} and Ca^{2+} to bind to oil surface, and those charges are somehow stabilizing the emulsion for first few days, with Mg inhibiting formation of calcite capsule. This situation is not as

effective as when calcite is formed, with oil droplets coalescing in a fluctuating layer with increase of Mg content.

Even so, mineral capsules are very stable, with microscope images acquired after 1 month preparation similar to images of just 7 days old (Appendix 17).

3.3.3. Continuous Mineralization

The goal of this section was to try different approaches to grow a thick $CaCO_3$ shell (**Figure 3.22**), based on reference [11] and [14].

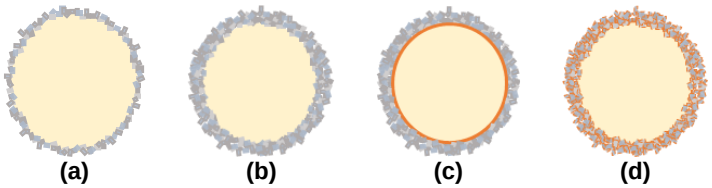

Figure 3.22. (a) $CaCO_3$ capsule before posterior mineralization; (b) after mineralization in ionic solutions; (c) capsule grows triggered by an organic matrix; (d) capsule grows with aid of organic matrix.

Mineralization photographs and microscope images are in **Figure 3.23**.

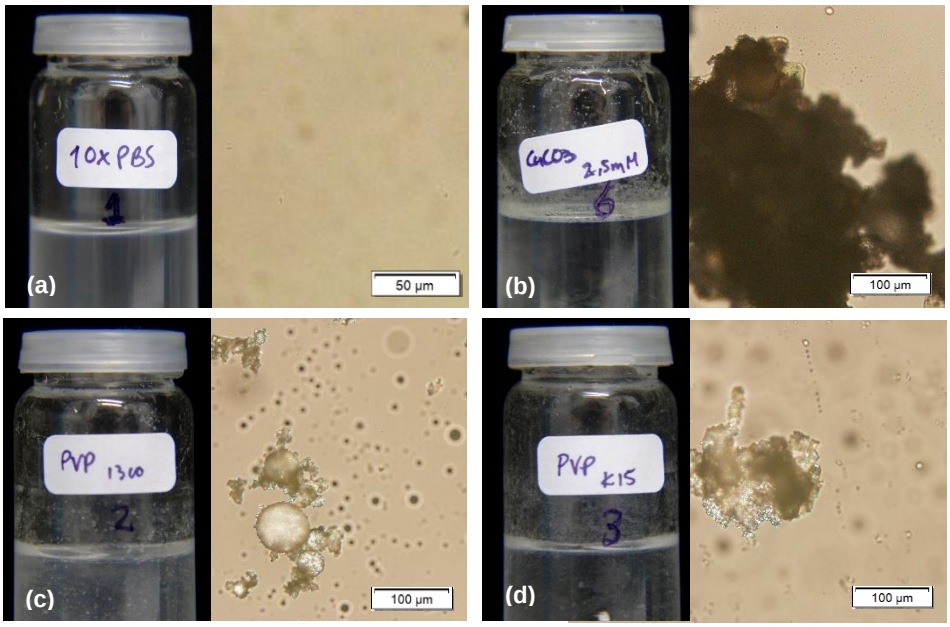

Figure 3.23. $CaCO_3$ (a) in 10 × PBS, disrupted at 24h (turbid solution); (b) formed agglomerates in $CaCO_3$ 2.5 mM solution; (c) remained intact with lot of $CaCO_3$ capsules in solution; (d) formed agglomerates.

For an approach as in **Figure 3.22 - b**, PBS and $CaCO_3$ precipitation solutions were used.

At 24h, ionic exchanges with PBS ions in solution led to dissolution of $CaCO_3$ capsules with oil being released **Figure 3.23 - a**. In reference [14] using SBF (similar ionic solution) worked for mineralization, but in that case, polymers were also used, which kept emulsion's stability while mineralizing. Attempts with PAA-Na to be used as emulsion stabilizer (as in **Figure 3.22 - c**) for posterior crystallization weren't successful (Appendix 18 – Table A18.1). It was seen in reference [11] the use of MAA for this purpose, but different molecular weight may be the cause of unsuccessful emulsion in this case. The process was not carried through for this case.

Next experiments were meant to compare $CaCO_3$ precipitation solution with and without PVP (**Figure 3.22 - d**). PVP with different molecular weight was used, for its role in speeding up mineralization process in SBF. [11] In this case a solution to precipitate $CaCO_3$ was used. For all attempts capsules were seen floating in solution, so the process was carried until the end. PVP of high molecular weight seems to have capped the capsules, maintaining them disperse (**Figure 3.23** - **c**)**.** On contrary when this polymer was not used or had low molecular weight, precipitation seems to have formed agglomerates (**Figure 3.23** - **d**)**.**

As for stabilization in air, all capsules collapsed after water was evaporated. **Figure 3.24** shows this event.

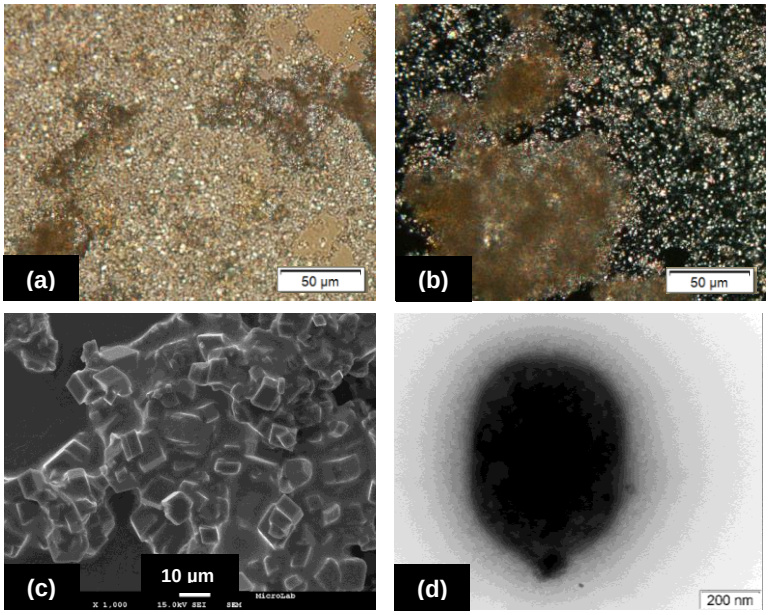

Figure 3.24. (a) Microscope image of collapsed droplets mineralized with "PVP 1300"; (b) Crossed polarizer showing crystals; (c) SEM image after $CaCO_3$ oil capsules dried in air- without further mineralization – it can be seen a soft layer from oil between crystals; (d) TEM image of a $CaCO_3$ particle/capsule.

It wasn't possible to stabilize mineralized oil droplets in air. The mineral capsule was not thick enough. However, comparing to literature, stabilization in air is only achieved for very small particles and capsules with no liquid core. For example in reference [46] stable particles were produced with sizes close to 200 nm. For core-shell capsules, successful air stabilization was achieved in [13] but also for sizes smaller than 2 µm. For larger capsules it is regular to find results using cryo-SEM, which means that those capsules are not stable in air either (20 µm capsules in [10]). One of the best results found is in [14] (CaP capsules around 100 µm), which was where the protocol for mineralization followed was based. But in this case the type of mineral and production method are different, which is enough for different results. TEM image shows a mineralized structure with diameter around 600 nm, which can be simply a particle or a shell-like structure. Color variation may indicate this is a capsule, but it is extremely small compared to the desired ones.

The stability of mineralized capsules is more likely to be achieved for smaller sizes. The process did not work for micrometer droplets but may have worked for nanometric ones.

Conclusions and Future Perspectives

The goal of this thesis included the development of a microfluidic device capable of producing uniform droplets by double W/O/W emulsion, to avoid problems related to common methods of encapsulation. For that purpose, a wet chemical modification to turn the outlet microchannel hydrophilic was seek. This modification had to be applied in closed channels and to be stable over time. An optimal solution was found with chemical oxidation by 1M NaOH aqueous solution followed by LbL adsorption of at least 3 BL of polyelectrolyte system, PDADMAC/PSS. This turned PDMS surface hydrophilic over time, in water and air, maintaining its optical properties, without the need of expensive equipment or clean room facilities. This also did not affect PDMS transparency, making possible to monitor droplet's production on microscope, essential to synchronize flows to produce the desired emulsions.
However, after several different attempts to selectively apply this modification just to the outlet channel, it was found that the flow controllers used weren't a good choice to control multiphase flows. During the process the balance between fluids' flows was disrupted by the step motor, and chemical solutions advanced for unwanted channels.
With this happening, the best suggestion for future work is to apply this modification with pressure controllers and pumping air as blocking solution, which will not affect PDMS water behavior for sure. As for chemical solution, the one found in this study seems ideal and easy to apply.

Since the microfluidic device was developed with the intention to produce homogenous emulsions to study $CaCO_3$ mineral stabilization - and in future drug content distribution and release - this time it was necessary to resort to conventional methods to produce the emulsions. With the development of this area in a very initial stage, it was chosen to study simple emulsions to acquire knowledge on interface stability. The results obtained can in future be applied to the microfluidic device.
It was found a surprising stabilization of oil droplets using only $CaCO_3$ precipitation *in-situ* under physiological conditions. These capsules were extremely stable in aqueous environment (evaluated up to 1 month), but on dry environment they collapsed. This was due to incomplete mineral capsule formation. In an attempt to try to grow a thick shell, posterior mineralization steps were carried, but that process is hard to control, with homogenous precipitation occurring in solution. In future, other options should be explored, like the stabilization of oil droplets with monomers to trigger nucleation on droplets surface, or applying LbL methods to previously formed $CaCO_3$ capsules. Since PAA-Na was not capable to stabilize oil droplets, and PVP was not enough to construct a thick capsule, probably by lack of charged mineralizable groups, it seems a good choice for future works the use of polyelectrolytes. These should enable a high density of surface charges on surface of droplets, to chelate Ca^{2+}, starting mineralization. This study has a lot of opportunities for optimization, with the major final goal to produce homogenous thermostable mineral capsules triggered by pH for controlled drug release.

References

[1] B. Bhushan, “Biomimetics: lessons from nature-an overview.,” Philos. Trans. A. Math. Phys. Eng. Sci., vol. 367, no. 1893, pp. 1445–86, 2009.

[2] K. Liang, R. Ricco, C. M. Doherty, M. J. Styles, S. Bell, N. Kirby, S. Mudie, D. Haylock, A. J. Hill, C. J. Doonan, and P. Falcaro, “Biomimetic mineralization of metal-organic frameworks as protective coatings for biomacromolecules,” Nat. Commun., vol. 6, no. 7240, pp. 7240, 2015.

[3] W. Chen, G. Wang, and R. Tang, “Nanomodification of living organisms by biomimetic mineralization,” Nano Res., vol. 7, no. 10, pp. 1404–1428, 2014.

[4] N. a. J. M. Sommerdijk and M. Cusack, “Biomineralization: Crystals competing for space,” Nat. Mater., vol. 13, no. 12, pp. 1078–1079, 2014.

[5] H. Nebel and M. Epple, “Continuous preparation of calcite, aragonite and vaterite, and of magnesium-substituted amorphous calcium carbonate (Mg-ACC),” Zeitschrift fur Anorg. und Allg. Chemie, vol. 634, no. 8, pp. 1439–1443, 2008.

[6] L. Brecevic and D. Kralj, “On Calcium Carbonates : from Fundamental Research to Application,” Croat. Chem. Acta, vol. 80, no.3-4, pp. 467–484, 2007.

[7] H.-B. Yao, J. Ge, L.-B. Mao, Y.-X. Yan, and S.-H. Yu, “25th anniversary article: Artificial carbonate nanocrystals and layered structural nanocomposites inspired by nacre: synthesis, fabrication and applications.,” Adv. Mater., vol. 26, no. 1, pp. 163–87, 2014.

[8] P. Zhu, Y. Masuda, and K. Koumoto, “The effect of surface charge on hydroxyapatite nucleation.,” Biomaterials, vol. 25, no. 17, pp. 3915–21, 2004.

[9] Y. Boyjoo, V. K. Pareek, and J. Liu, “Carbonate particles and their applications,” J. Mater. Chem. A Mater. Energy Sustain., vol. 2, no. 35, pp. 14270–14288, 2014.

[10] X. Wang, W. Zhou, J. Cao, W. Liu, and S. Zhu, “Preparation of core-shell $CaCO_3$ capsules via Pickering emulsion templates,” J. Colloid Interface Sci., vol. 372, no. 1, pp. 24–31, 2012.

[11] R. V. Bell, L. a. Rochford, R. T. M. de Rosales, M. Stevens, J. V. M. Weaver, and S. a. F. Bon, “Fabrication of calcium phosphate microcapsules using emulsion droplets stabilized with branched copolymers as templates,” J. Mater. Chem. B, vol. 3, no. 27, pp. 52–55, 2015.

[12] Y. Long, K. Song, D. York, Z. Zhang, and J. a. Preece, “Engineering the mechanical and physical properties of organic-inorganic composite microcapsules,” Colloids Surfaces A Physicochem. Eng. Asp., vol. 433, pp. 30–36, 2013.

[13] G. X. Wu, J. Ding, and J. M. Xue, “Synthesis of calcium carbonate capsules in water-in-oil-in-water double emulsions,” J. Mater. Res., vol. 23, no. 01, pp. 140–149, 2008.

[14] K. Du, X. Shi, and Z. Gan, “Rapid biomimetic mineralization of hydroxyapatite-g-pdlla hybrid microspheres,” Langmuir, vol. 29, no. 49, pp. 15293–15301, 2013.

[15] H. J. Shen, H. Shi, K. Ma, M. Xie, L. L. Tang, S. Shen, B. Li, X. S. Wang, and Y. Jin, “Polyelectrolyte capsules packaging BSA gels for pH-controlled drug loading and release and their antitumor activity,” Acta Biomater., vol. 9, no. 4, pp. 6123–6133, 2013.

[16] C. Wang, C. He, Z. Tong, X. Liu, B. Ren, and F. Zeng, “Combination of adsorption by porous $CaCO_3$ microparticles and encapsulation by polyelectrolyte multilayer films for sustained drug delivery,” Int. J. Pharm., vol. 308, no. 1–2, pp. 160–167, 2006.

[17] D. Volodkin, “$CaCO_3$ templated micro-beads and capsules for bioapplications,” Adv. Colloid Interface Sci., vol. 207, no. 1, pp. 306–324, 2014.

[18] M. Lee, W. Park, C. Chung, J. Lim, S. Kwon, K. H. Ahn, S. J. Lee, and K. Char, “Multilayer deposition on patterned posts using alternating polyelectrolyte droplets in a microfluidic device.,” Lab Chip, vol. 10, no. 9, pp. 1160–1166, 2010.

[19] G. M. Whitesides, “The origins and the future of microfluidics.,” Nature, vol. 442, no. 7101, pp. 368–373, 2006.

[20] R. Seemann, M. Brinkmann, T. Pfohl, and S. Herminghaus, “Droplet based microfluidics,” Reports Prog. Phys., vol. 75, no. 1, pp. 1-41, 2011.

[21] S.-Y. Teh, R. Lin, L.-H. Hung, and A. P. Lee, “Droplet microfluidics.,” Lab Chip, vol. 8, no. 2, pp. 198–220, 2008.

[22] M. G. Simon and A. P. Lee, “Microdroplet Technology: Principles and Emerging Applications in Biology and Chemistry”, Chapter 2, ed. P. Day et al., pp. 23–51, 2012.

[23] Y. Schaerli and F. Hollfelder, “The potential of microfluidic water-in-oil droplets in experimental biology.,” Mol. Biosyst., vol. 5, no. 12, pp. 1392–1404, 2009.

[24] J. N. Lee, C. Park, and G. M. Whitesides, “Solvent Compatibility of Poly(dimethylsiloxane)-Based Microfluidic Devices,” Anal. Chem., vol. 75, no. 23, pp. 6544-6554, 2003.

[25] T. Nisisako, S. Okushima, and T. Torii, “Controlled formulation of monodisperse double emulsions in a multiple-phase microfluidic system,” Soft Matter, vol. 1, no. 1, pp. 23, 2005.

[26] T. P. Lagus and J. F. Edd, “A review of the theory, methods and recent applications of high-throughput single-cell droplet microfluidics,” J. Phys. D. Appl. Phys., vol. 46, no. 11, pp. 1-21, 2013.

[27] C. De Menezes Atayde and I. Doi, “Highly stable hydrophilic surfaces of PDMS thin layer obtained by UV radiation and oxygen plasma treatments,” Phys. Status Solidi Curr. Top. Solid State Phys., vol. 7, no. 2, pp. 189–192, 2010.

[28] G. Slaughter and B. Stevens, “A cost-effective two-step method for enhancing the hydrophilicity of PDMS surfaces,” Biochip J., vol. 8, no. 1, pp. 28–34, 2014.

[29] D. Maji, S. K. Lahiri, and S. Das, “Study of hydrophilicity and stability of chemically modified PDMS surface using piranha and KOH solution,” Surf. Interface Anal., vol. 44, no. 1, pp. 62–69, 2012.

[30] K. S. Koh, J. Chin, J. Chia, and C. L. Chiang, “Quantitative studies on PDMS-PDMS interface bonding with piranha solution and its swelling effect,” Micromachines, vol. 3, no. 2, pp. 427–441, 2012.

[31] G. Sui, J. Wang, C. C. Lee, W. Lu, S. P. Lee, J. V. Leyton, A. M. Wu, and H. R. Tseng, “Solution-phase surface modification in intact poly(dimethylsiloxane) microfluidic channels,” Anal. Chem., vol. 78, no. 15, pp. 5543–5551, 2006.

[32] I. Hoek, F. Tho, and W. M. Arnold, “Sodium hydroxide treatment of PDMS based microfluidic devices.,” Lab Chip, vol. 10, no. 17, pp. 2283–2285, 2010.

[33] A. R. Abate, J. Thiele, M. Weinhart, and D. a Weitz, “Patterning microfluidic device wettability using flow confinement.,” Lab Chip, vol. 10, no. 14, pp. 1774–1776, 2010.

[34] L. Yu, C. M. Li, Y. Liu, J. Gao, W. Wang, and Y. Gan, “Flow-through functionalized PDMS microfluidic channels with dextran derivative for ELISAs.,” Lab Chip, vol. 9, no. 9, pp. 1243-1247, 2009.

[35] Y.-J. Ko, S.-M. Ha, H.-J. Kim, D.-H. Lee, and Y. Ahn, “Development of a PDMS-Glass Hybrid Microchannel Mixer Composed of Micropillars and Micronozzles,” J. Solid Mech. Mater. Eng., vol. 2, no. 4, pp. 445–454, 2008.

[36] W.-A. C. Bauer, M. Fischlechner, C. Abell, and W. T. S. Huck, “Hydrophilic PDMS microchannels for high-throughput formation of oil-in-water microdroplets and water-in-oil-in-water double emulsions.,” Lab Chip, vol. 10, no. 14, pp. 1814–1819, 2010.

[37] J. Yan, W. A. C. Bauer, M. Fischlechner, F. Hollfelder, C. F. Kaminski, and W. T. S. Huck, “Monodisperse water-in-oil-in-water (W/O/W) Double emulsion droplets as uniform compartments for high-throughput analysis via flow cytometry,” Micromachines, vol. 4, no. 4, pp. 402–413, 2013.

[38] G. Lamour, A. Hamraoui, A. Buvailo, Y. Xing, S. Keuleyan, V. Prakash, A. Eftekhari-Bafrooei, and E. Borguet, “Contact angle measurements using a simplified experimental setup,” J. Chem. Educ., vol. 87, no. 12, pp. 1403–1407, 2010.

[39] J. Park, J. H. Bae, W. H. Kim, M. H. Kim, C. M. Keum, S. D. Lee, and J. S. Choi, “Effects of interfacial charge depletion in organic thin-film transistors with polymeric dielectrics on electrical stability,” Materials (Basel)., vol. 3, no. 6, pp. 3614–3624, 2010.

[40] B. Wang, Z. Abdulali-Kanji, E. Dodwell, J. H. Horton, and R. D. Oleschuk, “Surface characterization using chemical force microscopy and the flow performance of modified polydimethylsiloxane for microfluidic device applications,” Electrophoresis, vol. 24, no. 9, pp. 1442–1450, 2003.

[41] U. M. Bhalerao, J. Acharya, A. K. Halve, and M. P. Kaushik, “Controlled drug delivery of antileishmanial chalcones from Layer-by-Layer (LbL) self assembled PSS/PDADMAC thin films,” RSC Adv., vol. 4, no. 10, p. 4970, 2014.

[42] S. Köstler, A. V. Delgado, and V. Ribitsch, “Surface thermodynamic properties of polyelectrolyte multilayers,” J. Colloid Interface Sci., vol. 286, no. 1, pp. 339–348, 2005.

[43] C. M. Kuo, “Poly (dimethylsiloxane),” Polymer Data Handbook, pp. 411, 1999.

[44] T. K. Giri, C. Choudhary, Ajazuddin, A. Alexander, H. Badwaik, and D. K. Tripathi, “Prospects of pharmaceuticals and biopharmaceuticals loaded microparticles prepared by double emulsion technique for controlled delivery,” Saudi Pharm. J., vol. 21, no. 2, pp. 125-141, 2013.

[45] R. Babou-Kammoe, S. Hamoudi, F. Larachi, and K. Belkacemi, “Synthesis of $CaCO_3$ nanoparticles by controlled precipitation of saturated carbonate and calcium nitrate aqueous solutions,” Can. J. Chem. Eng., vol. 90, no. 1, pp. 26–33, 2012.

[46] V. Lauth, M. Maas, and K. Rezwan, “Coacervate-directed synthesis of $CaCO_3$ microcarriers for pH-responsive delivery of biomolecules,” J. Mater. Chem. B, vol. 2, no. 44, pp. 7725–7731, 2014.

[47] M. J. Schick and A. T. Hubbard, “Emulsions and Emulsion Stability”, Chapter 2, vol. 132. pp. 669, 2006.

[48] K. K. Sand, J. D. Rodriguez-Blanco, E. Makovicky, L. G. Benning, and S. L. S. Stipp, “Crystallization of $CaCO_3$ in water-Alcohol mixtures: Spherulitic growth, polymorph stabilization, and morphology change,” Cryst. Growth Des., vol. 12, no. 2, pp. 842–853, 2012.

[49] M. Ye, S. Kim, and K. Park, “Issues in long-term protein delivery using biodegradable microparticles,” J. Control. Release, vol. 146, no. 2, pp. 241–260, 2010.

Appendix 1

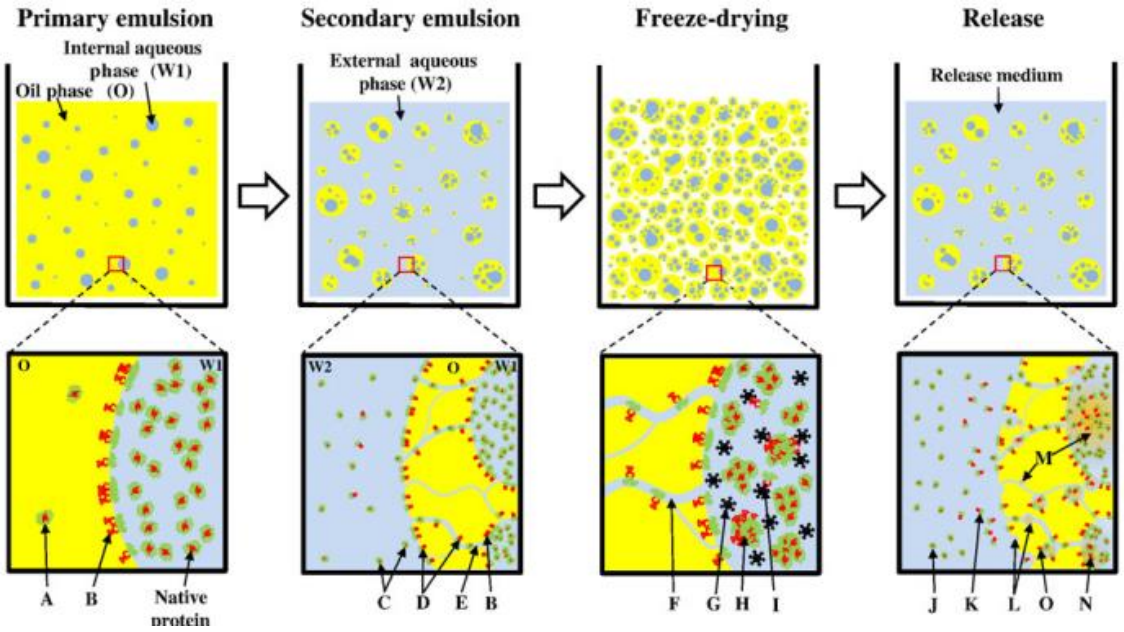

Figure A1.1. Typical W/O/W double emulsion method to prepare microspheres containing protein drug (upper panel) and microscopic events during fabrication process (lower panel). The sequence of fabrication is primary emulsion, secondary emulsion, solvent extraction/evaporation (not shown), freeze-drying, and drug release test. With negligible partition of protein into oil phase (A), the organic solvent–water interface during W1/O emulsion results in protein denaturation (B). During generation of secondary emulsion, water channels connecting internal (W1) and external (W2) aqueous phases (E) allow proteins to escape from droplets (C), and provide more chances of protein denaturation by increased surface area of the oil–water interface (D). The water channels become pores (F) of microspheres hardened by freeze-drying. Ice crystal (G) is known to provide a hazardous condition inducing protein denaturation (I). Irreversible aggregation (H) between protein molecules can be formed if stabilizer or cryoprotectant is not added. Normally, microspheres made by double emulsion have a broad range of particle size distribution as well as different protein amount in each microparticle. In a release test, a burst release of protein at the initial period (b24 h) is mostly due to the protein release (K) from the proteinaceous film on the particle surface (D). With time, proteins are release from particles (J) by diffusion and degradation (L) of polymer (e.g., PLGA). Microparticle degradation cumulates acidic products inside particles (M), which further facilitates protein denaturation (N). Protein adsorption on hydrophobic polymer surface (O) often leads to incomplete release of protein drugs.", quoted from [49]

Appendix 2

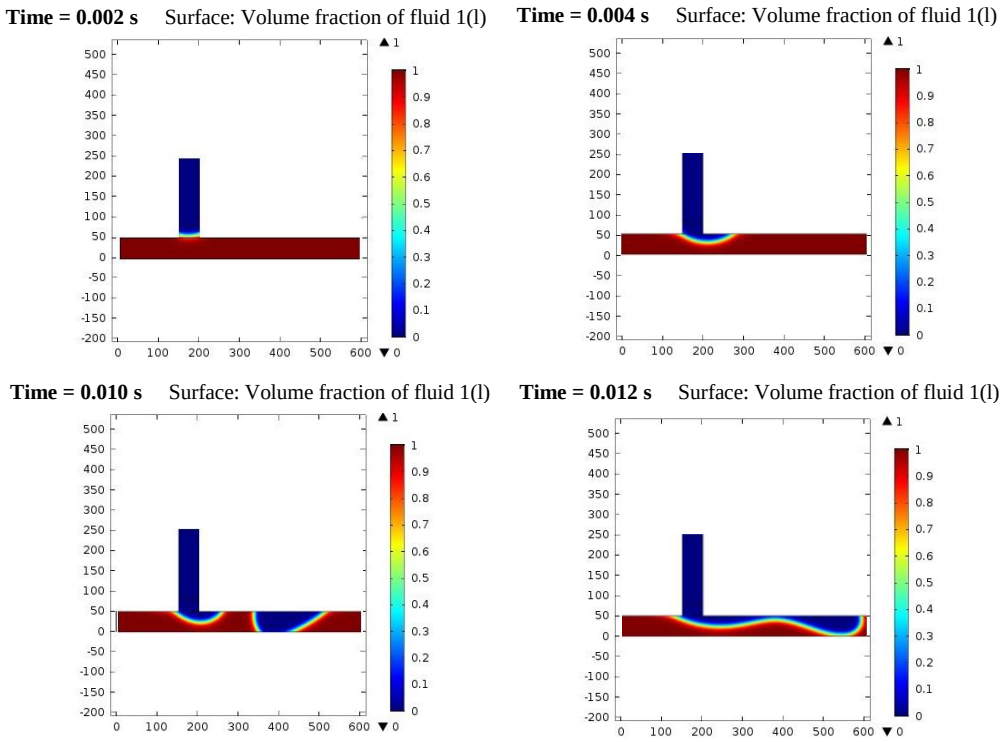

Figure A2.1. T-junction geometry with microfluidic channels of 50 µm width and depth. Simulation parameters: no slip boundary condition; Qd = 20 µl/h; Qc = 50 µl/h. Results showed for times indicated in respective picture.

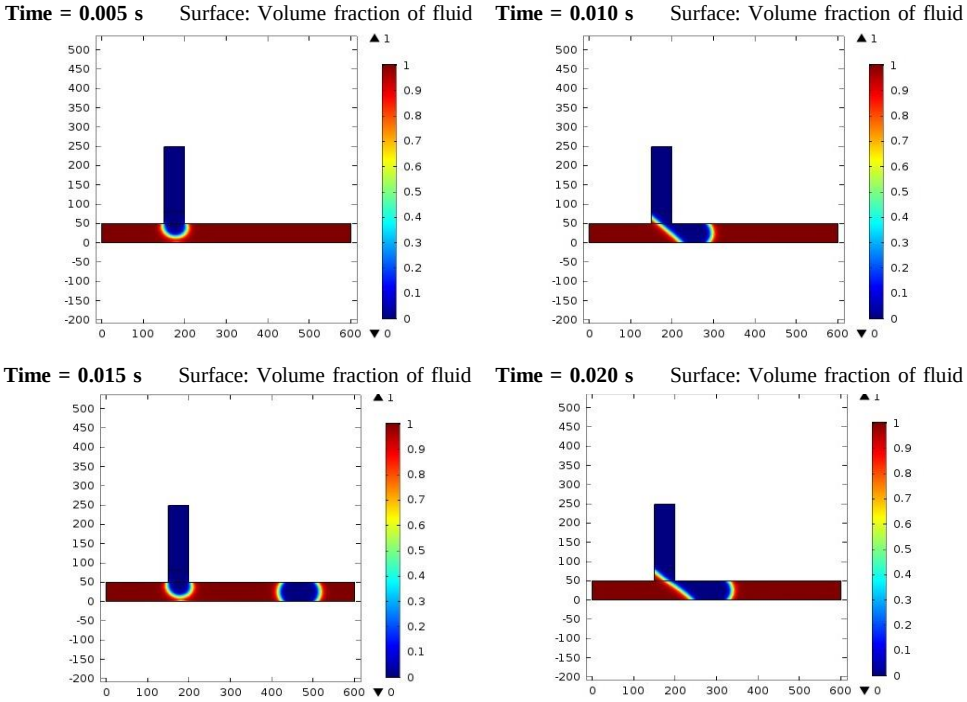

Figure A2.2. T-junction geometry with microfluidic channels of 50 µm width and depth. Simulation parameters: wetted wall boundary condition; Qd = 20 µl/h; Qc = 50 µl/h. Results showed for times indicated in respective picture.

Observations: Channels must meet a certain wetting wall condition, for formation of droplets. These last have to make a certain contact angle with channel's walls. In general channel has to be repellent to the fluid of the droplet, which is characterized by the contact angle with that fluid.

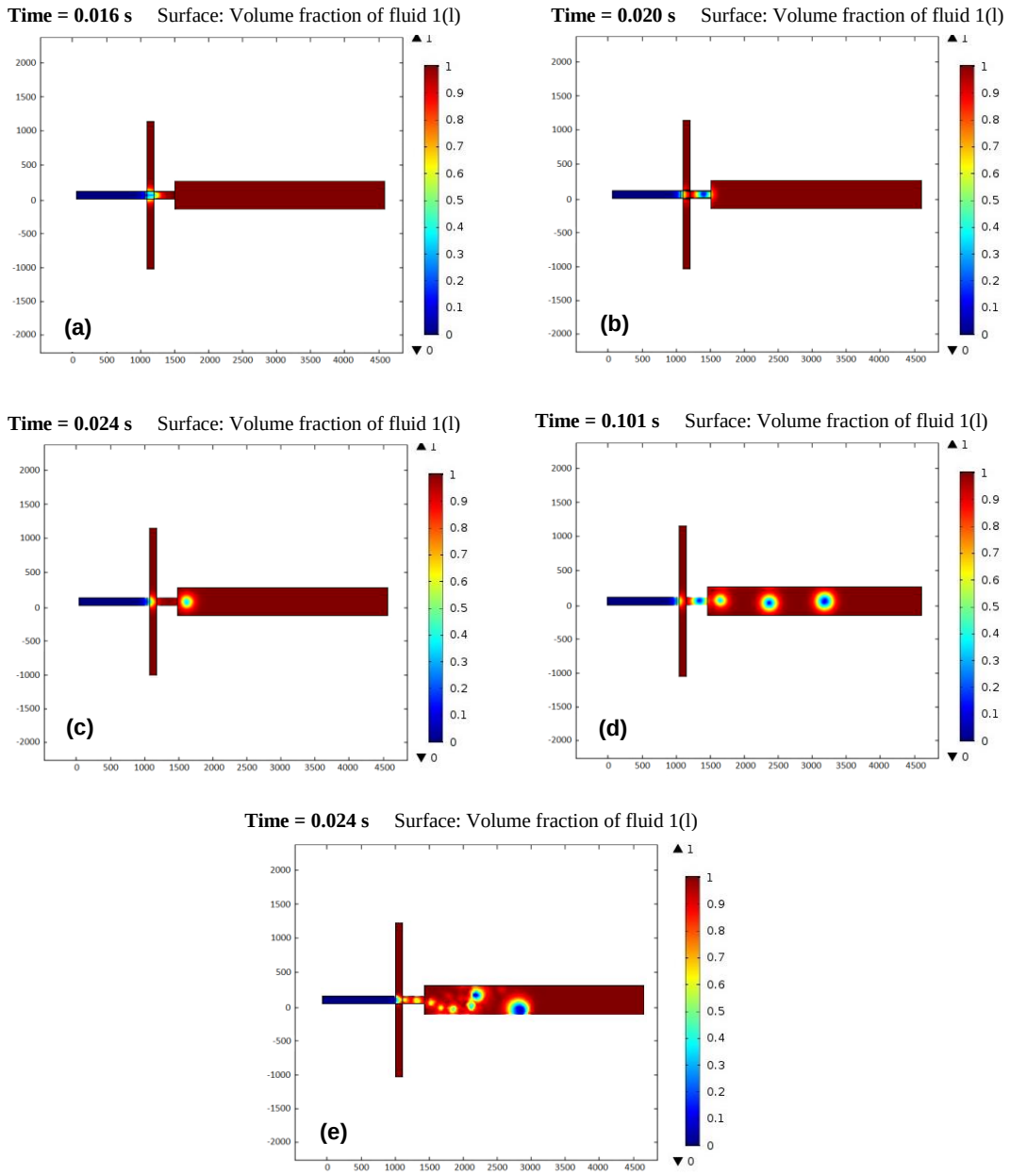

Figure A2.3. Flow focusing microfluidic device with inlet channels of 100 µm width and depth and (a, b, c, d) an expansion chamber of 400 µm width with 90º walls (similar to step-emulsification). Simulation parameters: Qd = 6.66 µl/h; Qc = 7 x Qd µl/h; boundary condition: wetted wall (focusing channel) = 3π/4; wetted wall (vertical walls of expansion chamber) = π. (e) Fluid becomes unstable with increasing flow rate: Qd = 50 µl/h; Qc = 4 x Qd. µl/h. Results showed for times indicated in respective picture.

Observations: COMSOL don't take in account surfactant effect, so droplets coalesce if their interface touches. This can be seen by droplets with different sizes in **Figure A2.3 - e.**

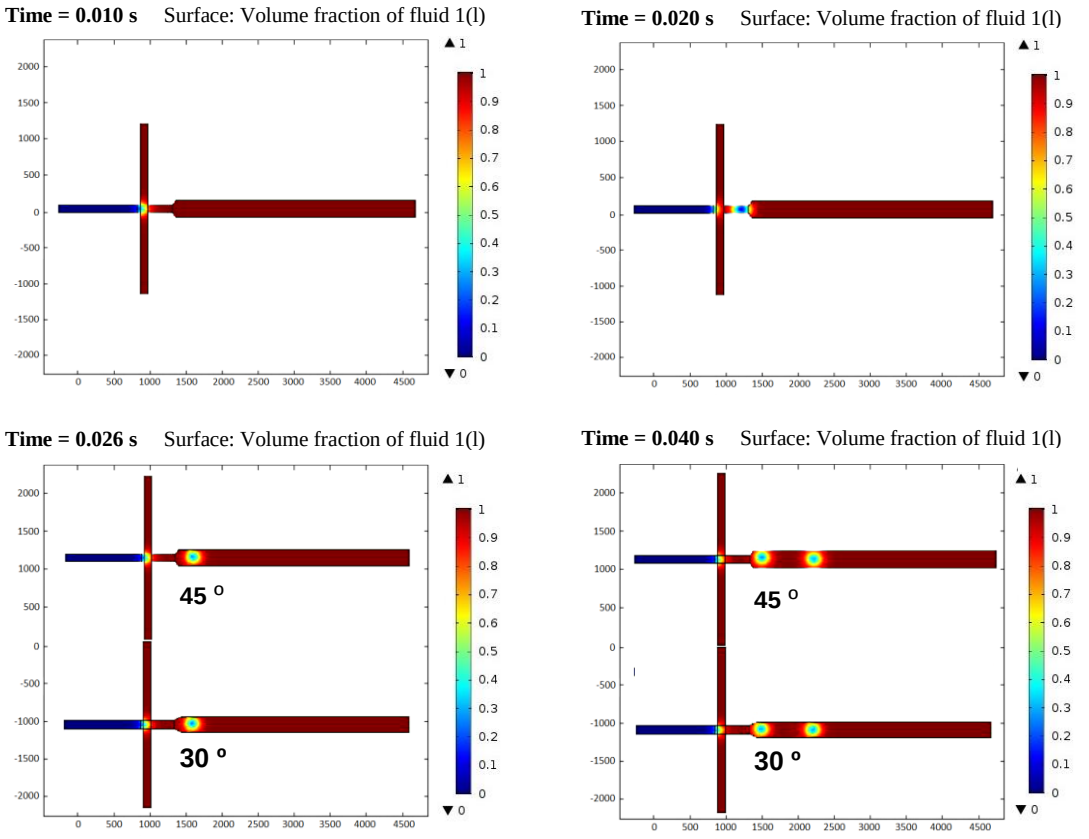

Figure A2.4. Flow focusing microfluidic device with inlet channels of 100 µm width and depth and an expansion chamber of 200 µm width with 45º or 30º walls. Simulation parameters: Qd = 6.66 µll/h; Qc = 7 x Qd µl/h; boundary condition: wetted wall (focusing channel) = 3π/4; wetted wall (walls of expansion chamber) = π. No difference in droplet production was observed. Results showed for times indicated in respective picture.

Observations: Water droplets with similar size are produced and these travel in straight line along the channel.

So, to avoid droplet instability associated with increased flow rate and pressure drops near the walls, and since these simulations represent only the first intersection of the microfluidic device, it should be chosen an expansion chamber with dimensions similar to the volume of droplets and with walls of 45º or less.

This way droplets will reach the second intersection to be encapsulated by water, in a simpler ans controllable manner.

To produce oil droplets, inverse conditions must be applied, where the wetting wall condition is respective to oil fluid instead.

Appendix 3

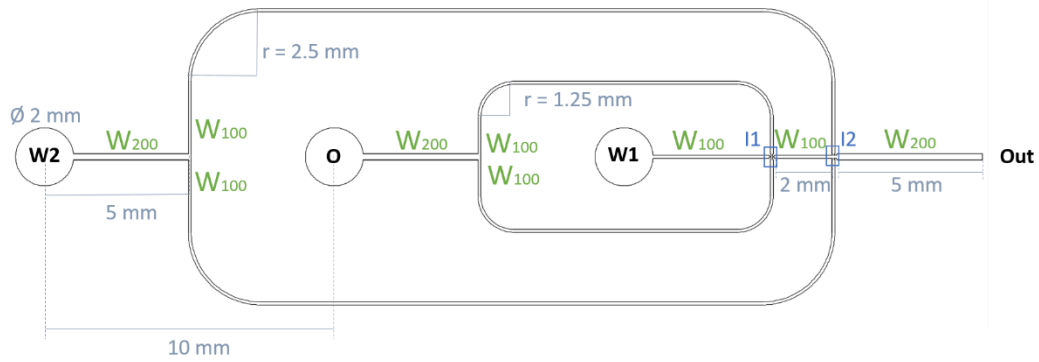

(a)

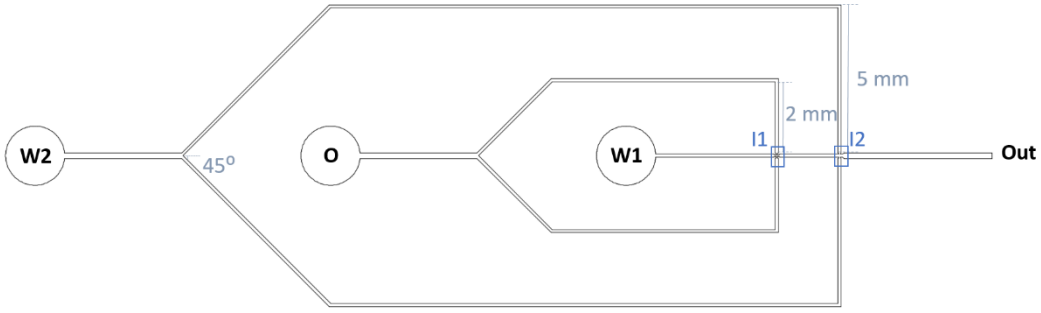

(b)

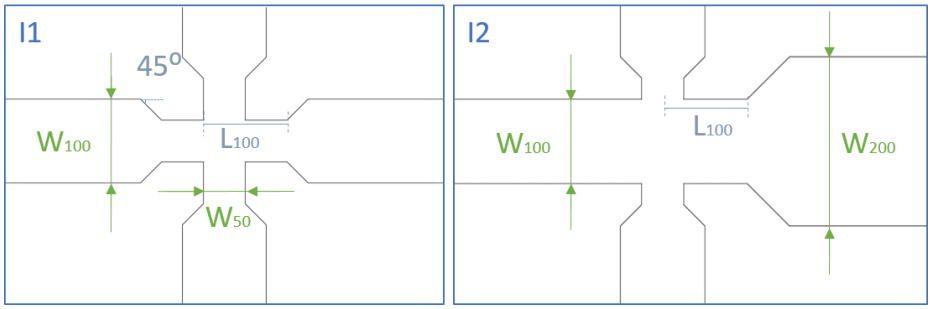

(c) **(d)**

Figure A3.1. AutoCAD drawing with dimensions of microfluidic devices for W/O/W emulsion: (a) with curve channels and (b) straight channels. Inlets have all same diameter and are named after emulsions phase. In (c) there is a magnification of first intersection, **I1**, and (d) the second intersection, **I2**. "W_X" refers to the width of respective channel and "L_X" refers to the length of marked path, with X dimension in micrometers.

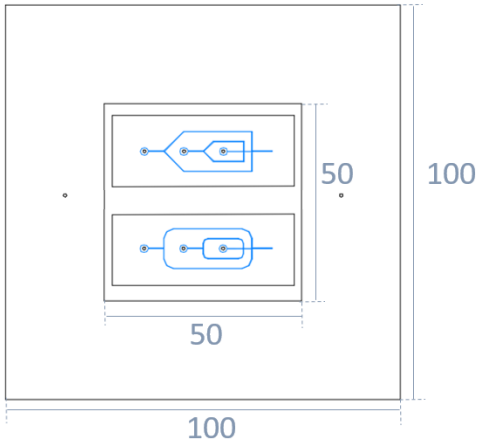

(a)

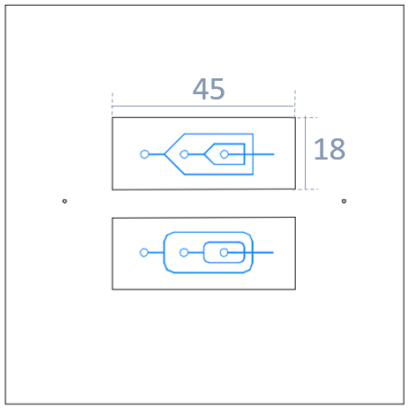

(b)

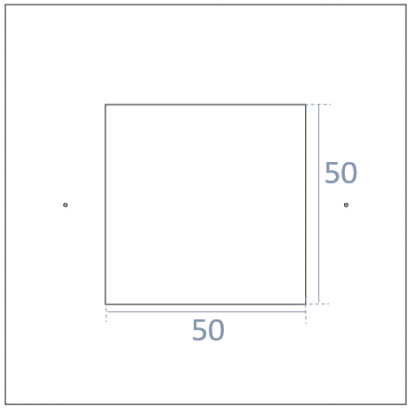

(c)

Figure A3.2. AutoCAD drawing of PMMA plates: (a) top: drill and contour; (b) medium: open holes of devices' size; (c) bottom: pocket for SU-8 mold. All measures in millimeters.

Appendix 4

Run Sheet: Glass Hard Mask

Responsible:

Sample ID:

Process start: Process end:

Step 1: Substrate cleaning and preparation

Date:	Operator:	Pre-treatment: No

Substrate: Glass sample of 0.7 mm thickness (1 × 1 in^2) 5 × 5 cm^2

Conditions:

- Washing with Alconox for 30 min in ultrasounds, followed by rinsing with deionised water (particle and grease removal)
- Drying with compressed air

Observations: 15 to 30 min in Alconox in ultrasounds.

Step 2: Al deposition

Date:	Operator:	Pre-treatment: No

Substrate: Glass sample of 0.7 mm thickness

Equipment: Nordiko 7000 at INESC-MN

Expected thickness: 1500 Å **Deposited thickness:** 1500 Å (during 40 sec)

Deposition Conditions:

	Mode	Power (W)	Ar Flux (sccm)	Pressure (mTorr)
Expected	Mod4 F1 metallization 40 sec	2000	50	3
Observed		2 kW 393 V/5.12 A	50	3

Observations: Al deposition of each glass sample made individually.

Step 3: Exposure		
Date:	Operator:	Pre-treatment: No

Substrate: Glass sample with Al layer

Equipment: Lasarray DWL 2.0 (Direct Write Laser system, Heidelberg) at INESC-MN

Step 3.1: Vapour Prime (30 min, Vapour Prime Oven)- Heating at 130ºC in vacuum with HDMS spraying (5 min)

Step 3.2: Coating (SVG) of 1.5 µm of positive photoresist (PFR7790G27cP- JSR Electronics) (program 6/2) – rotation of PR at 2800 rpm followed by soft-bake at 85ºC for 1 min.

Step 3.3: Exposure (DWL 2.0)

Exposure Conditions:

Map	Mask Name	E	F	Time	X0; Y0	Die Dimensions (µm)
AMSION	SusanaFCT_V02	45	-20	45 min	0,0 (don't have aligning cross)	
	AutoCAD File:					

Step 3.4: Development (SVG) – baking at 110ºC for 1min, followed by development during 1 min.

Masks: inverted (no PR on channels)

Step 3.5: Microscope verification of SV exposure

SusanaFCT_V02

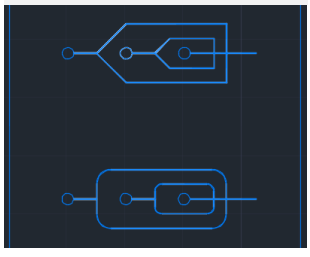

Substrate

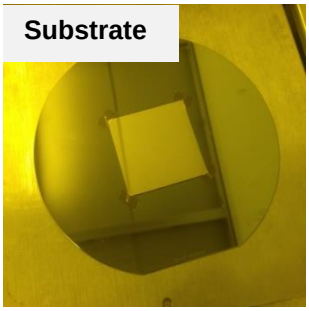

Step 3.2

Step 3.3

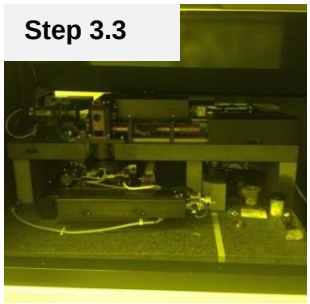

Step 3.4

Result

Step 4: Wet Etch

Date:	Operator:	Pre-treatment: No

Substrate: Glass sample with Al layer and PR

Equipment: Wet bench

Step 4.1: Etch

Solvent	T (ºC)	Time	Notes
Acetic Acid 3.3% Nitric Acid 3.1% Phosphoric Acid 3% pure	Room temperature	3min in solvent plus 2min in water, per sample	Manual agitation

Step 4.2: Substrate washing with deionized water

Observations: Etch rate ~ 6 Å/s.

Use protection glasses, coat and black thick gloves of clean room on top of white ones.

Use two glasses for solvent solution and water, and manipulate sample with a plastic tweezer.

Step 5: Resist Stripping

Date:	Operator:	Pre-treatment: No

Substrate: Glass sample with Al layer

Equipment: Lasarray DWL 2.0 (Direct Write Laser system, Heidelberg) at INESC-MN

Step 5.1: Stripping

Solvent	T (ºC)	Time	Notes
Microstrip	65	2 min	Manual agitation

Step 5.2: Substrate washing with IPA, followed by rinsing in deionized water and blow-dryed with compressed air gun

Mask

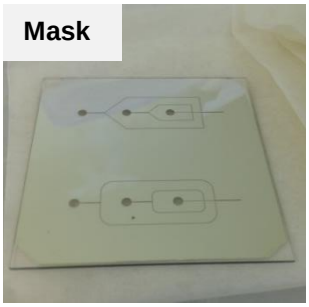

Run Sheet: PDMS microchannels microfabrication (SU-8, 100 µm)

Responsible:

Sample ID:

Process start: Process end:

Step 1: Substrate cleaning and preparation		
Date:	Operator:	Pre-treatment: No

Substrate: Silicon substrate form 6 in wafers <100> - International Wafer Service

Conditions:

- Immersing in Microstrip 3001
- Washing IPA, followed by rinsing with deionized water
- Heating in a hotplate @ 100ºC for 10 min, prior to spinning (to increase adhesion)
- Cool down the sample before spinning

Step 2: Sample Coating		
Date:	Operator:	Pre-treatment: No

Substrate: Silicon substrate form 6 in wafers <100> - International Wafer Service

Equipment: Spinner WS-650MZ-23NPP/LITE at INESC-MN

Expected thickness: 100 µm **Observed thickness:**

Coating Conditions:

Step 2.1: Pouring PR (SU-8) manually over silicon wafer, covering ¾ of the wafer and letting it rest for 5 min before start of the spinning

Step 2.2: Spin at 500 rpm for 10 sec, with 100 rpm/s acceleration

Spin at 1200 rpm for 30 sec, with 300 rpm/s acceleration

Observations: SU-8 must be poured carefully avoiding air bubbles. Measure thickness in profilometer.

Step 3: Soft-baking		
Date:	Operator:	Pre-treatment: No

Substrate: Silicon substrate form 6 in wafers <100> with PR

Equipment: Hot plate

Baking Conditions:

Step 3.1: Before soft-baking pre-bake for 10 min @65ºC

Step 3.2: Increase the hot plate temperature to 95ºC with the substrate on top. When 95ºC is achieved, bake for 30 min @ 95ºC

Step 3.3: Decrease the hot plate temperature to 75ºC and then cool down the sample for 5 min at room temperature on top of a glass

Step 4: UV exposure		
Date:	Operator:	Pre-treatment: No

Substrate: Silicon substrate form 6 in wafers <100> with PR

Equipment: Contact lithography system (UV lamp, by UV Light Technology LTD)

Exposure Conditions:

Step 4.1: Make contact between the quartz mask and the sample, trying to minimize the gap between them

Step 4.2: Expose the sample to 600 mJ/cm^2 (second slot) for 70 sec.

Observations: The mask is placed with side of pattern in contact with silicon substrate with SU-8.

Step 4.1

Step 4.2

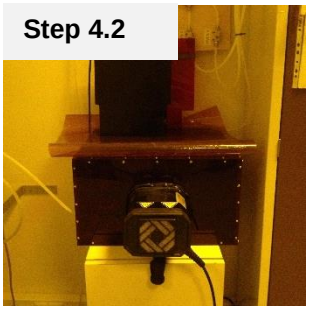

Step 5: Post exposure bake (PEB)		
Date:	Operator:	Pre-treatment: No

Substrate: Silicon substrate form 6 in wafers <100> with PR

Equipment: Hot plate

Exposure Conditions:

Step 5.1: Bake for 1 min @ 65ºC

Step 5.2: Increase the hot plate temperature to 95ºC with substrate on top. When 95ºC is achieved, bake for 10 min @ 95ºC

Step 5.3: Decrease hot plate temperature to 75ºC and then cool down the sample for 5 min @ room temperature on top of a glass.

Observations: Mask should be visible after 1 min of PEB. Otherwise there was insufficient exposure, heating or both.

Step 6: PR Development		
Date:	Operator:	Pre-treatment: No

Substrate: Silicon substrate form 6 in wafers <100> with PR

Developing Conditions:

Step 6.1: Development with PGMEA for 10 min with strong agitation.

Step 6.2: Rinsing with IPA and dry well (but gently)

Step 6.3: Hard-bake for 10 min @ 150ºC and letting the sample cool down on top of the plate

Observations: If a white residue is produced during rinse, the substrate is under developed, so immerse in PGMEA again.

Check the resist profile (by changing microscope focus) and measure with the profilometer (DEKTAK 3030ST).

If the structures peel off during development then either the exposure time or the PEB time were insufficient.

Step 6.1/6.2

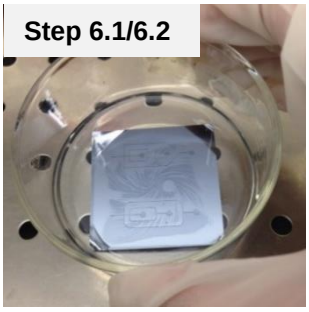

SU-8 mold

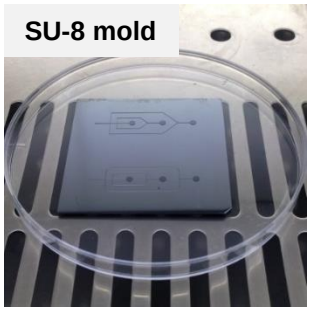

Run Sheet: PMMA plates fabrication

Responsible:

Sample ID:

Process start: Process end:

Step 1: PMMA Micro Machining

Substrate: 3 PMMA plates with 10 × 10 cm^2, two with a thickness of 2 mm and the other with 4 mm

Equipment: TAIG Micro Mill (Super tech & Associates) associated to high frequency motor

Step 1.1: Use double sided tape to fix PMMA plate to TAIG Micro Mill support and insert chosen tool

Step 1.2: Open DXF format AutoCAD file in DesKAM2000 and select a function to specific area. Save as DNC format.

Step 1.3: Run Mach2Mill CNC control Program (ArtSoft Corporation, 2000-2004) and open DNC format file. Adjust X, Y, Z positions and select respective velocity in high frequency motor.

Micro Machining Conditions:

PMMA Plate	Tool	Velocity (rpm)	Function
Top	Drill Ø 0.8 µm End Mill Ø 1.5 mm	6000-7000	Drill holes Contour for visual alignment
Medium	End Mill Ø 1.5 mm	7500	Multiple contour to open hole of chip size
Bottom	End Mill Ø 1.5 mm	7500	Double contour for 0.7 µm depth pocket

Observations: During micro machining use water to cool down de tool e clean polymer residues.

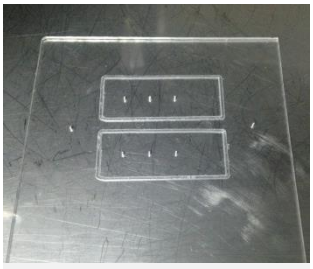

Top PMMA

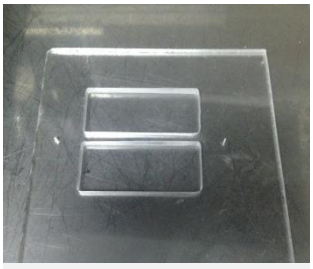

Medium PMMA

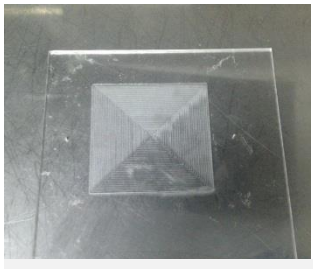

Bottom PMMA

Run Sheet: PDMS microchannels microfabrication and bonding

Responsible:

Sample ID:

Process start: Process end:

Step 1: PDMS mixture preparation

Step 1.1: PDMS (Sylgard 184 Silicone Elastomer Kit, Dow Corning) is prepared in plastic disposable cup by mixing the base and the curing agent in 10:1 (w/w) ratio.

Step 1.2: Degas for 1h to remove air bubbles, using the desiccator.

Step 1.1

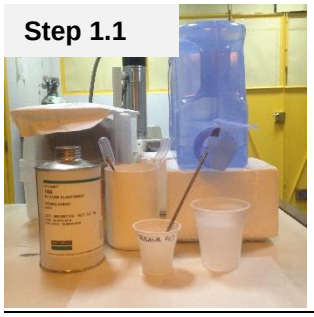

Step 1.2

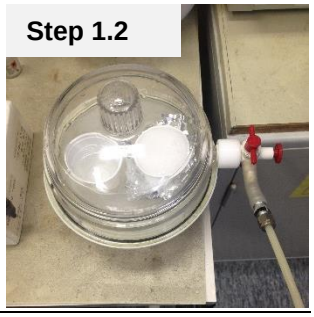

Step 2: PDMS casting and curing

Equipment: Oven

Step 2.1: Place SU-8 mold on bottom PMMA plate, and align metallic part of syringe needles with the outlet using tape.

Step 2.2: On top of that place medium PMMA plate and aligned top PMMA plate.

Step 2.3: Place syringe needles for holes on top PMMA plate and align with inlets of SU-8 mold.

Step 2.4: Lock up the structure using office springs

Step 2.4

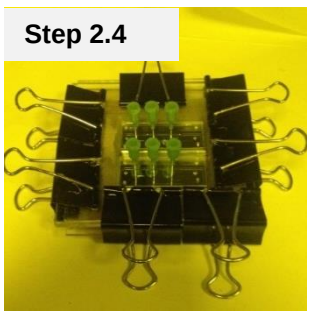

Step 2.5: Charge a syringe with PDMS mixture and fill void area trough hole on top PMMA

Step 2.6: Place in oven @ 70ºC for 1h and 30 min

Step 2.7: Prepare PDMS smooth non patterned layer by process in Step 1, and cast it on a petri dish or similar and follow Step 2.6.

Step 3: PDMS bonding

Substrate: Channel patterned PDMS and smooth PDMS slab

Equipment: Corona

Step 3.1: Perform Corona discharge for 2 min in each PDMS side to bring into contact, namely, side of PMDS with open channels and PDMS smooth substrate

Step 3.2: Bring into contact both PDMS substrates carefully to avoid trapping air bubbles

Observations: Don't bring electrical devices near Corona.

Use safety UV glasses and don't look directly to violet light produced during discharge.

Don't ouch metallic structures near Corona.

Do a scan of PDMS surface in multiple directions with Corona.

When joining PDMS substrates for bonding, don't bend the material.

Step 3.1

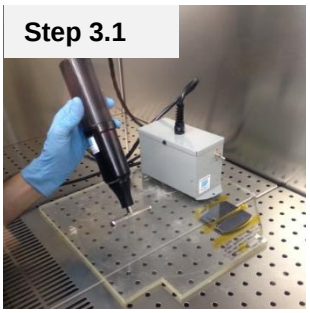

Appendix 5

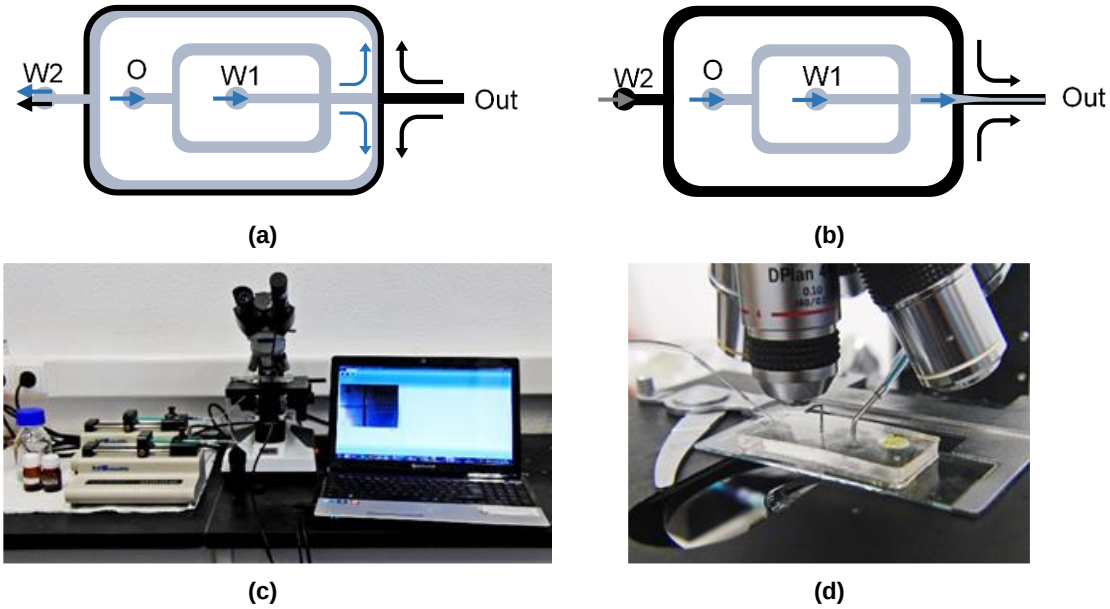

Figure A5.1. Flow confinement for outlet functionalization, where (a) chemical solution is injected either by outlet (**Out**) or (b) by inlet **W2**, while blocking solution is injected in inlets **O** and **W1;** (c) Setup for chemical modification of microchannels: flow controllers and loaded syringes connected by tubes to microfluidic device on microscope platform. A camera placed in right ocular is connected to pc to monitor fluids flows; (d) Inset of connections on microfluidic device: chemical solutions are injected through **Out**, blocking solution through inlet **O**, inlet **W1** is blocked and **W2** serve as outlet. Metallic part of 21G needles were used to connect tubes to inlets of the microfluidic device, and outlet tube was connected to a 26G and a 28G needle placed inside the device.

Appendix 6

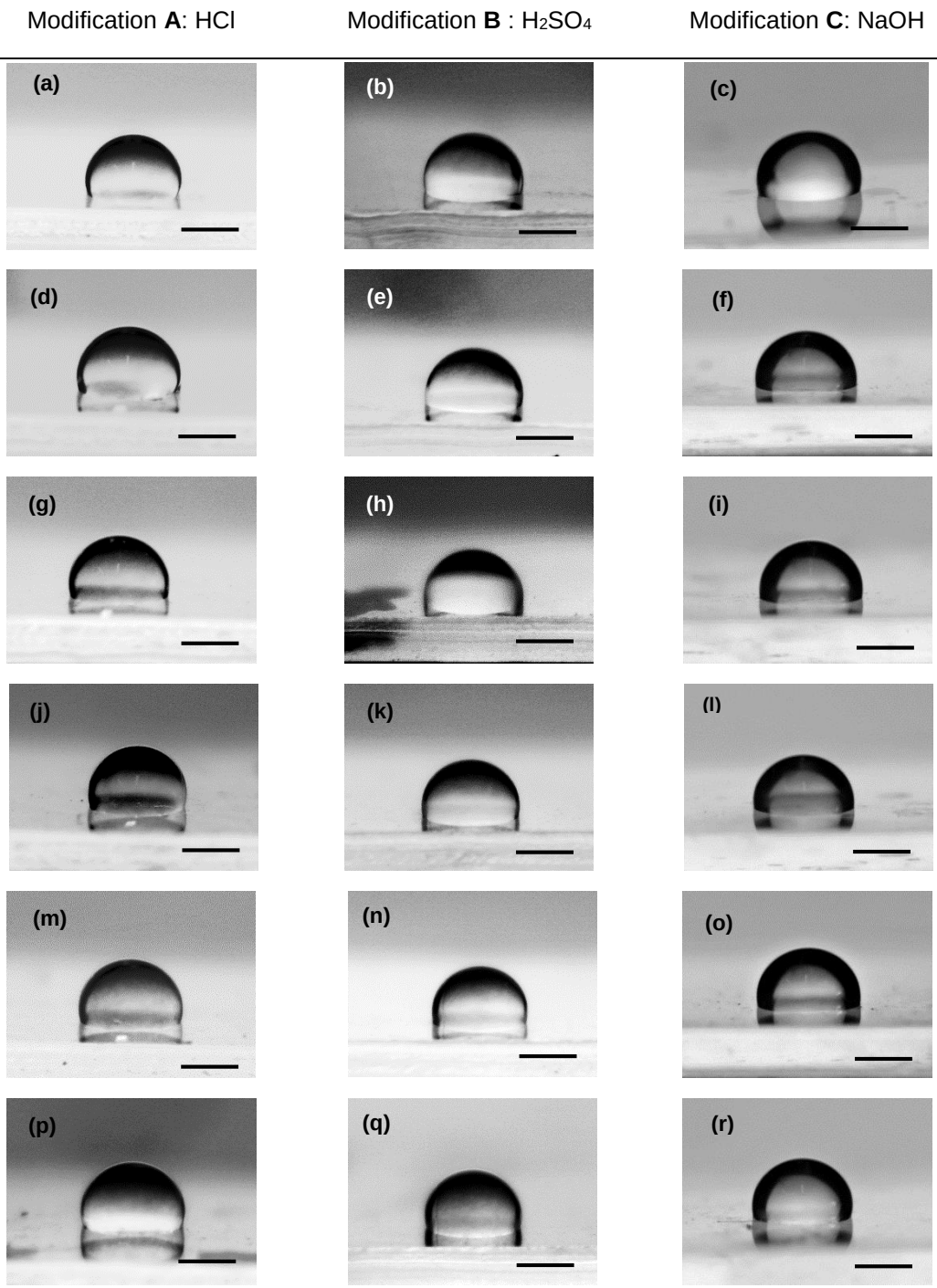

Figure A6.1. Photographs analysed for WCA of PDMS modified with (a, d, g, j, m, p) **A**; (b, e, h, k, n, q) **B**; (c, f, i, l, o, r) **C**. Scale bar = 500 µm.

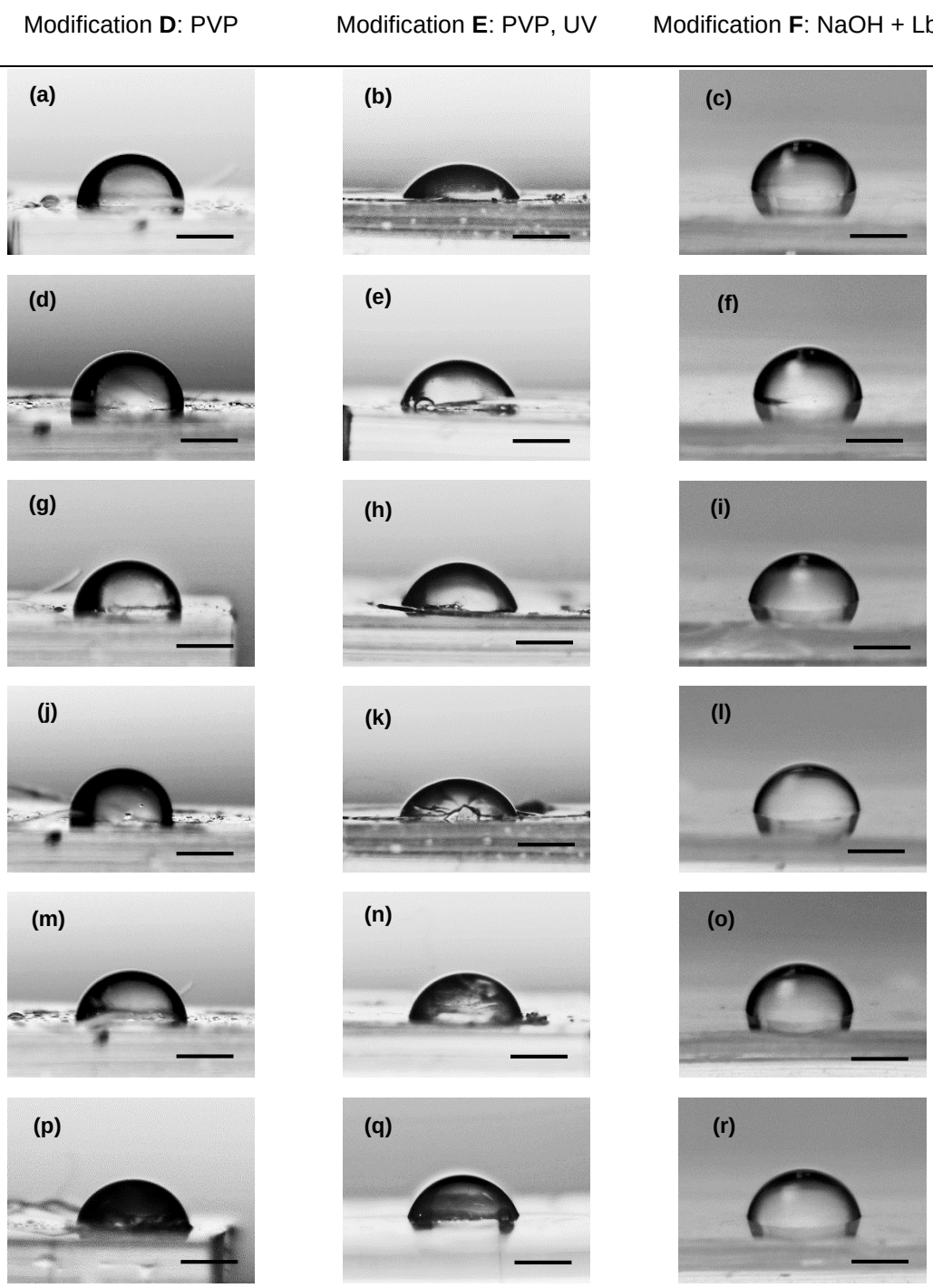

Figure A6.2. Photographs analysed for WCA of PDMS modified with (a, d, g, j, m, p) **D**; (b, e, h, k, n, q) **E**; (c, f, i, l, o, r) **F**. Scale bar = 500 µm.

Appendix 7

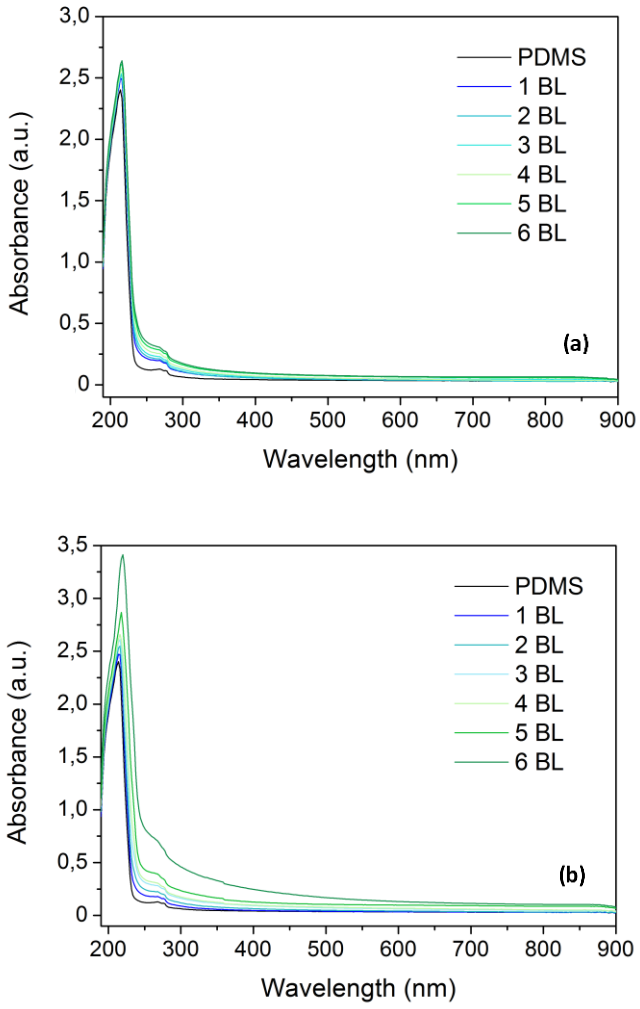

Figure A7.1. UV-Vis spectra in 190-900 nm range for modified PDMS with thickness of 0.869 ± 0.024 mm. Chemical treatment included 6 BL deposition of 5' per layer after oxidation with 1M NaOH for 15'. (a) Polyelectrolyte solution without salt; (b) Polyelectrolyte solution prepared in 0.5M NaCl - absorbance seems to increase exponentially.

Appendix 8

Table A8.1. DWCA (°) with and without oxidation with 1M NaOH for 15 minutes, and also with immersion of 3 BL substrates for 8h, followed by 5 days storage in air.

	5 minutes			15 minutes				
	1 BL	2 BL	3 BL	1 BL	2 BL	3 BL	3 BL NO NaOH	PDMS
t = 0 s	84 ± 3	69 ± 4	53 ± 4	74 ± 6	65 ± 4	67 ± 4	98 ± 5	110 ± 1
$t_{\text{stable WCA}}$ > 150 s	83 ± 3	64 ± 6	52 ± 4	71 ± 6	60 ± 6	61 ± 5	87 ± 5	108 ± 2
i8h								
t = 0 s			70 ± 2			66 ± 3	99 ± 8	
$t_{\text{stable WCA}}$ > 150 s			60 ± 1			58 ± 2	97 ± 4	
air5d								
t = 0 s			79 ± 5			74 ± 3		
$t_{\text{stable WCA}}$ > 150 s			69 ± 5			62 ± 1		

Appendix 9

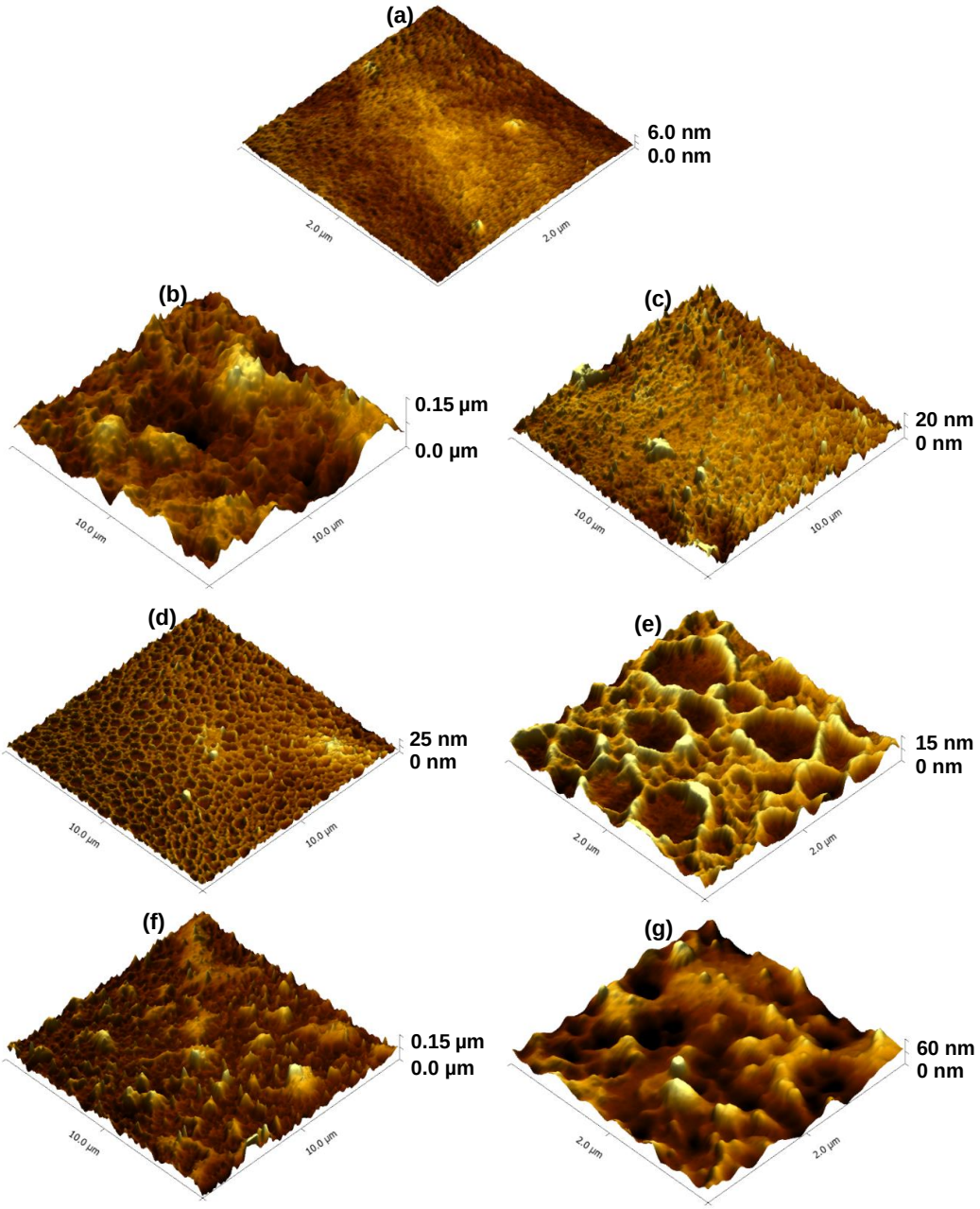

Figure A9.1. AFM 3D topographic images of (a) 2 × 2 µm^2 unmodified PDMS; (b) 10 × 10 µm^2 modified PDMS in 1M NaOH (24h) shows clearly increased roughness compared to (c) where modification occurred for only 15'; (d) after 3 BL (5'), magnification in (e); (f) after 6 BL (5') deposition, magnification in (g).

Appendix 10

Table A10.1. Approaches carried for turning the outlet channel of the microfluidic device hydrophilic.

Hydrophobic channels Water presented with color (blue or red); scale bar = 200 µm.	
10M NaOH (15') injected through Out 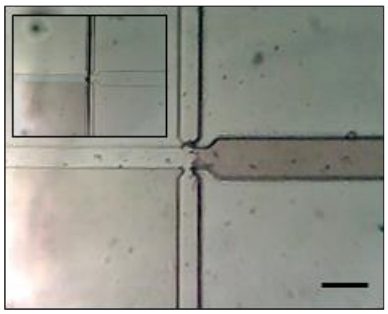	Higly concentrated NaOH solution produced well defined interface, but it damaged PDMS: channel turned white on naked eye perceived as brown under microscope. Q_{Out} = 0.08 ml/h; Q_{W1} = Q_O = 0.04 ml/h Blocking fluid: Milli Q.
1M (15'), 3 BL (15') injected through Out 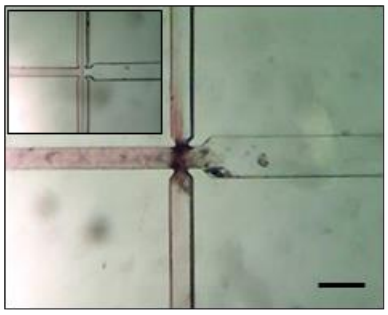	Hydrophilic? No. NaOH precipitates on the interface with colored water. Subsequent steps using polyelectrolytes blocked the intersection. Use color in solutions for chemical treatment instead. Q_{Out} = 0.08 ml/h; Q_{W1} = Q_O = 0.04 ml/h Blocking fluid: Milli Q.
1M (15'), 3 BL (15') injected through W2 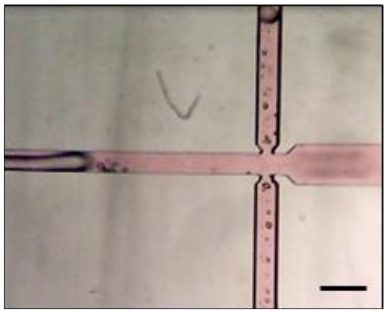	Hydrophilic? Yes. Oil droplets. W/O/W ? No. Channel between I1 and I2 was partially hydrophilic. This is due to chemical solution advancing for the channel during: - Changing between chemical solutions - Micro air bubbles that stop the oil flow Q_{W2} = 0.10 ml/h; Q_{W1} = Q_O = 0.04 ml/h Blocking fluid: Milli Q.

Table A10.2. Approaches carried, after hydrophilic modification, for turning the channel between **I1** and **I2** hydrophobic.

Hydrophilic channels

Water presented with color (blue or red); scale bar = 200 µm.

Comercial water repellent injected through Oil channel 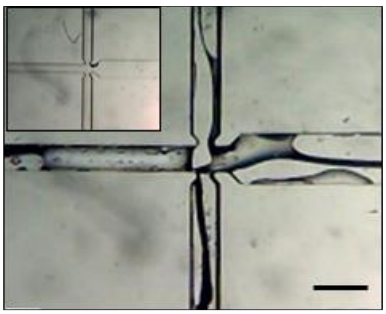	I1 to I2 hydrophobic? Partially. The mixture contains hydrophobic components. These adhered only partially to the walls. Other unknown components are possibly interfering with this modification. That question was not further evaluated. Q_O = 0.05 ml/h; Q_{Out} = 0.05 ml/h W1 was blocked. Blocking solution: Milli Q. Tap water was used as blocking solution for hydrophilic modification.
Triton-X injected trough Oil channel 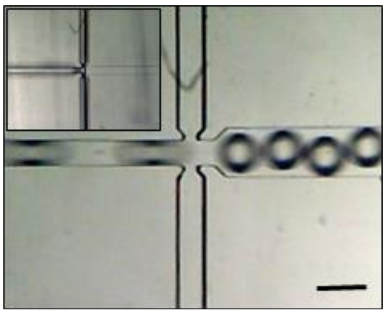	I1 to I2 hydrophobic? Channel remained perfectly hydrophilic. Triton-X is a non-ionic surfactant with a hydrophilic head and hydrophobic tail. It was expected it would adhere to walls orienting the tail to oil, but that didn't happened. This may be due to lack of functional groups to attract Triton-X, or due to the fact that this is non-ionic. That question was not further evaluated. (Sigma product information: http://www.snowpure.com/docs/triton-x-100-sigma.pdf) Q_O = 0.05 ml/h; Q_{Out} = 0.40 ml/h W1 was blocked. Blocking solution: Milli Q. Used phosphate buffer as blocking solution for first modification.

Appendix 11

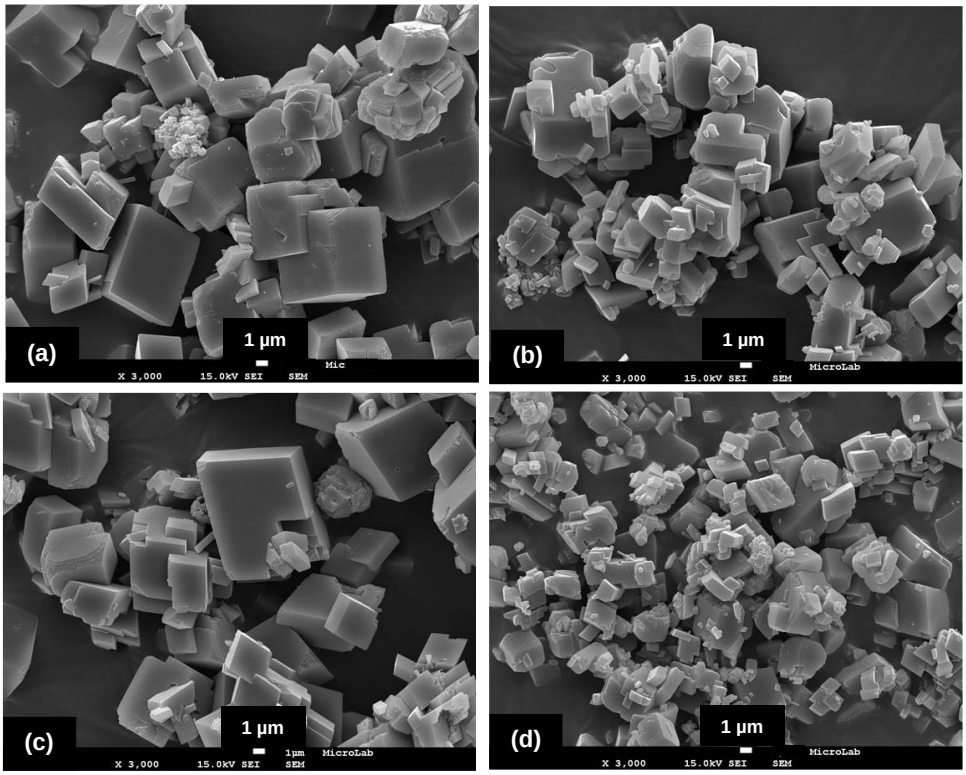

Figure A11.1. SEM micrographs of $CaCO_3$ synthesized by precipitation reaction between 0.5 M aqueous solutions of $CaCl_2.2H_2O$ and Na_2CO_3 at (a) 300 rpm, 30'; (b) 300 rpm, 2h; (c) 1200 rpm, 30'; (d) 1200 rpm, 2h.

Appendix 12

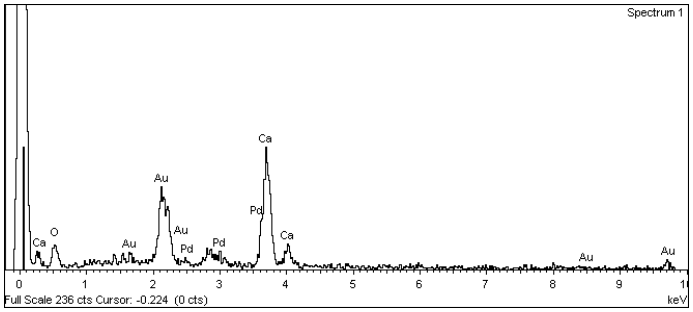

(a)

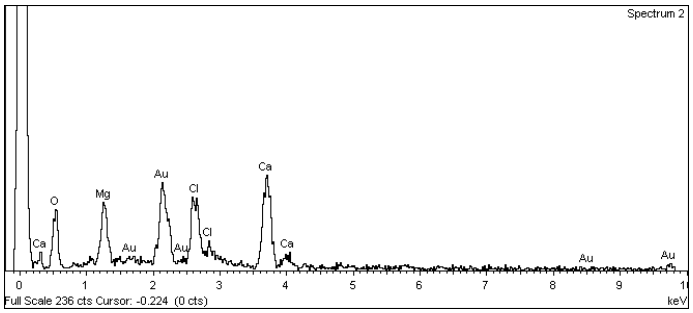

(b)

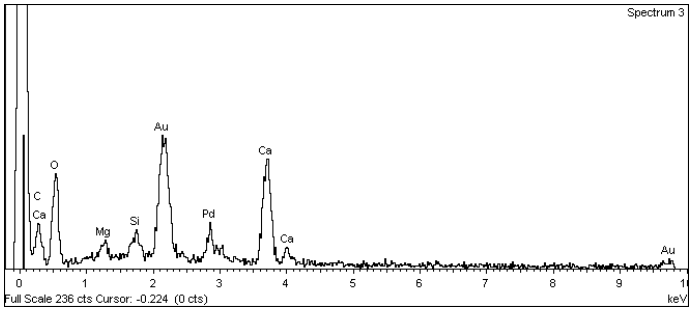

(c)

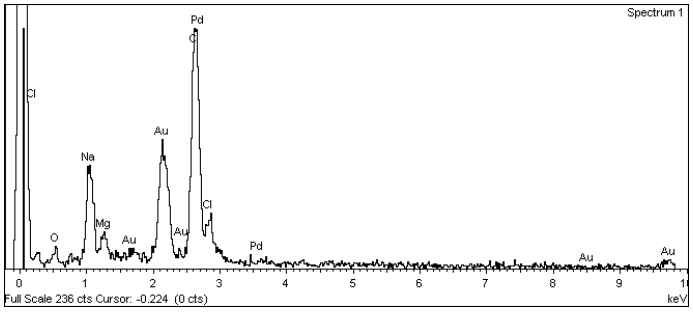

(d)

Figure A12.1. EDS for sample (a) 300 (2h) and [Mg]/[Ca] of (b) 2, (c) 4 and (d) 8.

Appendix 13

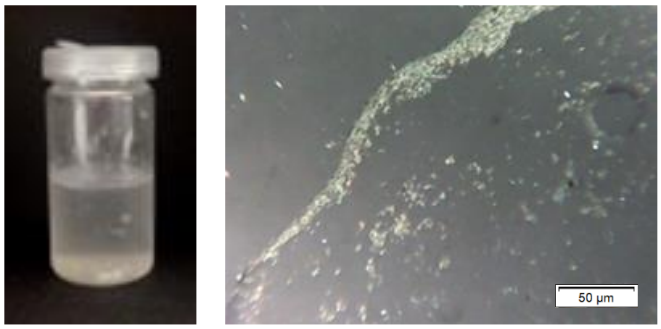

(a) **(b)**

Figure A13.1. Unsuccessful attempt to stabilize O/W emulsion with pre-synthesized $CaCO_3$ particles: (a) Photograph shows deposited crystal on bottom; (b) Microscope image revealed only crystal deposits and no emulsion.

Appendix 14

Table A14.1. W/O emulsions: 1, 2, 3, 4, 5 microscope images and respective photographs. When 2 or more images are displayed for same emulsion, top image correspond to a sample of top of the emulsion, medium image of medium sample, and bottom image of sample extracted from the bottom (in same scale).

	Immediately after preparation	24h later	Observations
1-PVA	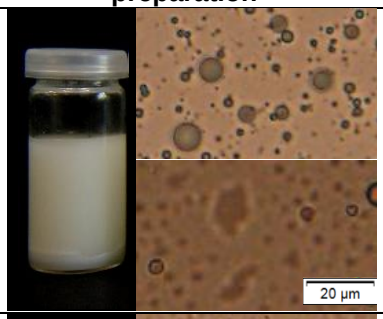	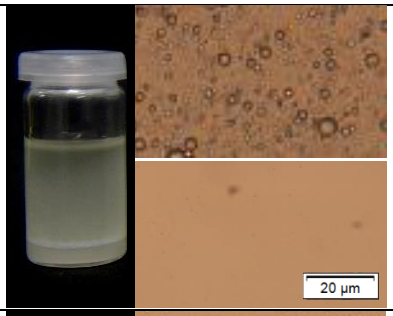	- Two phases are distinguishable at initial time and become more evident at 24h. - Water droplets are coalescing.
2-PAA-NA	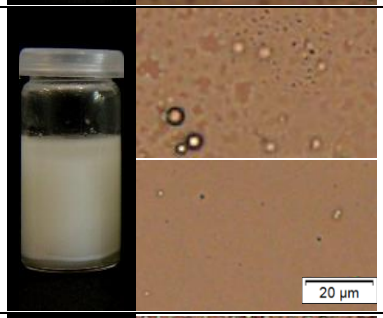	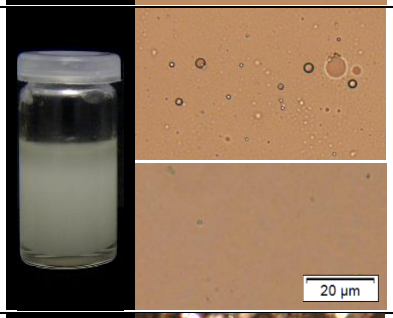	- Same as in 1. - Rare and very small water droplets at 24h.
3-PVA + salts	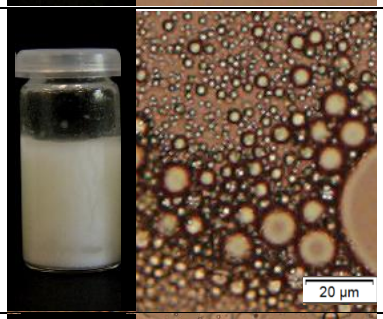	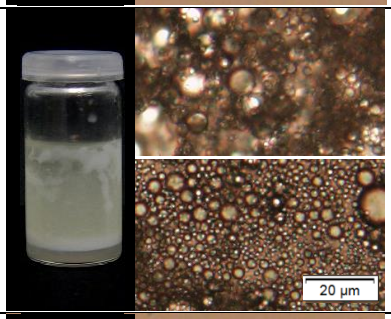	- Water droplets coalescing at initial time. - After 24h, some interaction between PVA and salts occurred seen by deposits on glass walls. - No signs of $CaCO_3$ crystals.
4-PAA-Na + salts	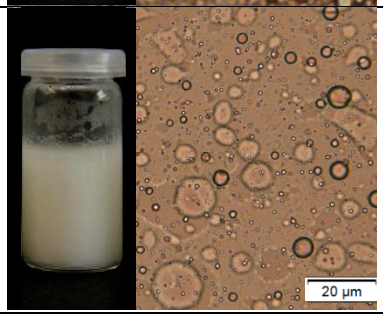	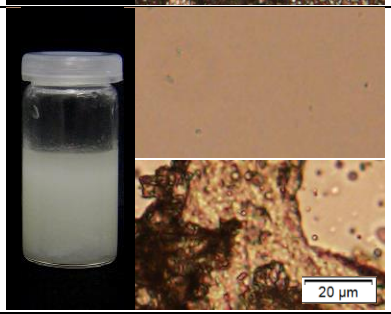	- Few water droplets seen at initial time. - After 24h, some interaction between PAA-Na and salts occurred seen by deposits on bottom. - No signs of $CaCO_3$ crystals.
5-$CaCO_3$	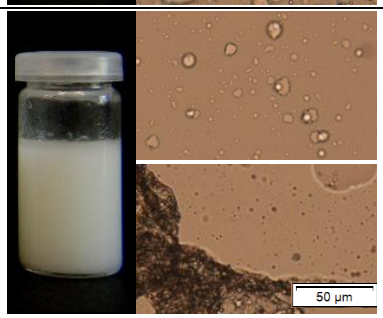	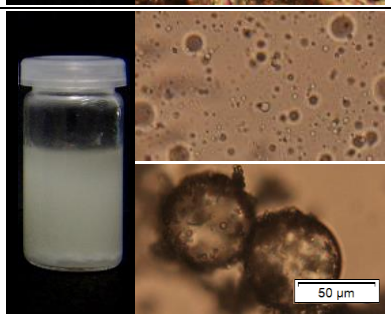	- Crystal deposits at bottom in initial time; few water droplets can be seen. - After 24h oil droplets surrounded by $CaCO_3$ were collected at bottom, indicating phase inversion.

Appendix 15

Table A15.1. W/O oleic acid emulsions (1, 5, 10 % (w/v)) microscope images and respective photographs. When 2 images are displayed for same emulsion, top image correspond to a sample of top of the emulsion and bottom image of sample extracted from the bottom of the emulsion (in same scale).

	Immediately after preparation	3 days later	Observations
1% (w/v) Oleic Acid	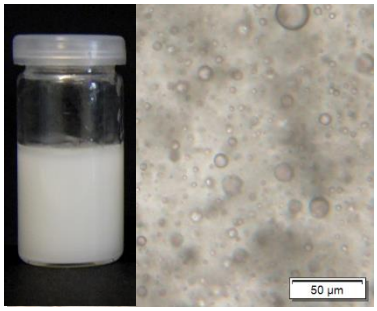	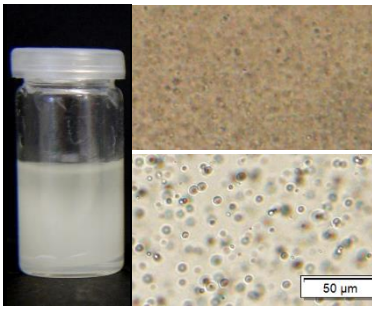	- Smaller water droplets on top of oil phase and bigger droplets on bottom. - Some droplets have coalesced: seen by water phase at bottom of the glass.
5% (w/v) Oleic Acid	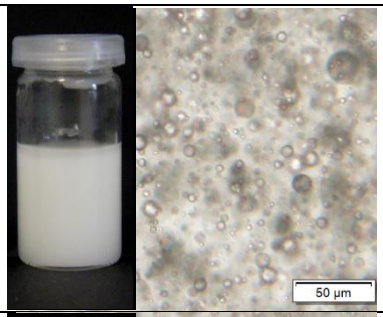	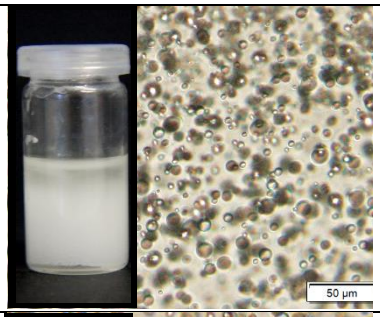	- Water remained emulsified. - **<u>Stable emulsion.</u>**
10% (w/v) Oleic Acid	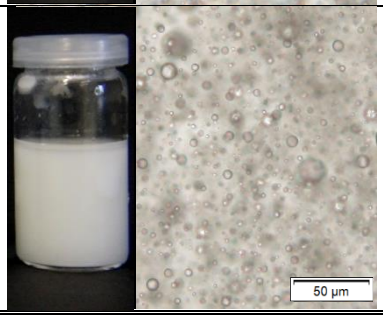	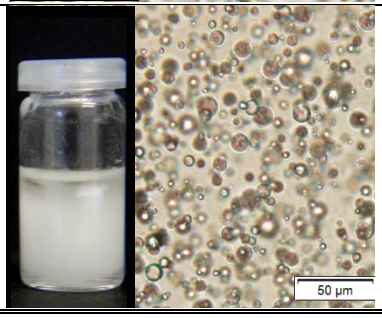	- **<u>Stable emulsion.</u>**

Appendix 16

Table A16.1. O/W emulsions: 1, 2, 3, 4, 5 microscope images and respective photographs. When 2 or more images are displayed for same emulsion, top image correspond to a sample of top of the emulsion, medium image of medium sample, and bottom image of sample extracted from the bottom (in same scale).

	Immediately after preparation	24h later	Observations
1-PVA	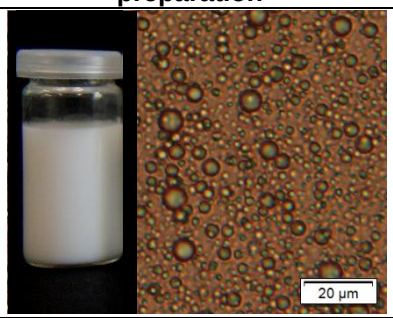		- Dispersion in droplets size. - **<u>Stable emulsion</u>** after 24h.
2-PAA-NA	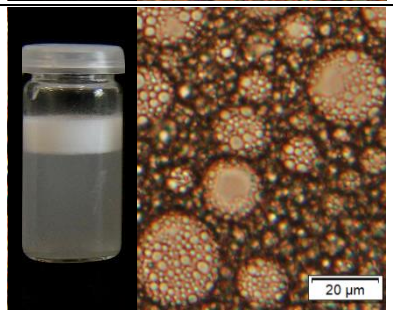		- Coalescing oil droplets fluctuating at initial time. - After 24h oil droplets grew into milimetric size, and a clean water phase was visible.
3-PVA + salts	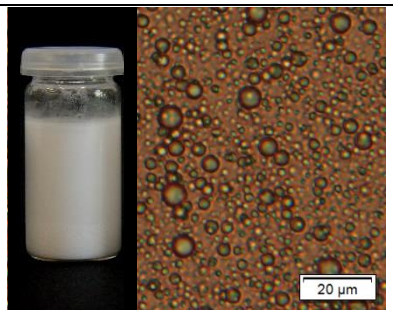		- At initial time similar results to 1. - At 24h oil droplets are coalescing, seen by bigger droplets in the upper part. - No signs of $CaCO_3$ crystals on droplets.
4-PAA-Na + salts	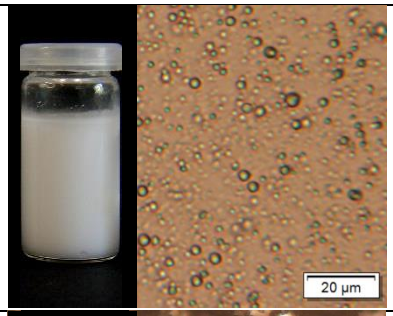		- Results similar to 3. - No signs of $CaCO_3$ crystals on droplets.
5-$CaCO_3$	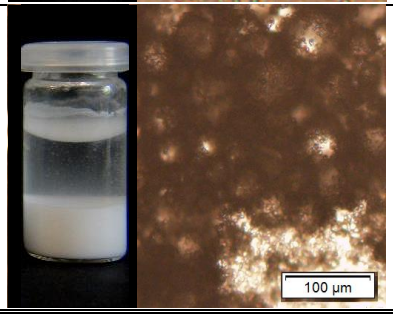		- Oil droplets deposit. - Not all the oil was emulsified, which can be modulated increasing salts' concentration or decreasing the oil fraction. - **<u>Stable emulsion</u>.**

Appendix 17

Table A17.1. O/W emulsion number 5, 6, 7, 8 microscope images and respective photographs. When 2 images are displayed for same emulsion, top image correspond to crossed polarizer and bottom image without polarizer (in same scale).

	Immediately after preparation	7 days later	1 month later
5-$CaCO_3$		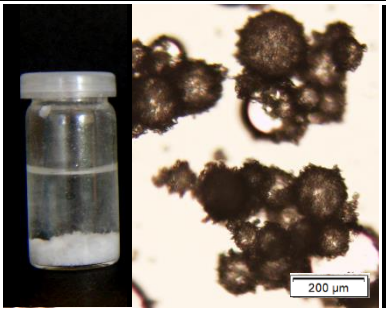	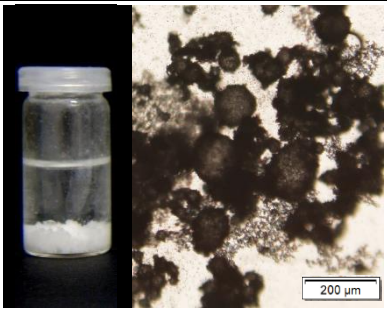
6- [Mg]/[Ca] = 2	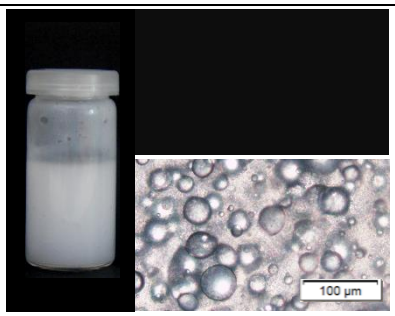	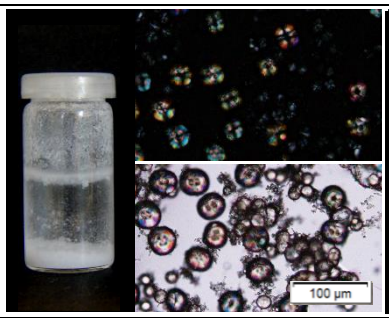	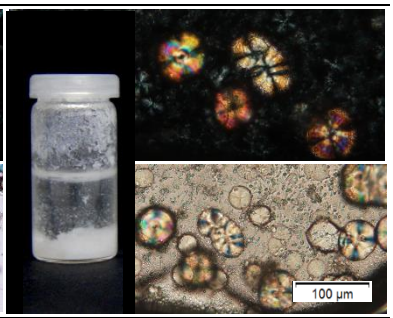
7- [Mg]/[Ca] = 4	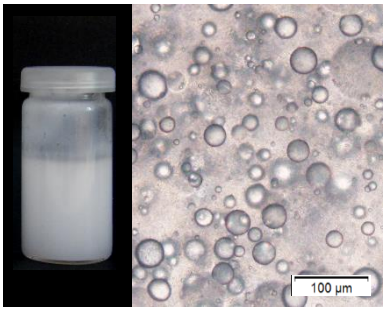	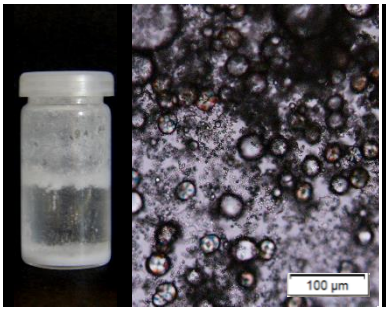	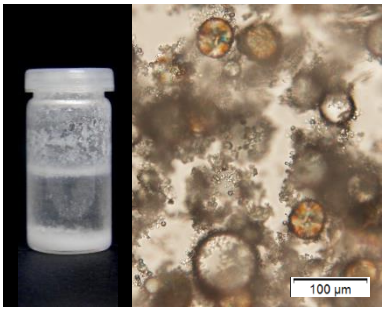
8- [Mg]/[Ca] = 8	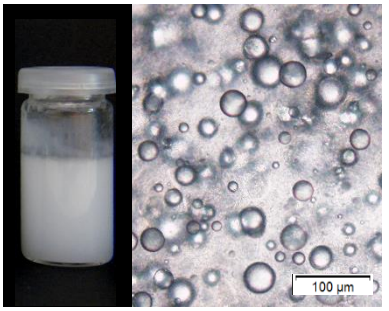	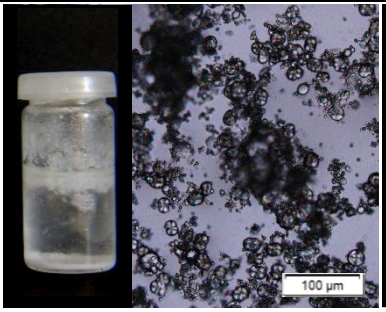	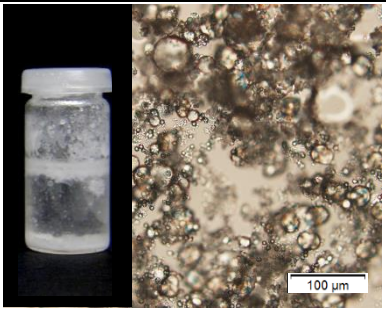

Appendix 18

Table A18.1. O/W PAA-Na emulsions (5 and 20% (w/v)) microscope images and respective photographs. When 2 images are displayed for same emulsion, top image correspond to a sample of top of the emulsion and bottom image of sample extracted from the bottom (in same scale).

	Immediately after preparation	3 days later	Observations
5% (w/v) PAA-Na	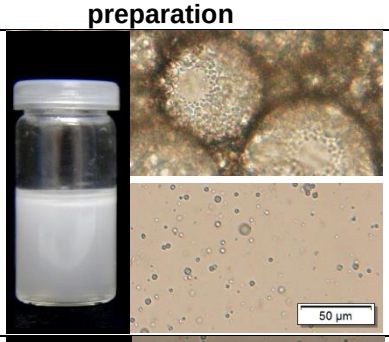	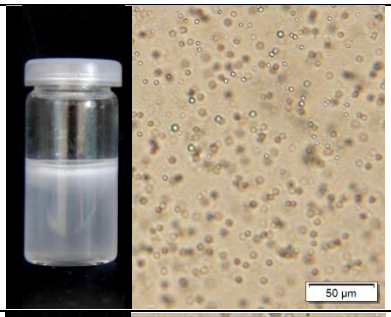	- Droplets are coalescing right at initial time.
20% (w/v) PAA-Na	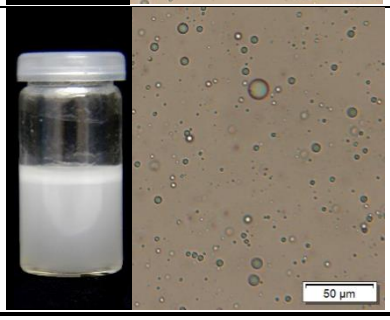	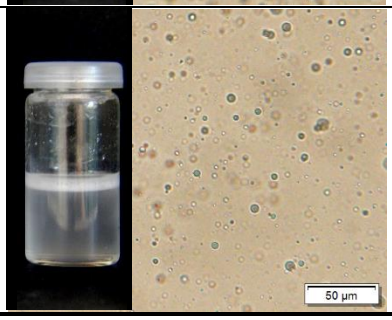	- After 3 days the two phases are almost separated.